IMPLICIT 3D STRUCTURAL MODELLING IN METAMORPHIC MOUNTAIN BELTS: REGIONAL AND LOCAL-SCALE APPLICATIONS IN THE PENNINE ALPS (NW ITALY)

Cognome / Surname: Arienti   Nome / Name: Gloria

Matricola / Registration number: 789518

Tutore / Tutor: Prof. Marco Giovanni Malusà

Supervisor: Prof. Andrea Bistacchi

Coordinatore / Coordinator: Prof. Marco Giovanni Malusà

Abstract

The overarching theme presented this thesis is the generation of large (x1) and local-scale (x2) 3D structural models of regions of the Pennine Alps, for which I introduce modelling workflows that combine high-resolution new and legacy structural datasets derived from fieldwork with implicit modelling algorithms. The implicit approach builds the tectonic architecture as an analogy between the relative distance among geological structures and a volumetric scalar field, within which geological structures are represented as isovalue surfaces. In particular, in this thesis I employ the Discrete Smooth Interpolator algorithm.

The study areas, situated in the northwestern Alps between Mont Blanc and Monte Rosa, lacked prior comprehensive three-dimensional representations. This region exhibits the Austroalpine-Penninic collisional wedge and the Helvetic-Ultrahelvetic sequence of thrust sheets. This tectonic sequence is represented in the first, regional-scale 3D model presented in this thesis, spanning approximately 1,500 km^2 along the Italian-Swiss boundary. The modelling workflow for the creation of this model incorporates structural interpretations on vertical cross-sections to propagate geological knowledge to the subsurface, ensuring the geological realism of the final outcome, resulting in a deterministic model that provides a comprehensive summary of the tectonic architecture and captures the state of the knowledge about the region. Geological structures represented by the model include hierarchical shear zones, isoclinal and/or recumbent folds, and networks of faults.

Successively, I redirect my attention to two more localised regions (extensions less than 30km^2) encompassed within the boundaries of the regional model, the Lago di Cignana area and the Tournalin-Roisetta ridge. With the objective of reducing subjectivity and uncertainty of the final outcomes, I employ implicit modelling techniques that leverage constraints provided by the structural database. For this, I perform three-dimensional interpolation of vectorial data, incorporate inequality constraints that act on the value of the implicit scalar field to integrate off-contact information in the interpolation (i.e., observations collected away from tectonic boundaries), and account for uncertainties in the structural database through stochastic simulations of vectorial data that replicate spherical distributions derived from the input database.

In the Lago di Cignana area, I adapt the modelling workflow to represent non-cylindrical, isoclinal recumbent folds exposed in the region and I employ interpolation and simulation of fold axes. The value of the uncertainty analysis is demonstrated by its ability to suggest, among the alternative possible scenarios, partial rotation within segments of the isoclinal folds, possible closures along the axial plane, and higher uncertainties localised at the fold hinges. Conversely, for the modelling of the Tournalin-Roisetta ridge, I interpolate and simulate schistosity data and incorporate off-contact observations that act on both the value and the gradient of the implicit scalar field. Results reveal that inequality constraints enable the creation of alternative, smoother solutions, and the uncertainty analysis indicates higher uncertainties away from direct measurements and reveals oscillations of up to 100 meters orthogonal to the layers.

Throughout the different chapters of this thesis, I provide descriptions of the modelling workflows elucidating the rationale behind the selection of the modelling strategies and present the three-dimensional outcomes of the implicit modelling approach applied to the Pennine Alps.

Table of contents

<div align="right">Chapter 1</div>

<div align="right"># **Introduction**</div>

Three-dimensional structural models are numerical representations of subsurface geological structures, generated through integration of both direct and derived observations with modelling algorithms. 3D models provide invaluable and accessible visualisations of the tectonic architecture, enhance three-dimensional reasoning and serve as a computational foundation for various subsurface studies, including resource exploration, underground water management, and engineering projects (e.g., risk assessment studies, tunnelling projects).

The primary objective of this PhD thesis is the employment of modelling approaches that integrate the outcomes of traditional high-resolution structural mapping studies with advanced modelling algorithms. The process is applied to generate comprehensive interpretations of the tectonic framework, both at a regional and local scale, within the northwestern European Alps. Situated at the heart of the Alpine collisional orogen, this region is the result of the Cretaceous-onwards convergence between the Adriatic and European continental plates, characterised by a complex history of orogenic nappe emplacement processes (Dal Piaz et al., 2003; Schmid et al., 2004). The structural geology and petrography of units exposed in the study area is the result of superimposed Alpine and in some cases pre-Alpine events, whose relics are still recognised at different scales in basement and pre-Mesozoic rocks. The boundaries that separate different tectono-metamorphic units (i.e., discrete crustal elements defined by a peculiar association of lithology, metamorphic imprint and deformative evolution) in the tectonic stack are the result of both contractional and extensional tectonic phases (e.g., Ballèvre and Merle, 1993; Wheeler and Butler, 1993; Reddy et al., 2003; Manzotti et al., 2014) and we refer to them throughout this thesis as tectonic boundaries and not as "simple" folded thrusts.

Particularly, the geographical focus of this thesis lies within the area that expands from Mont Blanc to

Monte Rosa, in the Pennine Alps. This region has been a subject of considerable cartographic and scientific interest since the release of Dufrénoy and de Beaumont's (1841) geological map, which was one of the first geological maps ever produced and encompassed our study area. This Alpine region bears substantial economic importance and significantly impacts the livelihoods of neighbouring populations, as it holds significance in agriculture by serving as a natural water storage facility. The area also hosts major civil and tunnelling engineering projects, establishing it as an important communication node, and it serves as a popular tourist destination. However, despite the economic importance and the long history of active scientific interest (Dal Piaz and Argentieri, 2021), no comprehensive three-dimensional representation of this specific area has been produced to date, a knowledge gap that this thesis seeks to fill.

Deformation structures in metamorphic terrains exhibit frequent thickness variations, large-scale boudinage (resulting in fragmentation of original lithological or stratigraphic units), complex multi-phase. Folds often display multi-scale and disharmonic patterns, commonly with non-cylindrical geometries. Generating 3D structural models in orogenic settings is therefore a multifaceted task whose resolution addresses different challenges. The initial step in the modelling process requires a comprehensive understanding of the tectonic processes responsible for shaping the often complex architectures, and this knowledge is crucial for identifying the deformation patterns to be modelled. Subsequently, choosing appropriate modelling algorithms becomes the second critical step for accurately representing the geological subsurface.

For the modelling presented in this thesis, I employ the implicit modelling approach, whose first applications to the geological problem were proposed by Houlding (1994) and Lajaunie et al. (1997). The implicit modelling approach represents geological structures as isovalues within a volumetric scalar field and constrains their geometries through simultaneous integration of geological information, fault data and unconformities to build a model that aligns with field observations. Over the past two decades, the implicit modelling approach has been gaining traction and it has been extensively applied to a diverse range of geographical regions in complex orogenic settings (Maxelon and Mancktelow, 2005; Bistacchi et al., 2008; Maxelon et al., 2009; Hillier et al., 2013; Perrouty et al., 2014; Philippon et al., 2015; Vollgger et al., 2015; de Kemp et al., 2016; Schneeberger et al., 2017; Thornton et al., 2018), demonstrating its suitability for the objectives of this thesis.

In the following sections, I articulate the motivation behind the modelling endeavours discussed in this PhD thesis and provide a general overview of the state of the art of modelling algorithms. Following this, I present the timeline of the work, concise descriptions of the three main chapters of the thesis, and an overview of the side projects undertaken throughout the PhD years.

1.1.   Motivation for 3D structural modelling in the Pennine Alps

The work presented in this thesis was carried out within the framework of the European Interreg Reservaqua project (ID 551749). The project, which initiated in July 2019 and concluded in March 2023, provided funding for a total of 2 years and 4 months of this PhD research. In the final eight months, support was received from the Italian national cartographic project (CARG project, https://www.isprambiente.gov.it/en).

The main objective of the Reservaqua project was to develop a programme for sustainable management of water resource in Alpine regions, with a specific focus on the impact of climate change. By addressing the vulnerabilities of the water supply systems in mountainous settings, this Interreg project aimed to fortify the management of water resources. This holds paramount importance, given that the European regions bordering the Alpine belt rely significantly on water stored in mountainous areas to meet their water supply needs and support agriculture, industry and tourism.

In this context, this PhD is dedicated to addressing part of the research questions of the Reservaqua project by developing a regional-scale 3D structural model located in the Italian-Swiss border region between Mont Blanc and Monte Rosa, whose location is highlighted in Fig. 1.1. The model covers approximately 1,500 km^2 and serves a dual purpose. Firstly, it encapsulates the wealth of geological field data collected over the past 30 years primarily as part of projects supported by the Autonomous Aosta Valley Region, Italian lead partner of the Reservaqua project, therefore consolidating the outcomes of the geological investigations. Secondly, the model provides the three-dimensional representation of the subsurface architecture, making it a valid foundation for future hydrogeological studies and enhancing the structural interpretation of the region. In addition, the collaboration for the Reservaqua project yielded two small-scale 3D structural models (areal extension less than 30 km^2), located within the same region covered by the regional-scale model (Fig. 1.1).

1.2.   3D structural modelling: overview of the state of art

At a fundamental level, modelling workflows can be categorised into two main approaches: model-driven and data-driven methods. Model-driven approaches, often referred to as knowledge-driven approaches, rely on existing a-priori geological knowledge organised within a conceptual model (Wellmann and Caumon, 2018). This conceptual model, based on a comprehensive understanding of the underlying geological processes, is used to transfer geological insights from the interpreter to the 3D model. Data-driven approaches, on the other hand, rely on vast databases (e.g., physical properties from geophysical databases) to directly guide model creation based on observed data (Wellmann and Caumon, 2018). This approach often employs statistical and predictive techniques to construct the model from the available data.
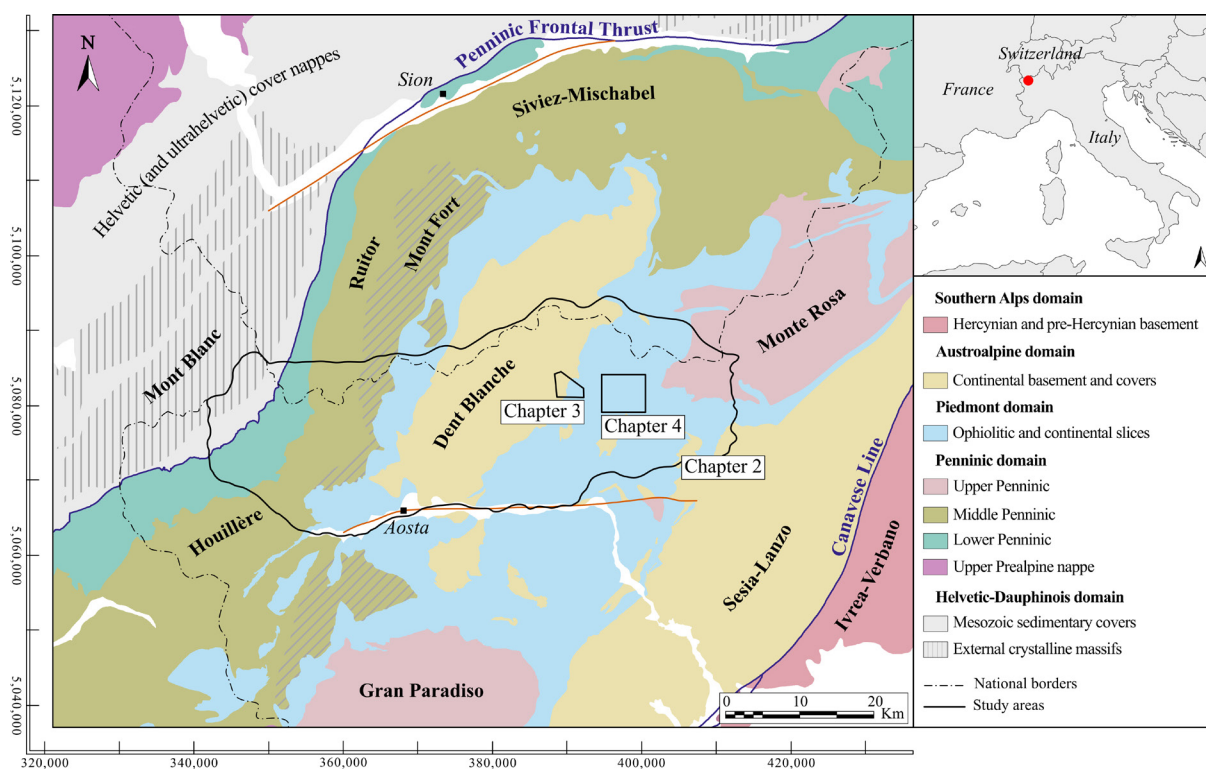
Figure 1.1. Tectonic setting of the northwestern Alps. Modified from Bigi et al. (1990) by Geol. Bruno Monopoli. Coordinates as WGS 1984 UTM Zone 32N.

Within the realm of modelling techniques, there are two more families to consider: explicit and implicit modelling approaches, which differ in the algorithms used for the creation of 3D surfaces. Explicit approaches (Sides, 1997; Caumon et al., 2009; Wellmann and Caumon, 2018) treat each structure as an individual entity, represented by nodes and cells, and the modelling takes place through interpolation of the input elements represented by their 3D spatial coordinates. While being valuable in many applications, explicit methods also display several limitations as they require significant interpreter time since they entail the progressive interpolation of each structure, and when dealing with structures that terminate inside the model's domain, such as finite faults. Modelling these geometries requires specific interpretations positioned at the closure location (Sides, 1997), and modelled geometries may result in unexpected intersections between surfaces, leading to the generation of geometries that do not represent geologically feasible scenarios (Caumon et al., 2004), overall increasing the time required for expert validation. Explicit modelling techniques are implemented in many commercial software packages, among which there are Move (www.petex.com/products/move-suite) and SKUA/GOCAD (https://www.aspentech.com/en/products/sse/aspen-skua).

The implicit approach, instead, is a sometimes considered more efficient alternative to the explicit approach. As mentioned earlier, the implicit method establishes an analogy between the three-

dimensional geological space (or geological time) and a scalar field that spans the entire model volume (Lajaunie et al., 1997; Chilès et al., 2004; Frank et al., 2007). In this approach, tectonic boundaries are portrayed as isovalue surfaces within this three-dimensional scalar field, and they can be extracted to derive a boundary representation of the 3D structural model. The scalar field is continuous throughout, except at the intersection with faults and unconformities, which are integrated into the interpolation process as mathematical discontinuities (Lajaunie et al., 1997; Frank et al., 2007; Caumon et al., 2013; Laurent et al., 2013; Godefroy et al., 2018; Grose et al., 2021a).

Implicit modelling approaches offer a crucial advantage in that they can seamlessly integrate a variety of geological information directly into the modelling workflow through the imposition of mathematical constraints. On-contact and off-contact observations are translated into the mathematical problem as position (both equality and inequality) constraints to guide the value of the scalar field, while structural datasets can be integrated as orientation constraints to affect the attitude of the isovalue surfaces (Chilès et al., 2004; Frank et al., 2007; Calcagno et al., 2008; Caumon et al., 2013; Hillier et al., 2013, 2014; Laurent et al., 2016; Grose et al., 2017, 2019). These constraints help reducing the subjective influence of the interpreter on the interpolation, relying instead on direct observations.

Implicit modelling approaches moreover offer the significant advantage of great adaptability to changes in the input database, making them well-suited for incorporating stochastic analysis for the integration of structural uncertainties (Caumon et al., 2007; Wellmann et al., 2010, 2014; Lindsay et al., 2012; Wellmann and Regenauer-Lieb, 2012; Cherpeau and Caumon, 2015; Jessell et al., 2018; Pirot et al., 2022).

Numerous different implicit modelling algorithms are available, and they can be further classified into meshless and mesh-based algorithms. The key distinction lies in whether a 3D mesh is used to facilitate the interpolation of the scalar field. Meshless methods, as the name suggests, employ mathematical formulations that do not rely on a mesh. Examples include Radial Basis Function interpolators (Carr et al., 2001), utilised in commercial software Leapfrog (https://www.seequent.com/products-solutions/leapfrog-software/) and in the open-source library Surfe (Hillier et al., 2014), dual kriging methods (Calcagno et al., 2008) implemented in Geomodeller (commercial; https://www.intrepid-geophysics.com/products/geomodeller/) and GemPy (open-source, De La Varga et al., 2019), as well as point-based moving least squares basis functions (Renaudeau et al., 2019). In meshless approaches, the mathematical formulation results in systems of equations of size $\sim N^2$, where N represents the number of data or interpolation points, which can become computationally demanding, particularly when dealing with large numbers of data points.

In contrast, mesh-based algorithms rely on three-dimensional meshes, which can be either cartesian (Irakarama et al., 2018) or tetrahedral (Frank et al., 2007; Caumon et al., 2013; Irakarama et al., 2022).

The computational complexity of mesh-bashed methods typically scales linearly with the mesh size, offering flexibility by adjusting the mesh resolution. Mesh-based algorithms are implemented in commercial software such as SKUA/GOCAD and Petrel (https://www.software.slb.com/products/petrel), as well as in the open-source library LoopStructural (Grose et al., 2021b).

The models presented in this thesis (Chapters 2, 3 and 4) have been generated using the implicit mesh-based Discrete Smooth Interpolator (DSI; Frank et al., 2007; Caumon et al., 2013) implemented in SKUA/GOCAD and in the RING Toolkit plugin, which solves the interpolation on the nodes of a tetrahedral mesh. Several factors influenced the choice of this software package, among which was the DSI's capacity to incorporate position and orientation observations collected during fieldwork, and the straightforward integration of fault elements in the modelling process. Additionally, the DSI interpolator has already been successfully applied to similar projects and geological settings (e.g., Bistacchi et al., 2008; Zanchi et al., 2009; Philippon et al., 2015), demonstrating its flexibility for modelling metamorphic terrains. Furthermore, University of Milan-Bicocca is academic sponsor of the RING consortium (https://www.ring-team.org/), which founded SKUA/GOCAD in 1989 and more recently implemented the RING Toolkit plugin (Frank et al., 2007; Caumon et al., 2013). This sponsorship not only facilitated access to the software for the research described in this thesis but also provided valuable access to expertise in the field.

1.3. Research progression

The PhD work detailed in this thesis extended over a period of 3 years, from December 2020 to November 2023. It was primarily conducted at the University of Milan-Bicocca in Italy under the supervision of Prof. Andrea Bistacchi, with the addition of two Erasmus+ Traineeships spanning a total of seven months, during the second and third years of the PhD (respectively three and four months). These traineeships have been both hosted at the RING team at the University of Lorraine in Nancy, France, under the guidance of Prof. Guillaume Caumon and Dr. François Bonneau. Below is a linear timeline outlining the principal tasks undertaken during the PhD. Additional collaborations are instead provided in Sect. 1.6.

With the focus on the creation of 3D structural models of portions of the northwestern Alps, the first year of PhD was dedicated to exploring the potential of various commercial and open-source technologies that could be tailored to the Alpine metamorphic tectonic setting, for both large and small-scale applications. For this, I conducted in-depths investigations into commercial software Move and SKUA/GOCAD and, simultaneously, contributed to the development of an open-source application (PZero; https://github.com/andrea-bistacchi/PZero) that supports libraries for 3D visualisation, interaction, and modelling of three-dimensional geometries, as it will be detailed in Sect. 1.4.

PZero emerged in the spring of 2020 as a collaborative effort between Prof. Andrea Bistacchi from the University of Milan-Bicocca and the Pro Iter Tunnelling & Geotechnical Department, a private Milan-based company (https://www.proiter.it/), which provided initial funding for the open-source project. I became involved with the project in December 2020, at a stage when the platform had already established key components, including a functional Graphical User Interface (GUI) and a robust data management system. Following a year of development within a private Git Bitbucket (https://bitbucket.org/product/) repository, the application transitioned to an open-source project, becoming publicly accessible in December 2021.

My collaboration with Pro Iter yielded a published paper authored by Luca Soldo (et al., 2022), one of the project's co-leaders. Furthermore, within the framework of this collaboration, a series of training sessions, totalling 16 hours, were conducted to facilitate knowledge transfer from the developers of the code to the employees of Pro Iter. My involvement in this modelling platform development project provided valuable hands-on experience and a deeper understanding of the 3D modelling problem, while also offering the opportunity to explore the scenario of existing open-source implicit interpolation algorithms. At the end of the first year of PhD the PZero modelling platform, while promising, was not yet mature enough for applications in the complex geological setting of the northwestern Alps, therefore shifting my focus to the commercial software packages.

During the first and second years, I moreover actively participated in and led fieldwork campaigns focused on data collection within the extents of the 3D regional models. The primary objective was to collect structural data to enhance and expand the existing database, contributing to the development of the 3D models presented in this thesis.

During the second year of my PhD, I engaged in a wide range of tasks. Firstly, I focused on the creation of the 3D regional-scale model of the northern Aosta Valley, task that has been completed in spring 2023. The modelling workflow is detailed in Chapter 2 and implemented using the commercial software Move and SKUA/GOCAD. Secondly, the first Erasmus+ traineeship took place, instrumental in exploring both implicit and explicit modelling approaches as implemented in SKUA/GOCAD. During this exchange, I delved into the detailed investigation of geological constraints, aiming to apply them to the metamorphic context of the northwestern Alps.

The beginning of the third year was dedicated to finalising the details of the regional-scale 3D model of the northern Aosta Valley and I additionally embarked on the second Erasmus+ Traineeship period lasting four months, during which I conducted further research on the application of geological constraints for small-scale modelling (Chapters 3 and 4 of the thesis). The rest of the third and last year was spent finalising the modelling and the Chapters presented in this thesis.

1.4. PZero

PZero (https://github.com/andrea-bistacchi/PZero) is an open-source 3D geological modelling platform entirely programmed in Python and leveraging various libraries. PZero can be used for standard modelling data management and visualisation, as well for both explicit and implicit interpolations.

PZero utilises several important libraries, including:

- PyQt (https://www.qt.io/qt-for-python) for the user-friendly GUI.
- VTK, (https://vtk.org/) which provides 2D and 3D visualisation tools and basic modelling solutions for various objects (points, lines, surfaces, volumes, and images) and supports common tessellation methods for creating and modifying 3D geometries.
- Pandas (https://pandas.pydata.org/) dataframes are implemented for collecting and managing PZero's objects and projects.
- Numpy (https://numpy.org/) for mathematical processing.
- Matplotlib (https://matplotlib.org/) as additional 2D visualisation tool.
- Shapely (https://shapely.readthedocs.io/en/stable/), which offers functions for managing two-dimensional objects.
- LoopStructural (https://github.com/Loop3D/LoopStructural; Grose et al., 2021b), for the implicit interpolation algorithms.

Designed to facilitate a traditional modelling workflow that incorporates geological data collected from fieldwork, boreholes and cross-sections, PZero includes a variety of input/output functions that enable data exchange and interoperability with other software packages. Some of the supported file formats managed by PZero are shapefiles, commonly used in Geographical Information Systems (GIS), Gocad Ascii files, which enable communication with SKUA/GOCAD, and text files.

I was involved in enhancing various functions within PZero, focusing on the GUI and the creation and management of 2D and 3D geometries. This required working with libraries such as VTK, Shapely, Pandas, and Numpy to implement these tools effectively. Additionally, I had the opportunity to explore the implicit modelling algorithms implemented in LoopStructural (Grose et al., 2021b) and adapt PZero's instances to be integrated into these algorithms.

1.5. Chapters overview

The main body of the thesis comprises three independent Chapters, each dedicated to modelling different subareas through the integration of implicit modelling techniques and high-resolution structural mapping. Since these Chapters are in the format of standalone contributions and follow the structure of traditional scientific articles, repetitions may occur especially regarding the description of the modelling algorithm, which is DSI (Frank et al., 2007; Caumon et al., 2013) throughout the thesis and as

implemented in SKUA/GOCAD and in the RING Toolkit plugin (Frank et al., 2007; Caumon et al., 2013). This thesis presents applications of these already fully implemented algorithms to the Pennine Alps. SKUA/GOCAD's Macro tools have however been employed to automate the uncertainty algorithms presented in Chapters 3 and 4.

The new structural map of the northern Aosta Valley (presented in Chapter 2) is used across the thesis as input dataset. The locations of the three study areas are indicated in Fig. 1.1, while the contributions of each Chapter to the overarching objective of the thesis are schematically represented in Fig. 1.2. This concentric diagram illustrates the modelling process, starting from data collection in the innermost circle, moving through different geological observations, to the integration of constraints in the modelling software and ultimately leading to the 3D outcomes.

Part of the work presented in this thesis has been presented at a total of 10 international conferences, spread during the three years of PhD.

1.5.1.   Chapter 2. Regional-scale 3D modelling in metamorphic belts: an implicit model-driven workflow applied in the Pennine Alps

Chapter 2 introduces the regional-scale 3D structural model of the bordering region between Italy and Switzerland spanning from Mont Blanc to Monte Rosa and covering an area of approximately 1,500 km^2. Within the Italian context, the model's scale is deemed regional. The workflow described in the Chapter employs a knowledge-driven modelling approach, relying on a surface input database consisting of a newly produced 1:75,000 structural map and structural datasets. The process begins with an orientation statistics analysis aimed at organising the structural database and defining structurally homogeneous domains. This is followed by structural interpretations, conducted on a network of vertical cross-sections (the conceptual model of Fig. 1.2). Subsequently, implicit interpolation is performed, using both the structural map and the structural interpretations as constraining data. The Chapter delves into the challenges of creating a regional-scale 3D structural model in orogenic settings characterised by multi-scale, disharmonic and isoclinal folding, shear zones organised in hierarchical relationships, and network of normal faults, and discusses how the 3D modelling impacts the interpretation of the area. The boundary representation of the 3D structural model is publicly available and linked in the Chapter.

This Chapter has been published in the *Journal of Structural Geology* (Arienti et al., 2024). The version of this work presented in Chapter 2 has been formatted and adapted to fit the format of this thesis.

The results of this paper have also been presented at the EGU General Assembly 2023 (Arienti et al., 2023a) and at the RING Meeting 2023 (Arienti et al., 2023b).

From fieldwork to 3D structural model
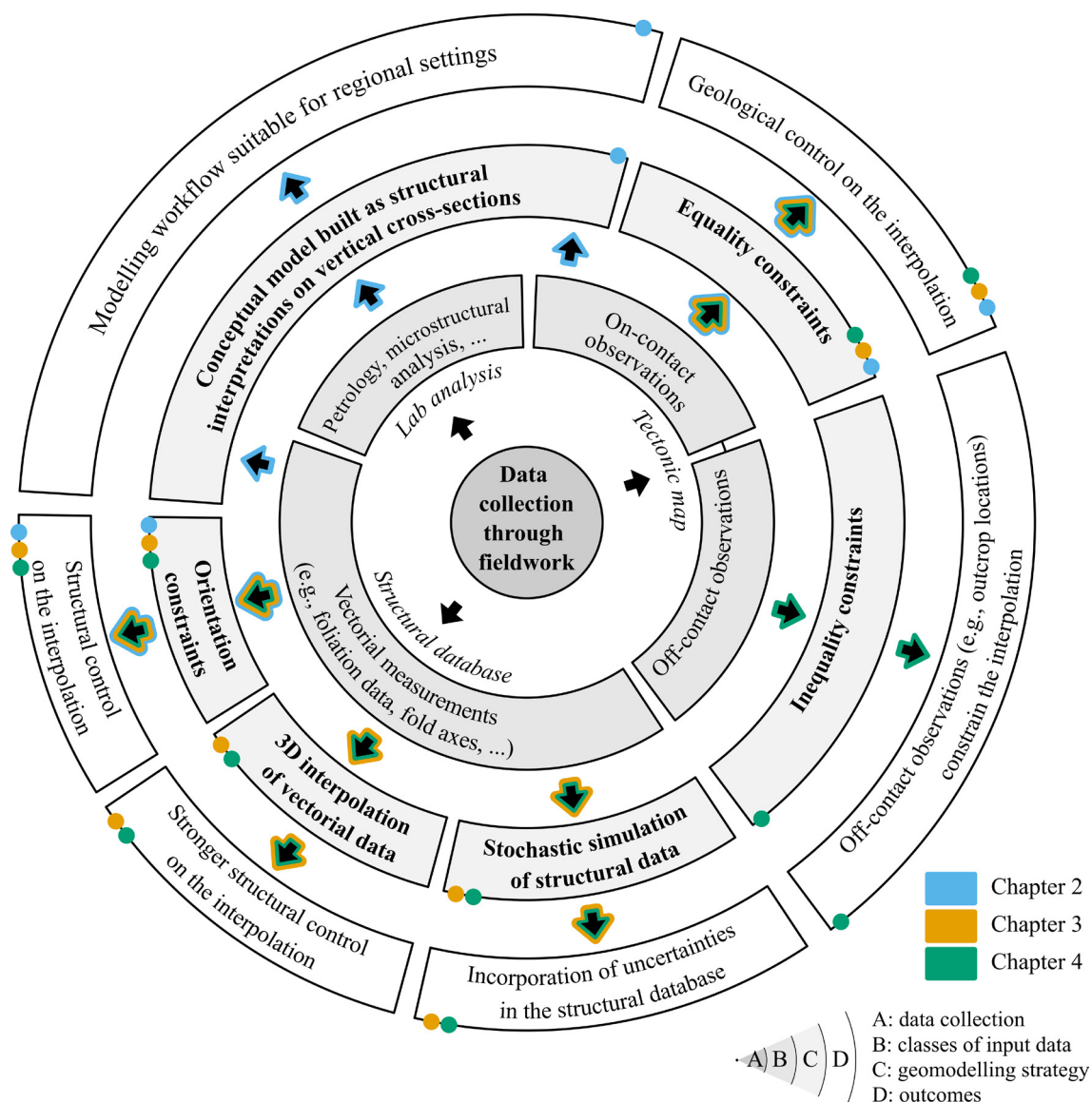
Figure 1.2. Overarching theme of the thesis.

1.5.2. Chapter 3. 3D structural implicit modelling of folded metamorphic units at Lago di Cignana with uncertainty assessment

Chapter 3 is dedicated to the 3D structural modelling of the tectonic contacts exposed in the vicinity of Cignana Lake (Lago di Cignana), covering an area of approximately 9 km^2 (Fig. 1.1) and falling within the boundaries of the regional-scale model presented in Chapter 2. The modelling, aimed at representing tectonic contacts with hierarchical relationships and open to isoclinal folds, all crosscut by normal brittle faults, leverages the surface structural map and implicit strategies without the need for interpretations

on vertical cross-sections. Modelling strategies include leveraging position and orientation constraints (equality and orientation constraints in Fig. 1.2), three-dimensional interpolation of fold axes (3D interpolation of vectorial data in Fig. 1.2) and densification of mapped boundaries constraints by projection along the interpolated fold axes. Additionally, the Chapter focuses on isoclinal recumbent folds exposed in the area and, after an orientation study aimed at characterising the vectorial sample of fold axes and its spherical distribution, produces suites of stochastically simulated fold axes that mirror the same distribution (stochastic simulation of structural data in Fig. 1.2). In this case study, I propose the cases for both von Mises-Fisher (Fisher, 1953) and Kent (or Fisher-Bingham; Kent, 1982) distributions. Suites of plausible alternative models are consequently generated, which reveal partial rotations of sections of the isoclinal recumbent folds and exhibit higher uncertainty values localised at the fold hinges.

The corresponding Chapter is scheduled for submission to a high-ranking scientific journal in the near future. Meanwhile, partial results from the paper have been presented at the RING meeting 2023 (Arienti et al., 2023b).

1.5.3.   Chapter 4. 3D implicit structural modelling leveraging inequality and structural constraints: a case study from the Pennine Alps

Chapter 4 centres on the tectonic contacts exposed along the Roisetta-Tournalin ridge, a north-south trending mountain range with peaks above 3,000 meters a.s.l. located in the northern Aosta Valley, within the area of the regional model (Fig. 1.1). The modelling workflow capitalises on a dense structural database of original and legacy metamorphic schistosity measurements, and on the 1:10,000 map of the outcrop locations. Modelling strategies include integration of off-contact position observations (inequality constraints in Fig. 1.2) in addition to on-contact observations and structural measurements (equality and orientation constraints in Fig. 1.2), and 3D interpolation of the normal directions to the foliation data (3D interpolation of vectorial data in Fig. 1.2). The workflow additionally employs stochastic simulations of structural data to address uncertainties identified in the foliation database (stochastic simulation of structural data in Fig. 1.2), which is analysed and simulated following a procedure similar to the one presented in Chapter 3, with the addition of a goodness-of-fit test for von Mises-Fisher distribution based on the work of Fisher and Best (1984).

The corresponding Chapter is scheduled for submission to a high-ranking scientific journal in the near future.

1.6.   Additional contributions

Throughout the duration of this PhD, I actively participated in additional projects, of which I provide a concise overview, emphasising the insights and skills gained during these experiences.

Within the framework of the Reservaqua project, which provided the motivation for modelling portions of the northwestern Alps at the Italian-Swiss border, I had the opportunity to collaborate with other researchers who were involved in various aspects of this broader European-Interreg project. Firstly, I collaborated with Professor Giorgio Vittorio Dal Piaz (Academy of Sciences of Turin, Italy) and other experts from LTS company (Land Technology and Services; http://www.ltsht.com/) in Treviso, Italy, including Bruno Monopoli and Giovanni Dal Piaz. These experts created the new structural map of the northern Aosta Valley, which is used as the input surface database in this thesis. This dataset was sourced from 1:10,000 geological maps and structural data collected over the last thirty years and published at the Geoportale of the Regione Autonoma Valle d'Aosta (https://geoportale.regione.vda.it/), and upscaled to 1:75,000. The structural map will be detailed in a future publication (Dal Piaz et al., in preparation) focused on the geological and tectonic setting of the region.

I additionally participated in a study on the characterisation of the fracturing state of metamorphic rocks in the area, contributing to the collection of Digital Outcrop Models (DOMs; e.g., Bellian et al., 2005) employing photogrammetric methodologies using both terrestrial and Unmanned Aerial Vehicles (UAV). I participated in organising photogrammetric surveys with a focus on the generation of DOMs that offer uniform and void-free coverage with high resolution, achieving pixel sizes of about 1 cm down to just a few millimetres per pixel. The data collected were successively analysed to extract fracturing parameters through point cloud analysis and statistical methods, utilising techniques detailed in Bistacchi et al. (2022). This aspect of my work has already been presented at the EGU General Assembly 2023 (Benedetti et al., 2023; Casiraghi et al., 2023).

Finally, I also had the opportunity to collaborate to the supervision of a master's student thesis fieldwork, during which samples of pseudotachylytes (structures formed by high-stress seismic fault slip and the frictional melt of host rock; Sibson, 1975) were collected for subsequent isotope dating analysis. The post-metamorphic brittle faults that generated the pseudotachylytes in question are located within the boundaries of the area of the 3D regional-scale model. Subsequently, step-heating $^{40}Ar/^{39}Ar$ analyses were conducted to determine the absolute age of the fault slip events. These results have been presented at the EGU General Assembly 2023 (Lugoboni et al., 2023) and will serve as the primary outcome of an independent scientific research publication (Lugoboni et al., in preparation).

1.7. References

Arienti, G., Bistacchi, A., Caumon, G., Bonneau, F., Dal Piaz, Giorgio V, Dal Piaz, Giovanni, Monopoli, B., Bertolo, D., 2023a. Three-dimensional modelling of a complex metamorphic nappe stack from field survey only: the case study of the Aosta Valley (Italian NW-Alps). EGU General Assembly 2023. Vienna, Austria, EGU23-8856. https://doi.org/https://doi.org/10.5194/egusphere-egu23-8856

Arienti, G., Bistacchi, A., Caumon, G., Dal Piaz, G., Monopoli, B., 2023b. 3D geomodelling in polydeformed metamorphic mountain belts: an implicit geomodel-driven workflow applied to large scale modelling of

the Northern Aosta Valley (North-Western Alps, Italy). RING Meeting Proceedings 2023. ASGA, Nancy, France.

Arienti, G., Bistacchi, A., Caumon, G., Dal Piaz, G., Monopoli, B., Bertolo, D., 2024. Regional-scale 3D modelling in metamorphic belts: An implicit model-driven workflow applied in the Pennine Alps. Journal of Structural Geology 180, 105045. https://doi.org/10.1016/j.jsg.2023.105045

Ballèvre, M., Merle, O., 1993. The Combin Fault: compressional reactivation of a Late Cretaceous-Early Tertiary detachment fault in the Western Alps. Schweizerische Mineralogische Und Petrographische Mitteilungen 73, 205–227. https://doi.org/https://doi.org/10/gfsjrz

Bellian, J.A., Kerans, C., Jennette, D.C., 2005. Digital Outcrop Models: Applications of Terrestrial Scanning Lidar Technology in Stratigraphic Modeling. Journal of Sedimentary Research 75, 166–176. https://doi.org/10.2110/jsr.2005.013

Benedetti, G., Casiraghi, S., Bistacchi, A., Arienti, G., Bertolo, D., 2023. Point cloud analysis and segmentation procedures in the PZero software. EGU General Assembly 2023. Vienna, Austria, EGU23-9549. https://doi.org/https://doi.org/10.5194/egusphere-egu23-9549

Bigi, G., Castellarin, A., Coli, M., Dal Piaz, G. V, Sartori, R., Scandone, P., Vai, G.B., 1990. Structural Model of Italy 1:500.000, Sheet 1, C.N.R. Progetto Geodinamica, SELCA Firenze. SELCA, Firenze.

Bistacchi, A., Massironi, M., Dal Piaz, Giorgio V, Dal Piaz, Giovanni, Monopoli, B., Schiavo, A., Toffolon, G., 2008. 3D fold and fault reconstruction with an uncertainty model: An example from an Alpine tunnel case study. Computers and Geosciences 34, 351–372. https://doi.org/10.1016/j.cageo.2007.04.002

Bistacchi, A., Massironi, M., Viseur, S., 2022. 3D Digital Geological Models: From Terrestrial Outcrops to Planetary Surfaces. 3D Digital Geological Models. Wiley, 1–9. https://doi.org/10.1002/9781119313922.ch1

Calcagno, P., Chilès, J.P., Courrioux, G., Guillen, A., 2008. Geological modelling from field data and geological knowledge. Part I. Modelling method coupling 3D potential-field interpolation and geological rules. Physics of the Earth and Planetary Interiors 171, 147–157. https://doi.org/10.1016/j.pepi.2008.06.013

Carr, J.C., Beatson, R.K., Cherrie, J.B., Mitchell, T.J., Fright, W.R., McCallum, B.C., Evans, T.R., 2001. Reconstruction and representation of 3D objects with radial basis functions. Proceedings of the 28th Annual Conference on Computer Graphics and Interactive Techniques. Association for Computing Machinery, 67–76. https://doi.org/10.1145/383259.383266

Casiraghi, S., Bistacchi, A., Agliardi, F., Arienti, G., Monopoli, B., Dal Piaz, G., Bertolo, D., 2023. Structural interpretation of Digital Outcrop Models on point clouds using a semi-automatic workflow: case studies on fractured metamorphic rocks (Aosta Valley, Italy). EGU General Assembly 2023. Vienna, Austria, EGU23-9632. https://doi.org/https://doi.org/10.5194/egusphere-egu23-9632

Caumon, G., Collon-Drouaillet, P., Le Carlier de Veslud, C., Viseur, S., Sausse, J., 2009. Surface-Based 3D Modeling of Geological Structures. Mathematical Geosciences 41, 927–945. https://doi.org/10.1007/s11004-009-9244-2

Caumon, G., Gray, G., Antoine, C., Titeux, M.O., 2013. Three-dimensional implicit stratigraphic model building from remote sensing data on tetrahedral meshes: Theory and application to a regional model of la Popa Basin, NE Mexico. IEEE Transactions on Geoscience and Remote Sensing 51, 1613–1621. https://doi.org/10.1109/TGRS.2012.2207727

Caumon, G., L. Tertois, A., Zhang, L., 2007. Elements for Stochastic Structural Perturbation of Stratigraphic Models. EAGE Conference on Petroleum Geostatistics. European Association of Geoscientists & Engineers. https://doi.org/10.3997/2214-4609.201403041

Caumon, G., Lepage, F., Sword, C.H., Mallet, J.L., 2004. Building and editing a sealed geological model. Mathematical Geology 36, 405–424. https://doi.org/10.1023/B:MATG.0000029297.18098.8a

Cherpeau, N., Caumon, G., 2015. Stochastic structural modelling in sparse data situations. Petroleum Geoscience 21, 233–247. https://doi.org/10.1144/petgeo2013-030

Chilès, J.P., Aug, C., Guillen, A., Lees, T., 2004. Modelling the geometry of geological units and its uncertainty in 3D from structural data: the potential-field method. Proceedings of International Symposium on Orebody Modelling and Strategic Mine Planning. Perth, 313–320.

Dal Piaz, G.V., Bistacchi, A., Monopoli, B., Dal Piaz, G., Arienti, G., n.d. Structural map of the Northern Aosta Valley.

Dal Piaz, G. V, Argentieri, A., 2021. 150 years of plans, geological survey and drilling for the Fréjus to Mont Blanc tunnels across the Alpine chain: an historical review. Italian Journal of Geosciences 140, 169–204. https://doi.org/10.3301/IJG.2020.29

Dal Piaz, G. V, Bistacchi, A., Massironi, M., 2003. Geological outline of the Alps. Episodes Journal of International Geoscience 26, 175–180. https://doi.org/10.18814/EPIIUGS/2003/V26I3/004

de Kemp, E.A., Schetselaar, E.M., Hillier, M.J., Lydon, J.W., Ransom, P.W., 2016. Assessing the workflow for regional-scale 3D geologic modeling: An example from the Sullivan time horizon, Purcell Anticlinorium East Kootenay region, southeastern British Columbia. Interpretation 4, SM33–SM50. https://doi.org/10.1190/INT-2015-0191.1

De La Varga, M., Schaaf, A., Wellmann, F., 2019. GemPy 1.0: Open-source stochastic geological modeling and inversion. Geoscientific Model Development 12, 1–32. https://doi.org/10.5194/gmd-12-1-2019

Dufrénoy, M.M., de Beaumont, E., 1841. Tableau d'assemblage des six feuilles de la Carte géologique de la France.

Fisher, N.I., Best, D.J., 1984. Goodness-of-fit tests for Fisher's distribution on the sphere. Australian Journal of Statistics 26, 142–150. https://doi.org/10.1111/j.1467-842X.1984.tb01228.x

Fisher, R.A., 1953. Dispersion on a sphere. Proceedings of the Royal Society of London 217, 295–305.

Frank, T., Tertois, A.L., Mallet, J.L., 2007. 3D-reconstruction of complex geological interfaces from irregularly distributed and noisy point data. Computers and Geosciences 33, 932–943. https://doi.org/10.1016/j.cageo.2006.11.014

Godefroy, G., Caumon, G., Ford, M., Laurent, G., Jackson, C.A.-L., 2018. A parametric fault displacement model to introduce kinematic control into modeling faults from sparse data. Interpretation 6, B1–B13. https://doi.org/10.1190/INT-2017-0059.1

Grose, L., Ailleres, L., Caumon, G., Jessell, M.W., Armit, R., 2021a. Modelling of faults in LoopStructural 1.0. Geoscientific Model Development 14, 6197–6213. https://doi.org/https://doi.org/10.5194/gmd-14-6197-2021

Grose, L., Ailleres, L., Laurent, G., Armit, R., Jessell, M., 2019. Inversion of geological knowledge for fold geometry. Journal of Structural Geology 119, 1–14. https://doi.org/10.1016/j.jsg.2018.11.010

Grose, L., Ailleres, L., Laurent, G., Jessell, M., 2021b. LoopStructural 1.0: Time-aware geological modelling. Geoscientific Model Development 14, 3915–3937. https://doi.org/10.5194/gmd-14-3915-2021

Grose, L., Laurent, G., Aillères, L., Armit, R., Jessell, M., Caumon, G., 2017. Structural data constraints for implicit modeling of folds. Journal of Structural Geology 104, 80–92. https://doi.org/10.1016/j.jsg.2017.09.013

Hillier, M., de Kemp, E., Schetselaar, E., 2013. 3D form line construction by structural field interpolation (SFI) of geologic strike and dip observations. Journal of Structural Geology 51, 167–179. https://doi.org/https://doi.org/10.1016/j.jsg.2013.01.012

Hillier, M.J., Schetselaar, E.M., de Kemp, E.A., Perron, G., 2014. Three-Dimensional Modelling of Geological Surfaces Using Generalized Interpolation with Radial Basis Functions. Mathematical Geosciences 46, 931–953. https://doi.org/10.1007/s11004-014-9540-3

Houlding, S.W., 1994. The Geological Characterization Process. 3D Geoscience Modeling. Springer Berlin Heidelberg, Berlin, Heidelberg, 7–26. https://doi.org/10.1007/978-3-642-79012-6_2

Irakarama, M., Laurent, G., Renaudeau, J., Caumon, G., 2018. Finite Difference Implicit Modeling of Geological Structures. 80th EAGE Conference and Exhibition 2018: Opportunities Presented by the Energy Transition. European Association of Geoscientists and Engineers, EAGE, 1–5. https://doi.org/10.3997/2214-4609.201800794

Irakarama, M., Thierry-Coudon, M., Zakari, M., Caumon, G., 2022. Finite Element Implicit 3D Subsurface Structural Modeling. Computer-Aided Design 149, 103267. https://doi.org/10.1016/j.cad.2022.103267

Jessell, M.W., Pakyuz-Charrier, E., Lindsay, M.D., Giraud, J., de Kemp, E.A., 2018. Assessing and Mitigating Uncertainty in Three-Dimensional Geologic Models in Contrasting Geologic Scenarios. Society of Economic Geologists 21. https://doi.org/10.5382/SP.21.04

Kent, J.T., 1982. The Fisher-Bingham Distribution on the Sphere. Journal of the Royal Statistical Society 44, 71–80.

Lajaunie, C., Courrioux, G., Manuel, L., 1997. Foliation fields and 3D cartography in geology: Principles of a method based on potential interpolation. Mathematical Geology 29, 571–584. https://doi.org/10.1007/BF02775087

Laurent, G., Ailleres, L., Grose, L., Caumon, G., Jessell, M., Armit, R., 2016. Implicit modeling of folds and overprinting deformation. Earth and Planetary Science Letters 456, 26–38. https://doi.org/10.1016/j.epsl.2016.09.040

Laurent, G., Caumon, G., Bouziat, A., Jessell, M., 2013. A parametric method to model 3D displacements around faults with volumetric vector fields. Tectonophysics 590, 83–93. https://doi.org/10.1016/j.tecto.2013.01.015

Lindsay, M.D., Aillères, L., Jessell, M.W., de Kemp, E.A., Betts, P.G., 2012. Locating and quantifying geological uncertainty in three-dimensional models: Analysis of the Gippsland Basin, southeastern Australia. Tectonophysics 546–547, 10–27. https://doi.org/10.1016/j.tecto.2012.04.007

Lugoboni, Z., Arienti, G., Barberini, V., Bistacchi, A., Cannella, C., Caprarulo, S., Villa, I.M., 2023. 40Ar/39Ar dating of pseudotachylytes: a case study on post-metamorphic brittle fault in the NW Alps. EGU General Assembly 2023. Vienna, Austria, EGU23-7367. https://doi.org/https://doi.org/10.5194/egusphere-egu23-7367

Lugoboni, Z., Bistacchi, A., Villa, I.M., Monopoli, B., Arienti, G., n.d. 40Ar/39Ar dating of post-metamorphic brittle faults in the NW Alps.

Manzotti, P., Zucali, M., Ballèvre, M., Robyr, M., Engi, M., 2014. Geometry and kinematics of the Roisan-Cignana Shear Zone, and the orogenic evolution of the Dent Blanche Tectonic System (Western Alps). Swiss Journal of Geosciences 107, 23–47. https://doi.org/10.1007/s00015-014-0157-9

Maxelon, M., Mancktelow, N.S., 2005. Three-dimensional geometry and tectonostratigraphy of the Pennine zone, Central Alps, Switzerland and Northern Italy. Earth-Science Reviews 71, 171–227.

https://doi.org/10.1016/j.earscirev.2005.01.003

Maxelon, M., Renard, P., Courrioux, G., Brändli, M., Mancktelow, N., 2009. A workflow to facilitate three-dimensional geometrical modelling of complex poly-deformed geological units. Computers & Geosciences 35, 644–658. https://doi.org/10.1016/j.cageo.2008.06.005

Perrouty, S., Lindsay, M.D., Jessell, M.W., Aillères, L., Martin, R., Bourassa, Y., 2014. 3D modeling of the Ashanti Belt, southwest Ghana: Evidence for a litho-stratigraphic control on gold occurrences within the Birimian Sefwi Group. Ore Geology Reviews 63, 252–264. https://doi.org/10.1016/j.oregeorev.2014.05.011

Philippon, M., de Veslud, C.L.C., Gueydan, F., Brun, J.P., Caumon, G., 2015. 3D geometrical modelling of post-foliation deformations in metamorphic terrains (Syros, Cyclades, Greece). Journal of Structural Geology 78, 134–148. https://doi.org/10.1016/j.jsg.2015.07.002

Pirot, G., Joshi, R., Giraud, J., Lindsay, M.D., Jessell, M.W., 2022. loopUI-0.1: indicators to support needs and practices in 3D geological modelling uncertainty quantification. Geoscientific Model Development 15, 4689–4708. https://doi.org/10.5194/gmd-15-4689-2022

Reddy, S.M., Wheeler, J., Butler, R.W.H., Cliff, R.A., Freeman, S., Inger, S., Pickles, C., Kelley, S.P., 2003. Kinematic reworking and exhumation within the convergent Alpine Orogen. Tectonophysics 365, 77–102. https://doi.org/10.1016/S0040-1951(03)00017-9

Renaudeau, J., Malvesin, E., Maerten, F., Caumon, G., 2019. Implicit Structural Modeling by Minimization of the Bending Energy with Moving Least Squares Functions. Mathematical Geosciences 51, 693–724. https://doi.org/10.1007/s11004-019-09789-6

Schmid, S.M., Fügenschuh, B., Kissling, E., Schuster, R., 2004. Tectonic map and overall architecture of the Alpine orogen. Eclogae Geologicae Helvetiae 97, 93–117. https://doi.org/10.1007/s00015-004-1113-x

Schneeberger, R., de La Varga, M., Egli, D., Berger, A., Kober, F., Wellmann, F., Herwegh, M., 2017. Methods and uncertainty estimations of 3-D structural modelling in crystalline rocks: a case study. Solid Earth 8, 987–1002. https://doi.org/10.5194/se-8-987-2017

Sibson, R.H., 1975. Generation of Pseudotachylyte by Ancient Seismic Faulting. Geophysical Journal International 43, 775–794. https://doi.org/10.1111/j.1365-246X.1975.tb06195.x

Sides, E.J., 1997. Geological modelling of mineral deposits for prediction in mining. Geologische Rundschau 86, 342–353. https://doi.org/https://doi.org/10.1007/s005310050145

Soldo, L., Arienti, G., Bistacchi, A., Mezzanzanica, M., Regondi, L., Pizzarotti, E.M., 2022. Modellazione Geologica digitale e sua integrazione nelle moderne metodologie di progetto di opere infrastrutturali - Digital Geological Modelling within the modern infrastructure design methodologies. Gallerie e Grandi Opere Sotterranee 142, 27–40.

Thornton, J.M., Mariethoz, G., Brunner, P., 2018. A 3D geological model of a structurally complex alpine region as a basis for interdisciplinary research. Scientific Data 5, 180238. https://doi.org/10.1038/sdata.2018.238

Vollgger, S.A., Cruden, A.R., Ailleres, L., Cowan, E.J., 2015. Regional dome evolution and its control on ore-grade distribution: Insights from 3D implicit modelling of the Navachab gold deposit, Namibia. Ore Geology Reviews 69, 268–284. https://doi.org/https://doi.org/10.1016/j.oregeorev.2015.02.020

Wellmann, F., Caumon, G., 2018. 3-D Structural geological models: Concepts, methods, and uncertainties. Advances in Geophysics 59, 1–121. https://doi.org/10.1016/bs.agph.2018.09.001

Wellmann, J.F., Horowitz, F.G., Schill, E., Regenauer-Lieb, K., 2010. Towards incorporating uncertainty of structural data in 3D geological inversion. Tectonophysics 490, 141–151.

https://doi.org/10.1016/j.tecto.2010.04.022

Wellmann, J.F., Lindsay, M., Poh, J., Jessell, M., 2014. Validating 3-D structural models with geological knowledge for improved uncertainty evaluations. Energy Procedia. Elsevier Ltd, 374–381. https://doi.org/10.1016/j.egypro.2014.10.391

Wellmann, J.F., Regenauer-Lieb, K., 2012. Uncertainties have a meaning: Information entropy as a quality measure for 3-D geological models. Tectonophysics 526–529, 207–216. https://doi.org/10.1016/j.tecto.2011.05.001

Wheeler, J., Butler, R.W.H., 1993. Evidence for extension in the western Alpine orogen: the contact between the oceanic Piemonte and overlying continental Sesia units. Earth and Planetary Science Letters 117, 457–474. https://doi.org/10.1016/0012-821X(93)90097-S

Zanchi, A., Francesca, S., Stefano, Z., Simone, S., Graziano, G., 2009. 3D reconstruction of complex geological bodies: Examples from the Alps. Computers and Geosciences 35, 49–69. https://doi.org/10.1016/j.cageo.2007.09.003

Regional-scale 3D modelling in metamorphic belts: an implicit model-driven workflow applied in the Pennine Alps

Gloria Arienti[1], Andrea Bistacchi[1], Guillaume Caumon[2,3],
Giovanni Dal Piaz[4], Bruno Monopoli[4], Davide Bertolo[5]

[1]Dipartimento di Scienze dell'Ambiente e della Terra, Università degli Studi di Milano-Bicocca, 20126 Italy
[2]RING, GeoRessources – ENSG, Université de Lorraine - CNRS, 54000 France
[3]Institut Universitaire de France (IUF), 75000 France
[4]LTS s.r.l., Treviso, 31020 Italy
[5]Regione Autonoma Valle d'Aosta, Struttura Attività Geologiche, 11100 Italy

Abstract

Leveraging a high resolution geological and structural dataset acquired over decades of fieldwork, we build the 3D structural model of a portion of the highly deformed core of the Alpine orogen, in the Northern Aosta Valley. The model represents tectonic contacts separating the tectono-metamorphic units outcropping along the section between Mont Blanc and Monte Rosa, and it covers an area of ca. 1500 km2. The input source data include original 1:10,000 geological surveys synthetised in a 1:75,000 tectonic map, and a dense database of structural stations. After a first orientation statistics study of the structural field database, our workflow develops through structural interpretation in vertical cross-sections that allow including in the modelling process structural drivers such as crosscutting relationships, interference patterns, kinematic constraints and fold morphology from detailed field studies. Three-dimensional interpolation on a tetrahedral mesh using the implicit Discrete Smooth Interpolator method follows, using also foliation and fold axes data as interpolation constraints. After describing the workflow and the model, we discuss the difficulties of modelling in polydeformed metamorphic complexes. In particular, we address the issue of modelling shear zones, refolded, isoclinal and/or recumbent folds and dense networks of faults, that characterise the geology of the Northern Aosta Valley.

2.1.   Introduction

Three-dimensional modelling of geological structures plays an essential role in the investigation and quantification of geological and tectonic processes in space and time. The importance of 3D modelling has been established in the past decades with applications in a variety of fields, from oil and gas (e.g.,

Kroeger et al., 2019), mining (e.g., Sides, 1997; Vollgger et al., 2015) and geothermal exploration (e.g., Milicich et al., 2018). Three-dimensional models have also been of great importance in geoengineering (e.g., Xiong et al., 2018; Soldo et al., 2022), groundwater projects (e.g., Hassen et al., 2016) and for CO_2 and gas storage studies (e.g., Kaufmann and Martin, 2009; Thanh et al., 2019). Geological modelling has moreover been used in combination with geophysical inversion for the enforcement of geological realism and to better assess subsurface uncertainty (e.g., Guillen et al., 2008; Giraud et al., 2023; Liang et al., 2023; Jessell et al., 2010; Caumon, 2010).

Methods used to model the geological structures in three-dimensional space can be categorised into two first-order classes: data-driven and model-driven approaches (Wellmann and Caumon, 2018). Data centric methods retrieve physical properties from large geophysical datasets (e.g., geophysical imaging or borehole measurements), then interpret these data as geological features of interest (Wellmann and Caumon, 2018). On the other hand, model-driven approaches (also referred to as knowledge-driven approaches) revolve around geological conceptual models built based on a priori identification of geological objects and their associated knowledge (Perrin et al., 2005).

In the broad framework of model-driven approaches, another fundamental distinction must be made between explicit and implicit representations. Explicit surface modelling consists in directly building geological interfaces as triangulated surfaces or regular 2D grids by interpolating input data, with each node of the surface characterised by its x, y, z position in 3D (Caumon et al., 2009). However, this class of methods may involve significant expert input from the interpreter (Caumon et al., 2009; Wellmann and Caumon, 2018) when it comes to complexly folded tectonic settings, unconformities and finite internal faults (i.e., faults with a finite area that have the tip line within the modelling domain), requiring considerable expert working time to reach an acceptable modelling outcome.

On the other hand, implicit surface approaches exploit the analogy between a generalised geological "time", as recorded in stratified formations, and a continuous and derivable (excepts at faults and unconformities) scalar field (Houlding, 1994). The whole 3D volume is modelled all at once, from prior information about stratigraphic units, faults and unconformities, to build a continuous scalar field from which stratigraphic surfaces can be extracted as equipotential implicit isosurfaces or level sets. From the first mathematical definitions of this approach (Lajaunie et al., 1997), many steps have been taken towards the integration of geological information into the scalar field, enhancing the mathematical constraints that guide the interpolation of structural field data in the three-dimensional volume (Frank et al., 2007; Calcagno et al., 2008; Hillier et al., 2013; Laurent, 2016) such as fold data (Hillier et al., 2014; Laurent et al., 2016; Grose et al., 2017) and faults (Laurent et al., 2013; Godefroy et al., 2018).

Furthermore, implicit interpolation methods fall into two categories: meshless and mesh-based methods. Meshless approaches use Radial Basis Function interpolators (Carr et al., 2001; Hillier et al., 2014), dual

kriging methods (Calcagno et al., 2008; De La Varga et al., 2019) or point-based moving least squares basis functions (Renaudeau et al., 2019). They benefit from a mathematical formulation that does not require a mesh, but their implementation results in a dense system of equations of size $\sim N^2$, where N is the number of data (or interpolation) points, that may become unmanageable even by modern workstations when N is large (in medium-sized models it is common to have $N > 10{,}000$). On the other hand, mesh-based interpolation algorithms work on tetrahedral (Frank et al., 2007; Caumon et al., 2013; Irakarama et al., 2022) or Cartesian (Irakarama et al., 2018) meshes, whose computational complexity and memory weight generally scale linearly with the mesh size, hence can be easily tuned by changing the mesh resolution.

Most of the methods mentioned above have been developed to specifically address the representation of gently deformed sedimentary sequences in tectonic settings on which the attention of the oil-and-gas exploration is focused (e.g., Mallet, 2014). Consequently, dealing with complex structures in basement and cover metamorphic units employing implicit methods remains a major challenge. Geometries such as polyphasic isoclinal and/or recumbent folds, major thrusts and stacks of tectono-metamorphic units, and dense networks of faults concur to the substantial complexity of the geology of metamorphic units in the core of mountain belts, which are a frontier for ambitious 3D structural modelling projects (de Kemp, 2000; Maxelon and Mancktelow, 2005; Bistacchi et al., 2008; Philippon et al., 2015; Thornton et al., 2018).

To aid the modelling of complex folded geometries, methodologies have been proposed to integrate structural principles (Maxelon et al., 2009; Hillier et al., 2014; Laurent et al., 2016; Grose et al., 2017; Pizzella et al., 2022). However, the challenge extends beyond the representation of complex geometries, as the modelling process also involves the upscaling of the often too detailed geological database to align with the model's scale. For this, upscaling strategies for structural data have been proposed (e.g., Carmichael and Ailleres, 2016), overall contributing to the ongoing research for automatic modelling workflows that, if achieved, would enhance both the reproducibility and efficiency of the modelling process. While such workflows have been proposed for less intricate tectonic settings (Jessell et al., 2021), this remains a topic of active research.

In this paper we use the geomodelling approach to build a 3D regional-scale structural model of the northern Aosta Valley (ca. 1,500 km[2] of extension in the Italian northwestern Alps), also including a narrow portion of the Swiss territory for the sake of a continuous interpretation. In the framework of the Interreg RESERVAQUA project, the creation of the 3D model is motivated by the development of a programme for sustainable water resource management in relation to climate change. The mountain regions bounding the Alpine belt are heavily dependent on water stored in the mountains in various forms to meet their hydric demand. Information on the distribution of water reserves is therefore crucial,

and it is why with our 3D structural model we fill the absence of a three-dimensional representation of this portion of the northwestern Alps. Not less important are the implications on regional tectonic studies of the area, whose interpretation is enhanced and validated by the three-dimensional reasoning allowed by the 3D modelling.

Our model covers the area between the massifs of Mont Blanc (Monte Bianco, 4,808 m a.s.l.) and Monte Rosa (4,634 m a.s.l.) in the Pennine Alps, where a vertical drop of ca. 4,300 m is observed between the highest peaks and the valley floors. This area includes other iconic mountains of the Alps, such as the Grand Combin (4,314 m a.s.l.) and the Monte Cervino (Matterhorn, 4,478 m a.s.l.), deep glacial valleys, high passes such as the Gran San Bernardo (Grand Saint-Bernard, 2,473 m a.s.l.) and a complete sample of tectono-metamorphic units of the core of this collisional mountain belt.

The input dataset is represented by the original 1:10.000 geological maps and related structural data stored within the Geoportale of the Regione Autonoma Valle d'Aosta (https://geoportale.regione.vda.it/), surveyed in the last thirty years for the CARG Project and the Regional Geological Map, mainly by Giorgio V. Dal Piaz (coordinator), Giovanni Dal Piaz, Bruno Monopoli, Alessio Schiavo Andrea Bistacchi, Matteo Massironi and Giovanni Toffolon, with the stratigraphic collaboration of Leonsevero Passeri and Gloria Ciarapica (Dal Piaz et al., 2010, 2016; Perello et al., 2011; Polino et al., 2015). Data are generalised in the tectonic map of Fig. 2.1.

In the following sections we will summarise the geological and tectonic complexity of the northern Aosta Valley. Successively, we will describe the steps of our workflow and then the resulting 3D structural model.

2.2. A summary of the geology of the northern Aosta Valley

The Alps are a European collisional belt that resulted from the Cretaceous to Present convergence of the Adria continental upper plate and of a subducting lower plate that included a Mesozoic ocean and the continental European lithosphere (Dal Piaz et al., 2003, and references therein). The Penninic-Austroalpine nappe stack, outcropping in the northwestern sector of the Alps, along our study transect, resulted from oceanic subduction, continental collisional and exhumation. It is composed of highly deformed ophiolitic units (Piedmont Zone, remnants of the Mesozoic Tethys Ocean), and continental units from both the European passive margin (Penninic system) and the Adriatic active margin and related extensional allochthons (Austroalpine system). More external units are the Europe-verging Helvetic and Ultrahelvetic basement slices and decollement cover nappes (marginally represented in our study area) and the Adria-verging southern Alps (not included in our transect).

The complex structural geology and petrography of units exposed in the Aosta Valley results from superposed Alpine and in some cases Pre-Alpine events. Several relics of Pre-Alpine metamorphic fabrics are still recognised at different scale in basement and pre-Mesozoic rocks. For instance, structures referred to the opening of the Mesozoic ocean are observed in the Piccolo San Bernardo region (Beltrando et al., 2012) and magmatic layering structures are preserved in some Permian gabbroic bodies (Manzotti et al., 2017), while pre-Alpine metamorphic fabrics are mapped from the micro- to the mega-scale in the Valpelline unit of the Dent Blanche Nappe (Gardien et al., 1994). However, more often the present-day structure of the nappe stack reflects Alpine thrusting during lithospheric subduction and continental collision, subsequent extensional deformation related to exhumation of units stacked in the collisional wedge, later uplift and erosion (Dal Piaz et al., 2003).

Detailed structural analysis in the last decades reveals that tectonic boundaries traditionally interpreted as "simple" folded thrusts (e.g., Escher et al., 1988), are actually the complex result of both contractional and extensional tectonic phases (e.g., Ballèvre and Merle, 1993; Wheeler and Butler, 1993; Reddy et al., 2003; Manzotti et al., 2014b). For this reason, most boundaries between tectono-metamorphic units (i.e., discrete crustal elements defined by a peculiar association of lithology, metamorphic imprint and deformative evolution) are not to be named simply as "thrusts" but are more generally referred to as tectonic boundaries (Dal Piaz et al., 2010).

These tectonic boundaries, in their last evolution, represent the most continuous geological discontinuities in the area, while smaller scale lithological contacts are strongly stretched and folded and more discontinuous. The tectonic boundaries are also the best markers between the contrasting metamorphic or chronologic domains, and to evidence the effect of two sets of post-metamorphic brittle normal faults that affect the area at all scales (Bistacchi and Massironi, 2000; Bistacchi et al., 2000, 2001; Sue et al., 2007).

In the following sections we introduce the tectonic architecture of the studied transect. We refer to the tectonic map (Fig. 2.1) and to the tectono-metamorphic legend (Fig. 2.2) to unfold the relative positions between tectonic structures. For more detailed descriptions on the tectonic and metamorphic evolution of the introduced units, we refer the reader to the cited literature.
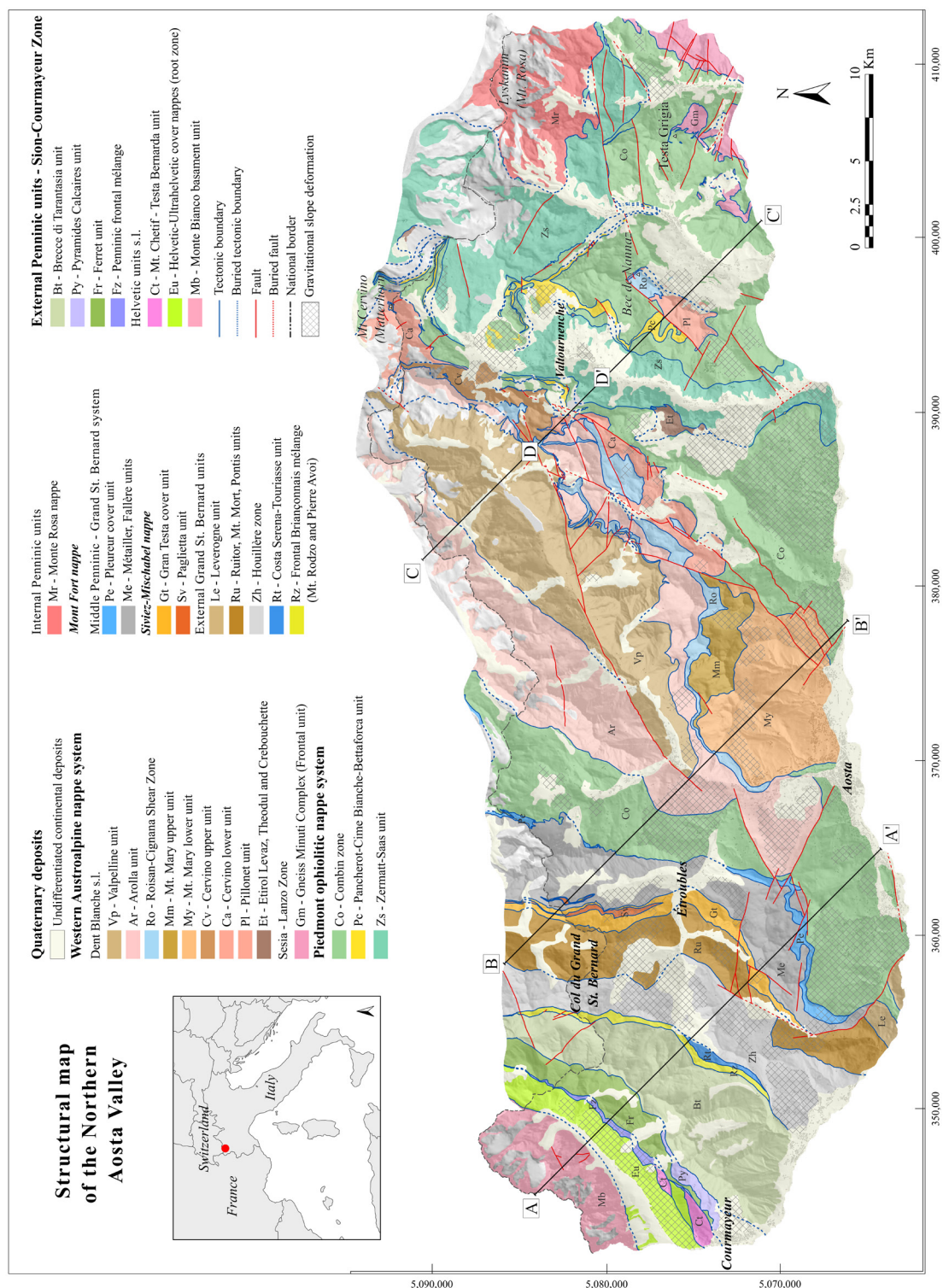
Figure 2.1. Tectonic map of the northern Aosta Valley, from Geoportale Regione Valle d'Aosta (https://geoportale.regione.vda.it/). The coordinates at the edge of the maps are provided as WGS 1984, UTM Zone 32.

2.2.1. The western Austroalpine nappe system

The structurally highest tectonic element of the northern Aosta Valley is represented by the collisional Adriatic nappe stack, showing eclogitic or blueschist peak metamorphism and greenschist facies regional overprint (Frey et al., 1974; Compagnoni et al., 1977; Compagnoni, 2003). The highest structural position is occupied by the Adriatic Dent Blanche-Sesia Lanzo system (Argand, 1909, 1911; Manzotti et al., 2014b, 2014a). The Dent Blanche system, usually referred to as Argand's Dent Blanche nappe s.l., comprises two different basement sub-nappes, the capping Dent Blanche s.s. and the underlying Mont Mary-Cervino superunit. The former is composed of the kinzigitic Valpelline unit and of the metamorphic Permian granitoids and mafic intrusives of the Arolla unit (Argand, 1906; Dal Piaz, 1999; Manzotti et al., 2014a; Dal Piaz et al., 2016). It is separated from the lower Mt Mary-Cervino Upper and Lower units (Reddy et al., 2003; Dal Piaz et al., 2016) by the Roisan Cignana Shear Zone (Canepa et al., 1990; Manzotti et al., 2014b; Dal Piaz et al., 2016). This shear zone is defined by high strain slices of Mesozoic meta-sediments and pre-Alpine continental rocks. Moving to the internal (eastern) side, the Adria-derived Austroalpine continental units are represented by the Pillonet klippe (Dal Piaz and Sacchi, 1969; Dal Piaz, 1976; Cortiana et al., 1998) and by the Sesia-Lanzo zone (Compagnoni et al., 1977; Lardeaux and Spalla, 1991), including in the transect considered here only the frontal Gneiss Minuti Complex. Other continental slices interpreted as Adria-derived extensional allochthons are tectonically interleaved within the ophiolitic units, and are collectively indicated as Austroalpine inliers (Dal Piaz, 1999; Dal Piaz et al., 2001, 2016).

2.2.2. The Piedmont ophiolitic nappe system

The Dent Blanche-Sesia Lanzo system overrides the Piedmont ophiolitic nappe system, Argand's (1916) *géosynclinal piémontais*, which in turn is composed by the Combin and Zermatt-Saas zones (Dal Piaz, 1965; Bearth, 1967; Caby, 1981). An interlayered corridor of continental carbonatic and silicoclastic sediments (Pancherot-Cime Bianche-Bettaforca unit; Dal Piaz et al., 2016) is found along or close to the basal contact of the Combin zone, overlying in the second case a lower Combin unit. The Combin and Zermatt-Saas ophiolitic units, separated by the Combin Fault tectonic contact (Ballèvre and Merle, 1993), show contrasting lithology and metamorphic history. Blueschist facies relics register peak metamorphic conditions for the Combin zone (Caby, 1981; Manzotti et al., 2021), while eclogitic and locally (ultra-) high pressure metamorphism (Ernst and Dal Piaz, 1978; Reinecke, 1991; Frezzotti et al., 2014) are recognised in the Zermatt-Saas unit.
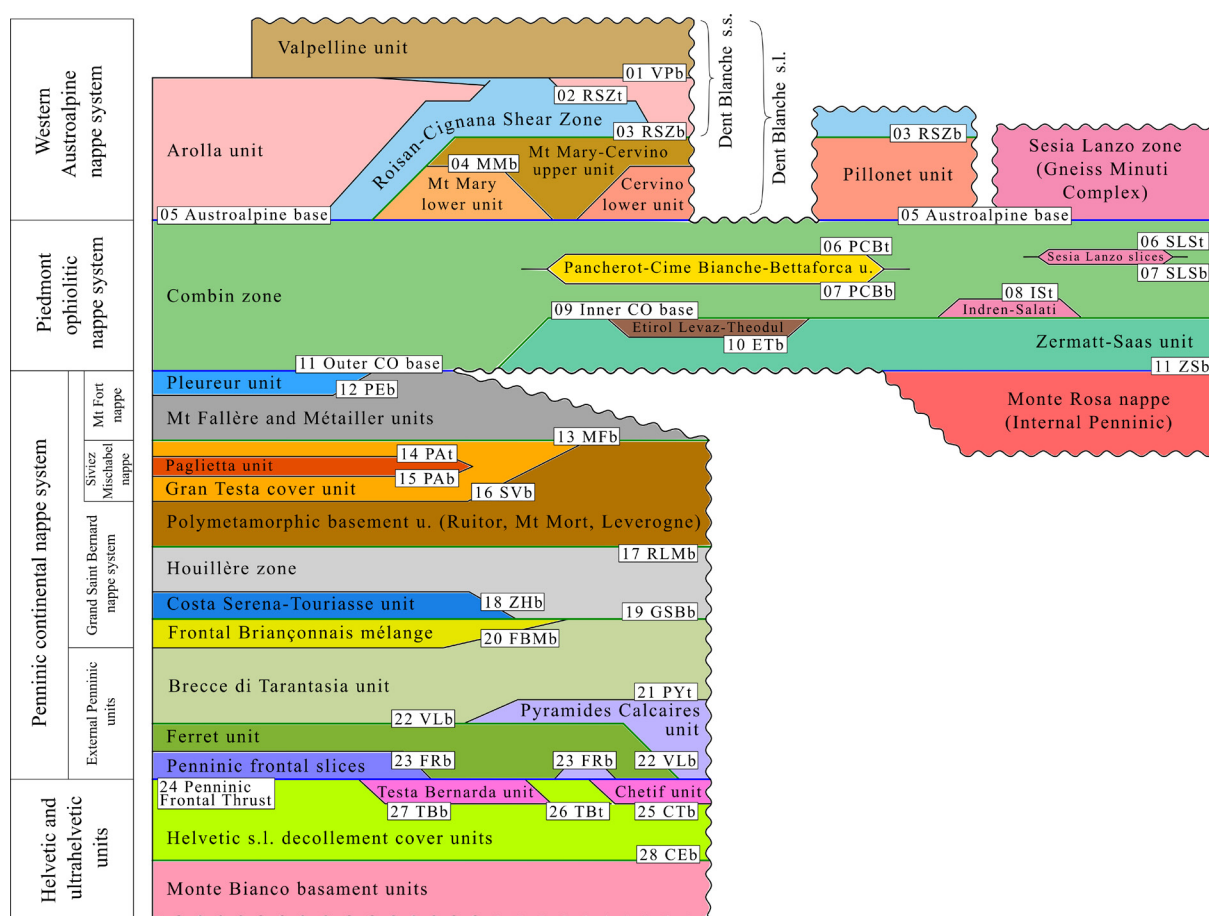
Figure 2.2. Hierarchical scheme of the tectono-metamorphic relationships of the nappe stack in the northern Aosta Valley. Major Alpine tectonic contacts separate different nappe systems (i.e., Austroalpine, Piedmont, Penninic and Helvetic and Ultrahelvetic nappe systems) and hold the highest hierarchical importance. Lower hierarchical positions are reserved for tectonic contacts that might interrupt against higher order elements and create tapered geometries. We refer to the text for the detailed description of the tectono-metamorphic legend and to Fig. 2.1 for the tectonic map.

2.2.3. The Penninic continental nappe system

In the northeastern portion of the study transect, the ophiolitic Zermatt-Saas unit lies over the eclogitic Monte Rosa continental nappe, derived from the European passive margin (Dal Piaz, 1999, 2001, 2004; Lapen et al., 2007; Steck et al., 2015).

Moving towards the western and structurally lower units, an intermediate sector is represented by the Grand Saint Bernard nappe system, a thick imbrication of thrust sheets characterised by alpine blueschist to greenschist facies metamorphism (Caby, 1968; Escher et al., 1988; Gouffon, 1993; Sartori et al., 2006; Bergomi et al., 2017). Within this system, the structurally highest and internal unit is the composite Mont Fort nappe (Gouffon, 1993; Burri et al., 1998; Pantet et al., 2020). This nappe is

composed of polymetamorphic basement units and associated cover metasediments (e.g., Pleureur unit; Burri et al., 1998) and it is in contact with the overlying Combin zone through the previously mentioned Combin Fault (Ballèvre and Manzotti, 2019). In a more external and lower structural position we find the Siviez-Mischabel and Ruitor units (Caby, 1968; Burri, 1983; Gouffon, 1993; Malusà et al., 2005). Finally, the Houillère zone (Bigi et al., 1990; Bertrand et al., 1996) and the Costa Serena-Touriasse units define the lowermost element of the Grand Saint Bernard nappe system.

The External Penninic units, or Sion-Courmayeur zone (Trümpy, 1954; Elter, 1960), constitute the most external portion of the Penninic nappe system and lie in the western region of the study transect. Here the peak metamorphism is low-T greenschist facies, with the exception of the Versoyen area which is affected by HP metamorphism. A sequence of younger thrusts defines an imbrication of thrust sheets of decolled cover units and thin basement slices (Dal Piaz et al., 2003). The External Penninic units are represented by the Brecce di Tarantasia unit (Trümpy, 1952, 1955; Elter and Elter, 1965; Loprieno et al., 2011), the Ferret unit (Cita, 1953; Burri and Marro, 1993), the Pyramides Calcaires unit (Antoine, 1971) and the Penninic frontal slices (cataclastic rocks marking to the Penninic Frontal thrust).

2.2.4. The Helvetic and Ultrahelvetic units

The External Penninic units are in contact, through the Penninic Frontal thrust (Ceriani et al., 2001; Perello et al., 2011), with the "root" of the underlying Helvetic and Ultrahelvetic units (Baretti, 1881; Cita, 1953; Elter, 1960) composed of shallower basement slices and decollement cover units. In the lowermost structural position exposed at the head of the Aosta Valley, we find the basement of the Monte Bianco (von Raumer and Bussy, 2004).

2.3. The geomodelling workflow

The complex tectono-metamorphic setting of the northwestern Alps and the nature of the input database composed of field data only (i.e., geological and structural data collected at surface) motivate the following geomodelling workflow. Spatial orientation analysis of geological and structural data is followed by structural interpretation on a series of vertical cross-sections, where interpretative models and prior knowledge gained from structural analysis are applied. Eventually, field data and cross-section interpretation are used as input for implicit interpolation, producing three-dimensional surfaces that represent boundaries of tectonic units interrupted by brittle fault surfaces. At each step, particular care is taken to reduce subjectiveness as much as possible. The following sections address in detail each step of the geomodelling workflow, schematically illustrated in Fig. 2.3.

Geomodelling workflow

```
┌─────────────────────────────────────────────┐
│                 INPUT DATA                    │
│   Tectonic map and database of structural data. │
└─────────────────────────────────────────────┘
                       │
                       ▼
┌─────────────────────────────────────────────┐
│               DATA ANALYSIS                   │
│        Preparation of structural data.        │
│  Upscaling of foliation data using vectorial means. │
│ Orientation statistics study and definition of structurally │
│            homogeneous sub-domains.           │
└─────────────────────────────────────────────┘
                       │
                       ▼
┌─────────────────────────────────────────────┐
│          STRUCTURAL INTERPRETATION            │
│              on vertical cross sections.      │
│  Expert geological knowledge and interpretation patterns │
│        to create a conceptual structural model. │
└─────────────────────────────────────────────┘
                       │
                       ▼
┌─────────────────────────────────────────────┐
│           IMPLICIT 3D INTERPOLATION           │
│          using mesh-based DSI algorithm.      │
│     Structural data constraints on the interpolator │
│        (gradient and tangent constraints).    │
│ Additional explicit refinement of the output triangulated surfaces. │
└─────────────────────────────────────────────┘
                       │
                       ▼
┌─────────────────────────────────────────────┐
│             3D STRUCTURAL MODEL               │
└─────────────────────────────────────────────┘
```

Figure 2.3. 3D geomodelling workflow. The input tectonic map collects geological information and structural measurements. Structural data (foliation and fold axis measurements) are analysed through an orientation statistics study and foliation data are upscaled to fit the regional extents of the area. Structural interpretations on a network of vertical cross-sections make up the conceptual model. Finally, the implicit DSI algorithm is applied to create the 3D structural model. Detailed description of the workflow in Sect. 2.3 of the text.

2.3.1. Input data

Input data for geomodelling projects can be of diverse nature including fieldwork observations, geophysical datasets, well logs, topography (i.e., Digital Elevation Models, DEM) and remote sensing (aerial or satellite) imagery. In our case subsurface data (wells and geophysics) are not available. The northern Aosta Valley is not crossed by any deep crustal seismic line, with the closest being the CROP-ECORS (e.g., Nicolas et al., 1990) and the NFP-20 (e.g., Pfiffner et al., 1997). The lack of subsurface data is partly counterbalanced by the rugged topography of this sector of the Alps, characterised by a difference in elevation of ca. 4,300 m (from ca. 500 m near Chatillon to 4,809 m on top of Mont Blanc), and by large mountain faces with continuous outcrops.

Our input field data are thus the collection of all the geological, petrographic and structural observations that have been gathered in the field, and of remote sensing and topographic datasets. The project benefits

from a recent and homogeneous seamless 1:10,000 geological map (Dal Piaz et al., 2010, 2015; Perello et al., 2011; Polino et al., 2015; and Monte Bianco and Gran San Bernardo sheets under way) which has been synthesized in 1:150,000 and 1:100,000 geotectonic maps of the Aosta Valley (Giusti et al., 2003; Bonetto et al., 2010) and more recently in a 1:75,000 structural map covering ca. 1,500 km^2 (Fig. 2.1). The dataset is strongly interdisciplinary and, for instance, dense meso-structural observations collected on outcrops (attitude of bedding, foliations, lineations, fold axes and axial surfaces, fractures, faults, etc.) are complemented by petrographic and microstructural studies that help building a consistent structural framework, with different deformation events arranged in a consistent relative chronology. Remote sensing datasets are represented by a 2 m resolution DEM, obtained from a LIDAR survey, and 20 cm/pixel aerial orthophotos (provided by the Autonomous Aosta Valley Region). All these data are organised in a Geographic Information System (GIS) aimed at structural analysis.

2.3.2. Defining the tectono-metamorphic legend

As in a geological map, the legend of a 3D geomodel is essential to list all the structural and geological features that are represented in the model and define their structural and chronological relationships (including primary and secondary stratigraphic, intrusive and deformation structures). Moreover, the legend defines a unique name for each structural element, which can be used for display, spatial queries and interoperability purposes.

As opposed to the case of sedimentary settings in which the legend is typically represented in the form of a stratigraphic column, sometimes including unconformities as the only complexity (Mallet, 2004), polydeformed metamorphic orogenic settings require a different approach to represent their structure and define the tectonic evolution. In this work we define the tectono-metamorphic legend of Fig. 2.2 as the 2D schematization of complexly deformed 3D tectono-metamorphic units, intended as discrete elements with a specific metamorphic and lithological history separated by tectonic boundaries.

Tectonic boundaries are represented in the tectono-metamorphic legend as hierarchical lines. First order elements hold the higher importance and, in our model area, do not interrupt against other structures. These are usually major discontinuities that accommodate large displacements (e.g., Austroalpine, Piedmont and Penninic base in Fig. 2.2). Lower order lines may interrupt against higher order ones, defining lenses and tapered geometries, and they might represent either (i) structures of lower tectonic importance, or (ii) older discontinuities that have been cut by more recent ones (e.g., the Roisan Cignana Shear Zone separating the Dent Blanche s.s. units from the Mont Mary units).

2.3.3.   Structural data analysis

Structural data consist of orientation data of compositional layering, schistosities and mineral lineations (related to different tectonic phases and PT conditions), fold and crenulation axes and axial surfaces of different folding events, and brittle fractures and fault surfaces. Analysis and processing of these data was performed with two goals: (i) defining structurally homogeneous domains, where well-defined interpretation rules could apply, and (ii) interpolating smooth orientation fields that can be used for modelling at the regional scale.

The analysis aimed at defining structurally homogeneous domains (i.e., areas characterised by foliation with constant mean attitude and/or folded along the same mean fold axis) has been performed by applying spherical statistics to data. In stereogram views for data visualisation, mean vectors (Borradaile, 2003) have been computed on populations of fold axis and foliation data (on the normal vectors to the foliation plane). Tentatively, homogeneous domains have been defined with the same boundaries as tectono-metamorphic units, then adjoining domains showing the same statistics have been merged (independently from isotopic ages and PT conditions). Conversely, when some domain revealed a relevant inhomogeneity (i.e., multimodal distribution of foliation data or fold axes), it has been split in two or more parts. The result of this analysis (Fig. 2.4A) is that each domain is either dominated by folding (hence characterised by average fold axes and/or axial surfaces), or by quasi-planar foliation (this could be either due to very intense lamination, or to almost no deformation).

Smoothing of structural data at the regional scale was performed by averaging orientation data at the nodes of a 650 m by 500 m regular grid (Fig. 2.4B). The calculation of the vector mean was performed as in Vollmer (1995) and in Carmichael and Ailleres (2016).

We excluded structural measurements located within the regions identified as gravitational slope deformation in the map (Fig. 2.1) from the entire structural analysis. These areas are affected by Deep-Seated Gravitational Slope Deformations, large slow slope instabilities commonly found in mountainous environments which might cause rotation and tilting of data, making them unreliable for the structural analysis.

Structural data analysis led to identifying three macro-regions that can be considered homogeneous in terms of regional-scale orientation statistics, and ductile and brittle deformation styles. The first area corresponds to the most internal sector, where the collisional wedge presents units with high-pressure metamorphism (the Penninic Monte Rosa, the Piedmont Zermatt-Saas unit and the Etirol-Levaz and Theodul lower eclogitic outliers) paired with structurally adjacent greenschist-facies units with blueschist relics (the Dent Blanche-frontal Sesia Lanzo system and the Combin unit). The Inner Combin base (Combin Fault in Ballèvre and Merle, 1993) is responsible for the relative juxtaposition of the

blueschist-greenschist units on top of the eclogitic units, showing a planar geometry that sharply cuts poly-folded older lithological and tectonic boundaries. This sector was also heavily affected by brittle post-nappe deformation, as two sets of normal faults offset the tectonic boundaries (NE-SW striking and NW-SE striking; Bistacchi and Massironi, 2000).

Moving towards the external sector, a change in deformation style is registered. The Grand Saint Bernard system (Mont Fort nappe, Siviez-Mischabel nappe, Ruitor and Houillère units) is affected by backfolding in the style of the famous Siviez-Mischabel structure (Milnes et al., 1981; Cartwright and Barnicoat, 2002) involving both basement and cover units. Post-nappe brittle deformation also affected this area, but in a less penetrative way and NW-SE striking normal faults dominate.

Lastly, the external Penninic units and the Helvetic system define a sequence of sub-parallel thrust sheets with thin interposed slices and extensional-transtensional features along more important tectonic boundaries (the Penninic and Briançonnais frontal thrusts). Tectonic boundaries dip with an intermediate angle towards the SE. Moreover, in this sector almost no post-nappe brittle deformation has been mapped that is relevant at the scale of the 3D model. However, the difference in abundance and pervasiveness of large-scale brittle structures may be apparent, as related to the different competence of outcropping lithologies. In fact, this sector is dominated by soft lithologies (i.e., metasediments), in contrast with the crystalline basements of the collisional wedge, and fault structures might be masked by detrital covers.

2.3.4. Structural interpretation

Deformation structures in metamorphic terrains are characterised by frequent thickness variations, complex multi-phase and non-cylindrical folding patterns, and large-scale boudinage (resulting in fragmentation of original lithological or stratigraphic units). The geometry of folds, defined by amplitude, wavelength and curvature parameters, often displays multi-scale and disharmonic patterns and is influenced by the rheological characteristics of the rocks they deform. Therefore, a conceptual geological and structural model is needed most of the times to guide the interpolation of a consistent 3D model. In agreement with different authors (Kaufmann and Martin, 2009; Zanchi et al., 2009) we build the conceptual model using serialised vertical cross-sections, whose position, spacing and orientation is chosen according to (i) map and model scale, (ii) the distribution of outcrops, (iii) outcomes of orientation analysis and (iv) typical wavelengths of structures in the study area. In particular, the orientation of cross-sections is chosen perpendicular to fold axes and fault surfaces, so as to minimise distortion due to apparent dip effects. Spacing of cross-sections is chosen to be smaller than the wavelength of the smallest folds or fault blocks to be represented in the model. In our case, we built a network of 75 planar vertical cross-sections with horizontal spacing of ca. 1,500 m and distributed in

two perpendicular sets, with SE-NW (135°-315° N) and NE-SW directions (Fig. 2.5). The network of cross-sections has been built in the software Move (www.petex.com/products/move-suite), which implements useful tools for data projection and two-dimensional structural interpretation.

Finally, it is a good practice to locate key cross-sections in areas of strong structural complexity, where data sampling is ideally denser. In such areas, depending on the complexity of the structure, it could be useful to densify the interpretation by building additional intermediate cross-sections. This approach was implemented in three specific subareas of the 3D model for the representation of folds with strong lateral variability (see Sect. 2.4, the Valpelline base, the Mont Mary tectonic contact exposed in the Cignana Lake area, and the Outer Combin base; see Fig. 2.2 for the nomenclature of the tectonic contacts). We proceeded by progressively reducing the distance between cross-section planes by a factor of 2 until achieving a satisfactory representation, reaching a final distance between cross-sections of one fourth of the original value for the three subareas.

Interpretation on cross-sections is constrained by orientation data and traces of tectonic boundaries and faults, that are projected onto each section along the mean fold axis or along the mean strike of schistosity defined for each structurally homogeneous subdomain (see Sect. 2.3.3 and Bistacchi et al., 2008). Since the homogeneous subdomains cover large areas, local geometries occasionally rotate from the average attitude (e.g., due to local rotation of fold axes). To resolve these instances, we locally revisit the orientation statistics analysis, and projection is performed using locally adapted mean vectors.

As a general rule, the projection of structural data and traces of tectonic or lithological boundaries is performed within a buffer of generally half the horizontal spacing between two cross-sections, so that every object in the input dataset is projected onto one cross-section only. However, the maximum projection distance can be varied also according to higher/lower cylindricity of the data (which can be evaluated in the orientation analysis), data density, etc.

When all constraints have been properly projected (as in the synthetic example in Fig. 2.6), cross-sections in Fig. 2.5 are interpreted using classical "manual" digitization of all structures by an expert of regional geology. Sometimes the drawing can be aided by algorithms that allow automatically generating patterns of foliations or folds according to some geometric/structural rule (e.g., parallel vs. kink vs. similar folds).

In our workflow both the subsurface and the eroded space (i.e., below and above the topographic profile) are interpreted. This leads to higher continuity of the interpretation, better expression of structural rules used by the interpreter, better exploitation of rugged topography, and overall higher robustness of the interpretation by avoiding edge effects. Fig. 2.7 holds examples of cross-sections from our modelled area.
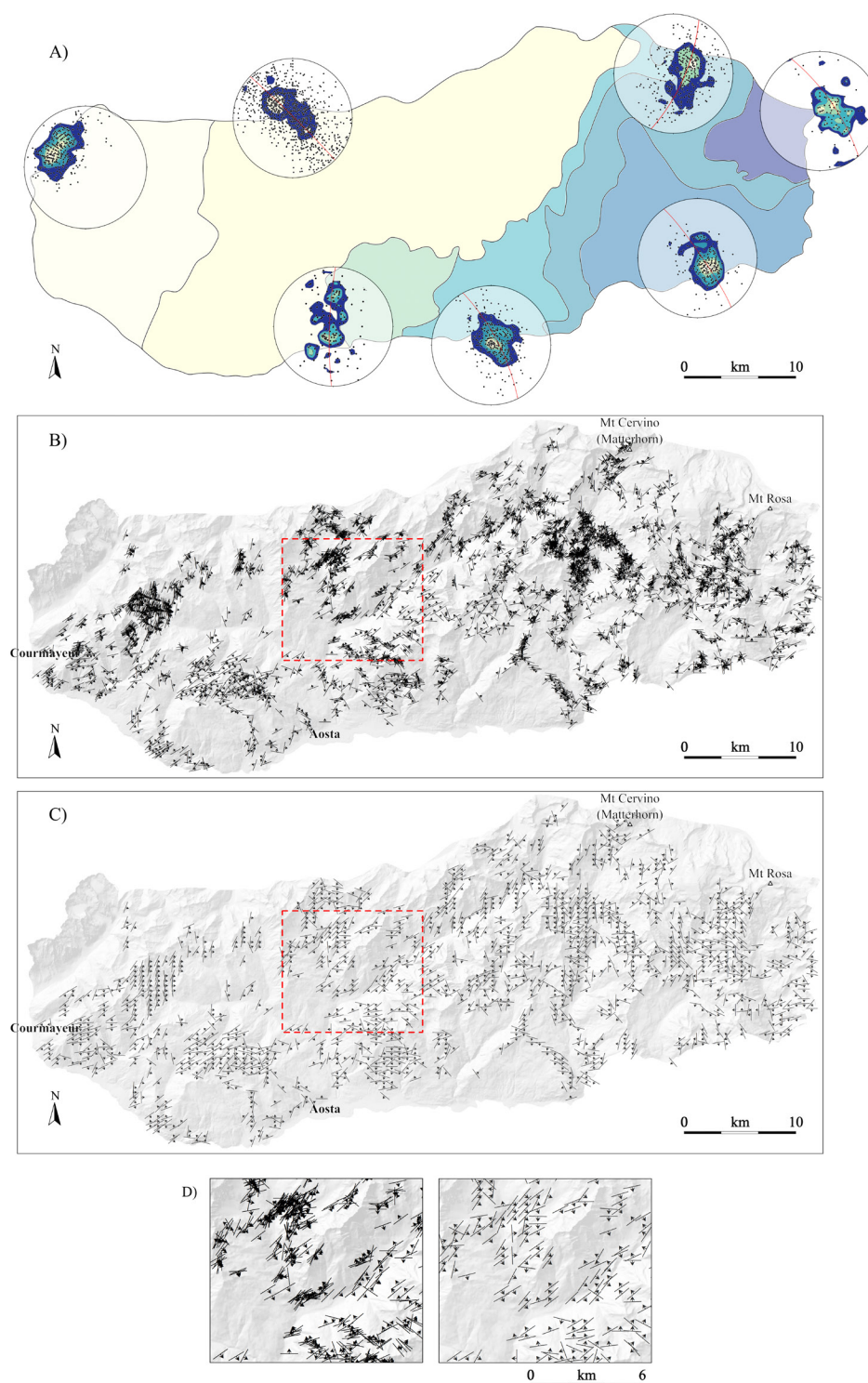
Figure 2.4. Structural analysis of the northern Aosta Valley, limited inside the national border to the north and to the Dora river to the south. (A) Homogeneous structural domains. Normal to foliation planes are plotted as dots in stereograms, including contouring with interval 1%. Best fitting as red great circles. (B) Primary foliation measurements at the location of observation. (C) Foliation orientations from B averaged on a 650 m by 500 m regular grid. (D) Details from B and C, from the areas highlighted by the dashed red rectangles.
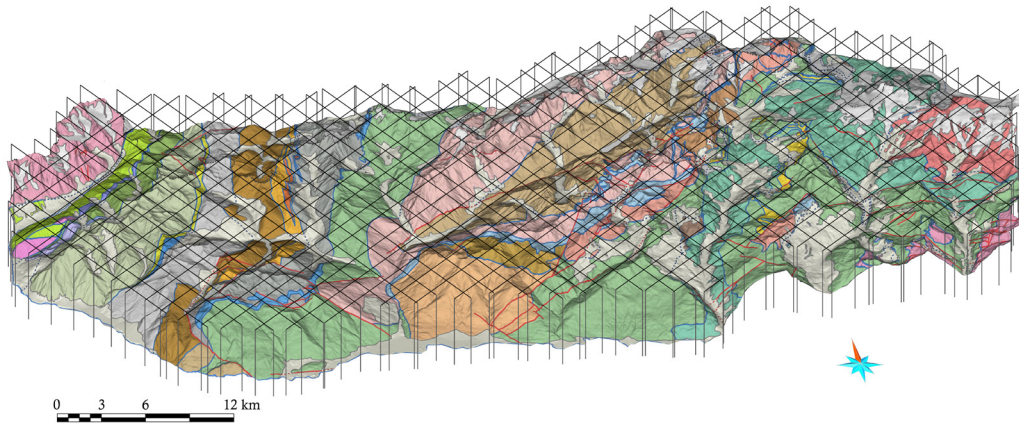
Figure 2.5. Network of vertical cross-sections on which the conceptual structural model is built, interpreted as detailed in Sect. 2.3.4 of the text. The tectonic map (Fig. 2.1) drapes the topography. Scheme of the tectono-metamorphic relationships in Fig. 2.2.
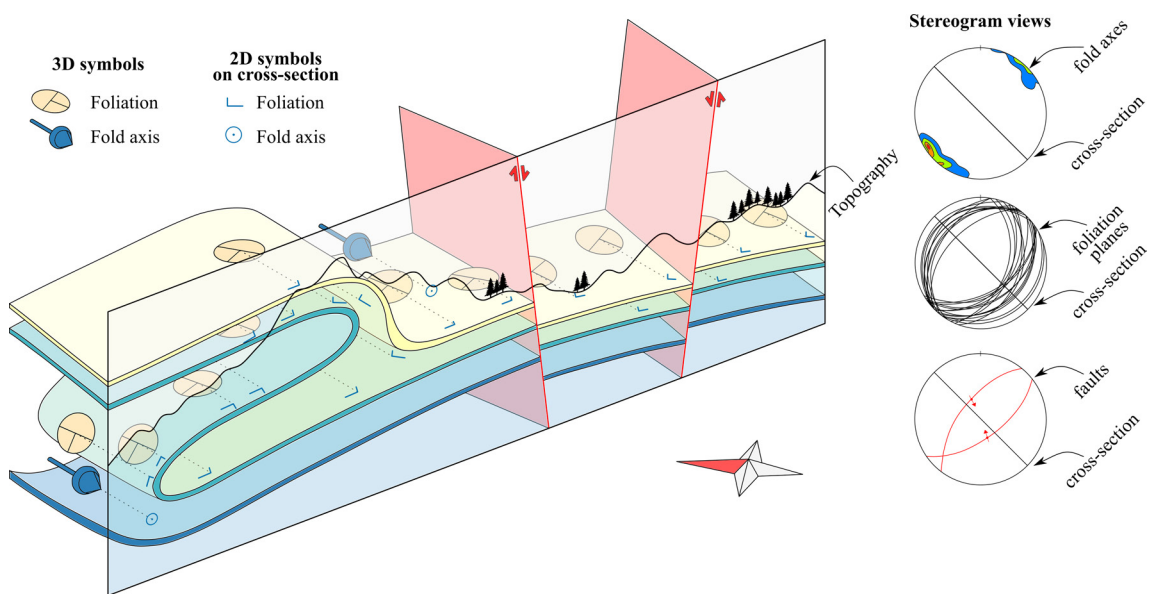
Figure 2.6. 3D view of a synthetic scenario showing isoclinal recumbent folding and normal faulting. An interpretative cross-section is built by projection of structural and geological data, collected during fieldwork, along the mean fold axis direction.
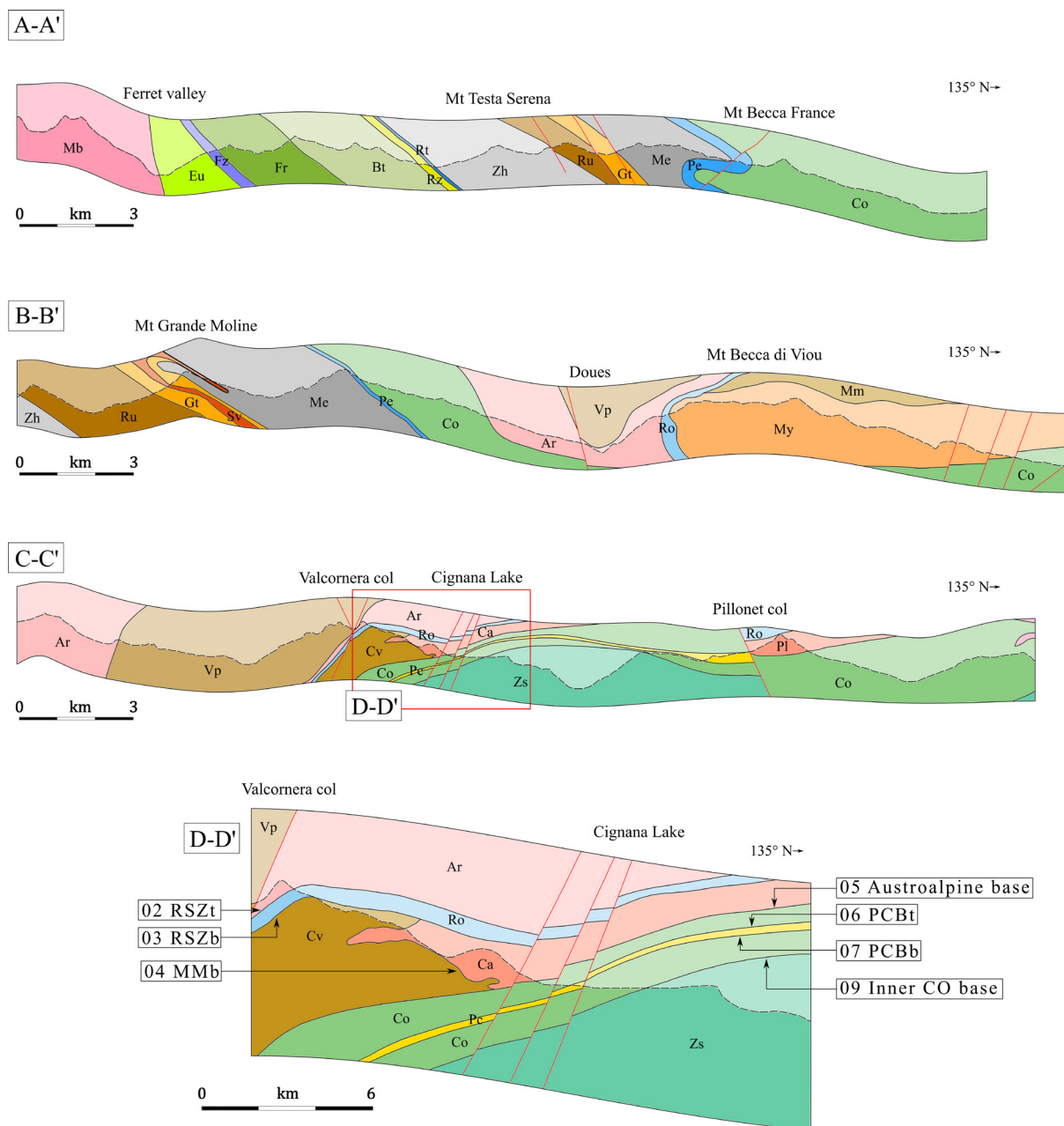
Figure 2.7. Representative NW-SE cross-sections from the model area. Cross-section locations as in Fig. 2.1. Colours as in the tectonic legend in Fig. 2.2. Topographic profiles as dashed black lines.

It is well known that building a conceptual structural model is susceptible to subjectiveness of interpretation (e.g., Bond, 2015). However, in our experience this is a lesser evil, necessary to guide the interpolation on the basis of concepts of structural analysis not easily implemented in interpolators used for simple sedimentary sequences with little deformation or very dense sampling interpreted from geophysical images.

2.3.5. Implicit interpolation

We perform the interpolation of implicit surfaces with SKUA/GOCAD (https://www.aspentech.com/en/products/sse/aspen-skua) and the RING Toolkit plugin, that implement the implicit Discrete Smooth Interpolator (DSI; Frank et al., 2007; Caumon et al., 2013). The interpolation is solved on a tetrahedral mesh using a least-squares weighted approach leveraging different kinds of geological and structural constraints. These are classified as hard (i.e., to be strictly honoured) or soft constraints (i.e., to be honoured in a least-squares sense).

Geological constraints are further distinguished in position and gradient constraints, respectively influencing the value of the scalar field or the orientation of its gradient (Frank et al., 2007; Caumon et al., 2013). Position constraints correspond to mapped tectonic contacts, interpretations on vertical cross-sections or observations along boreholes (not available for our model) and define the value of the scalar field at the corresponding locations. Gradient constraints allow instead the incorporation of structural data (e.g., foliation data and fold axes) to constrain the orientation of the implicit surfaces to conform to structural trends (Frank et al., 2007; Caumon et al., 2013).

Constraints obtained from the previous steps of our workflow are assigned different weights, or certainty levels, with the higher value corresponding to direct field observations such as outcropping tectonic boundaries and structural data. Meanwhile, conceptual interpretations in vertical cross-sections are assigned a lower weight/certainty level since they result from expert geological interpretation and can be at least partly imprecise or subjective. An additional constant gradient constraint is used to guarantee continuity across cells of the tetrahedral mesh and hence the well-posedness of the mathematical interpolation problem (Frank et al., 2007; Caumon et al., 2013). This constraint is generally isotropic and constant throughout the entire model volume, however the *Structure and Stratigraphy* workflow of SKUA/GOCAD enables, if requested, variations in the magnitude of the gradient of the scalar field, allowing large thickness lateral variabilities to be modelled.

Faults are introduced in the model in an early step, in the form of explicit triangulated surfaces, interpreted from their mapped trace as it curves along the DEM, and extended up- and down-dip proportionally to their map length. Cross-cutting relationships amongst fault surfaces are based on map relationships and relative chronology. Since fault surfaces interrupt the continuity of the implicit scalar field, they are introduced in SKUA/GOCAD as internal boundaries in the tetrahedral mesh, with tetrahedra being disconnected on opposite sides of a fault, resulting in mathematical discontinuities in the interpolated scalar field. This modelling strategy allows to introduce in the model both faults cutting through the whole domain and finite faults having tip lines inside the modelled volume (Frank et al., 2007; Caumon et al., 2013).

In Fig. 2.8 we schematically show the result of the implicit interpolation, which leverages the classes of constraints introduced before, on the synthetic scenario already presented in Fig. 2.6. This picture represents the implicit scalar field interpolated on a tetrahedral mesh in a three-dimensional volume, and surfaces of interest extracted a posteriori as isovalue nodes. The scalar field is interrupted by two normal faults, which dissect the conformable mesh. Foliation and fold axes are imposed as gradient constraints on the scalar field, allowing to easily model the isoclinal recumbent fold.

The tectonic boundaries of units outcropping in the western portion of the northern Aosta Valley (i.e., the External Penninic units and the Ultrahelvetic-Helvetic domain, Fig. 2.2) show in some cases lenticular geometries due to the presence of duplex structures in the stack of thrust sheets (Fig. 2.1). Some units of the Austroalpine and Piedmont nappe systems (Fig. 2.2) also show lenses with limited areal extent, in this case due to ductile shearing and regional boudinage (Fig. 2.1). In both cases, the geomodelling problem is resolved by interpolating with the *Structure and Stratigraphy* workflow in SKUA/GOCAD, which implements an implicit interpolator based on the previously mentioned DSI algorithm (Frank et al., 2007; Caumon et al., 2013). This workflow allows the definition of "unconformities" (using a term borrowed from stratigraphy) as interruptions of the continuity of the scalar field, that permit obtaining closed lenticular volumes.

Other portions of our model, such as the Dent Blanche s.l. and the basement units of the Grand Saint Bernard, include tight and isoclinal folds with long limbs and tight hinge zones (Fig. 2.1), which are better constrained by the RING Toolkit plugin implicit interpolator (Frank et al., 2007; Caumon et al., 2013). This tool allows imposing different kinds of structural constraints on the scalar field, each one based on different input data and with a different weight/certainty level. Fold axes and foliation data are used to constrain the gradient of the scalar field to be perpendicular to, respectively, the fold axis vector and the schistosity plane (Caumon et al., 2013). The definition of these additional structural constraints allows leveraging direct field observations, a better control on the modelled geometries, and lower tendency to create unintended artifacts (e.g., "handles" or "bubbles" in the implicit surfaces) when interpolation is conditioned by conceptual interpretation from vertical cross-sections. This approach leverages input data not considered in the SKUA/GOCAD *Structure and Stratigraphy* workflow - particularly foliation and fold axes, and results in a successful interpolation of tight isoclinal folds.

Successively, we export the implicit surfaces representing faults and tectonic boundaries, corresponding to isovalues in the scalar field, as triangulated surfaces. These output surfaces, constituting the boundary representation of the 3D model, undergo an enhancement step using the explicit tools of SKUA/GOCAD (Caumon et al., 2004) aimed at seamlessly merging the independently interpolated portions of the model, resolving local intersections with mesh-cutting tools. We also employ explicit tools to complete the representation of lenses created by regional scale boudinage (see the Pancherot-Cime Bianche-

Bettaforca lens and the Sesia-Lanzo slice, Fig. 2) which, unlike the other lenticular geometries, do not lie on a hierarchically higher tectonic contact in our model. For their modelling, after arbitrarily assigning higher hierarchy to one of the two bounding surfaces in the interpolation process, we apply mesh-cutting tools to terminate this surface at the intersection with the hierarchically lower one, where the lenticular bodies close. Finally, we leverage explicit tools to increase the equilaterality of the triangles composing the mesh, thereby improving the quality of the output.
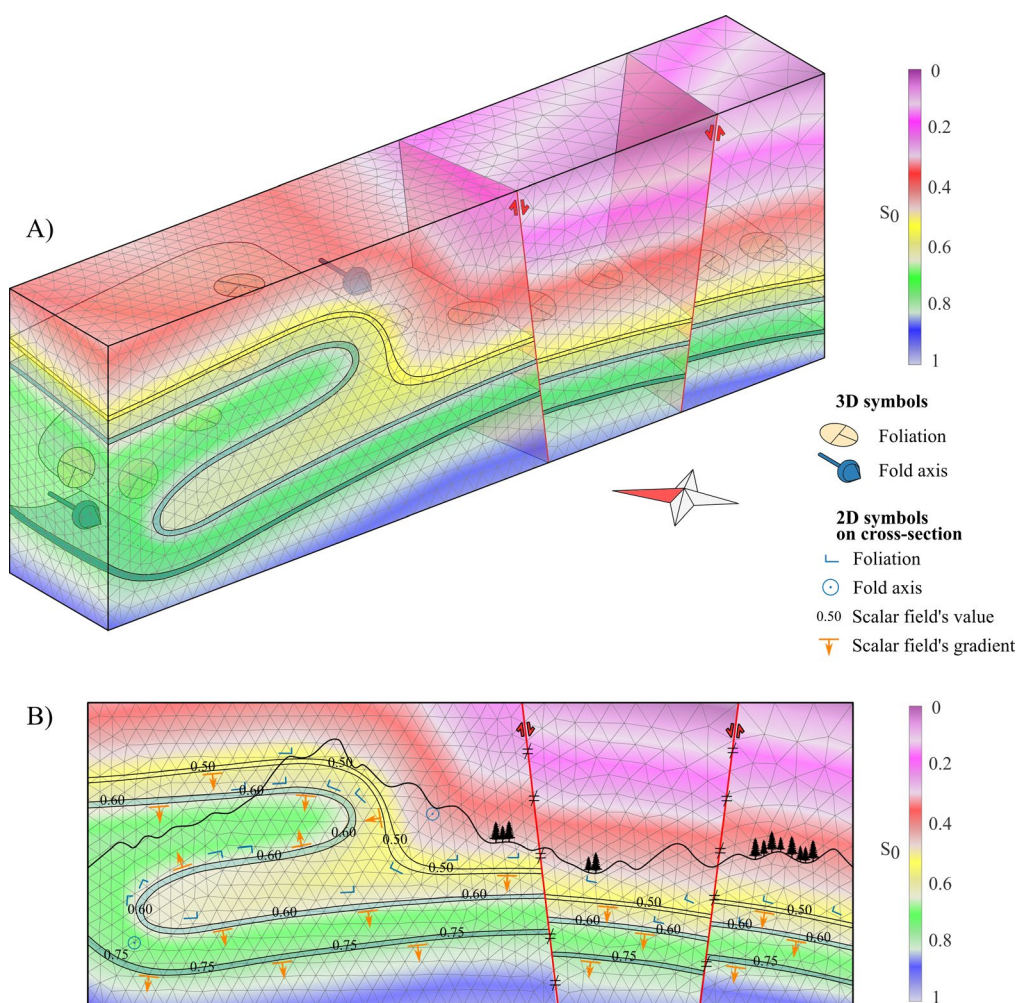

Figure 2.8. (A) 3D and (B) cross-section views of the synthetic scenario in Fig. 2.6 displaying isoclinal recumbent folding and normal faulting. The implicit approach is employed to interpolate the 3D structural model, using geological and structural data as value and gradient constraints.

2.4. The northern Aosta Valley 3D structural model

The 3D structural model of the northern Aosta Valley covers an area of ca. 1,500 km^2 and has a vertical extension of ca. 2,000 m, extending above and below the topographic surface. The boundary representation model is displayed in Figs. 2.9 and 2.10, and can be interactively explored on https://geologia3d.regione.vda.it.

A total of 29 tectono-metamorphic units is represented in the model, separated by 28 tectonic boundaries which are cut by 83 fault surfaces, all of them with finite surfaces and internal tip lines. The tetrahedral mesh used for the implicit interpolation has a vertical and horizontal resolution of 145 m (corresponding to the average edge length of the tetrahedra) totalling ca. 1.1×10^6 nodes and ca. 6.4×10^6 tetrahedra. This resolution allows for practical interpolation times on a desktop computer (between 10 and 30 minutes on average for the interpolation of the scalar field) and is suited for the representation of the gently deformed tectonic contacts of the external portion of the 3D model and for the complexity of the internal collisional wedge.

The core of the studied transect, represented by the western Austroalpine nappe system, constitutes one of the most complicated volumes of the 3D structural model. The region is characterised by frequent open and isoclinal folded geometries, whose continuity is interrupted by multiple internal hierarchical relationships and a network of brittle normal faults. The major tectonic contact internal to this system is the Roisan-Cignana Shear Zone (Manzotti et al., 2014a). Represented in our model by its bounding top and base surfaces, the Shear Zone is characterised by open undulations at the regional scale and abrupt lateral thickness variations. It closes, to the south, at the intersection with the hierarchically higher Dent Blanche Basal Thrust, whose regional expression is indicated as Austroalpine base in our model to highlight its position in the tectonic sequence (Fig. 2.2). Overhanging the Roisan-Cignana Shear Zone, only the mylonitic contact between the Valpelline and the Arolla unit outcrops. We represented the Valpelline base surface as a large scale mylonitic isoclinal synform, whose regional fold axes gently plunge towards the NE. The hinge of the regional fold outcrops in the Swiss Alps outside of our model area, north of the Dent d'Hérens-Tête de Valpelline ridge (Dal Piaz et al., 2016).

In underlying position, the tectonic contact internal to the Mont Mary superunit is represented by folded surfaces that interrupt at the intersection with the higher order Roisan-Cignana Shear Zone and Austroalpine base. In the area between the Cignana Lake and the Valconera col (Fig. 2.7, section CC'), the tectonic contact outcrops as a series of small-scale, isoclinal recumbent folds (Fig. 2.1). The limited thickness of the fold limbs is sub-scale as compared to the resolution of our 3D model and an accurate representation of the geometry would require a much finer mesh and impractical run-times. In fact, the DSI approach solves linear equations inside each tetrahedra, and higher curvature would be necessary to accommodate the narrow isoclinal geometry. Therefore, in our model this portion of the Mont Mary

tectonic contact slightly diverges from the tectonic map and we modelled it as a close recumbent fold. A higher resolution 3D model, focusing on this area, will be addressed in a future publication.

The units outcropping in the vicinity of the Pillonet col are correlated to the Mont Mary superunit and the Roisan-Cignana Shear Zone (Dal Piaz, 1976), although geographically separated by the Valtournenche valley. Therefore, in the 3D model the tectonic boundaries limiting the units in question are modelled as laterally continuous. The Austroalpine nappe system extends towards the east as Sesia Lanzo Zone, which is represented in our model by the Gneiss Minuti Complex only. Its related tectonic slices (i.e., the Sesia Lanzo and Indren-Salati slices, Fig. 2.2), detached by the main continental body, are modelled as independent slivers geometrically incorporated within the Piedmont ophiolitic sequence.

In lower tectonic positions, we model the easternmost portion of the Combin Fault (Ballèvre and Merle, 1993) and we refer to it as Inner Combin base (Fig. 2.2). While the name Combin Fault indicates a major Alpine tectonic contact responsible for the juxtaposition of the Combin zone with the Zermatt-Saas to the east and with the Mont Fort nappe to the west (Ballèvre and Merle, 1993), in our model we refer to the two portions of this tectonic contact using separate names. With this choice we want to highlight the different hierarchical importance that they hold in the tectono-metamorphic legend of our work (Fig. 2.2).

Incorporated into the ophiolitic Combin zone, we model the Pancherot-Cime Bianche-Bettaforca unit (Fig. 2.2) as a thin lens that spreads over the Valtournenche and Ayas valleys before laterally closing. Gentle open folds characterise this tectonic unit whose thickness, locally sub-scale compared to the model's resolution, has been resolved by modelling separately the top and bottom bounding surfaces. Three additional eclogitic continental lenses, named after close geographical elements, are found along the tectonic limit between the Combin and the Zermatt-Saas units. These are the elements of Etirol-Levaz, Crebuchette and Theodul. Due to coeval ages and conditions of metamorphism (Dal Piaz et al., 2001), these lenses are modelled to belong to the footwall of the Inner Combin base, together with the Zermatt-Saas unit.

In the northeastern sector of the 3D model, the Zermatt-Saas unit overrides the Monte Rosa nappe. As proposed by Lapen et al. (2007), these two eclogitic units show at least partially shared Alpine metamorphic history. Therefore, we model the separating tectonic contact (called Zermatt-Saas base in our model) with open folds geometry, to enhance its reworking under HP metamorphic conditions.
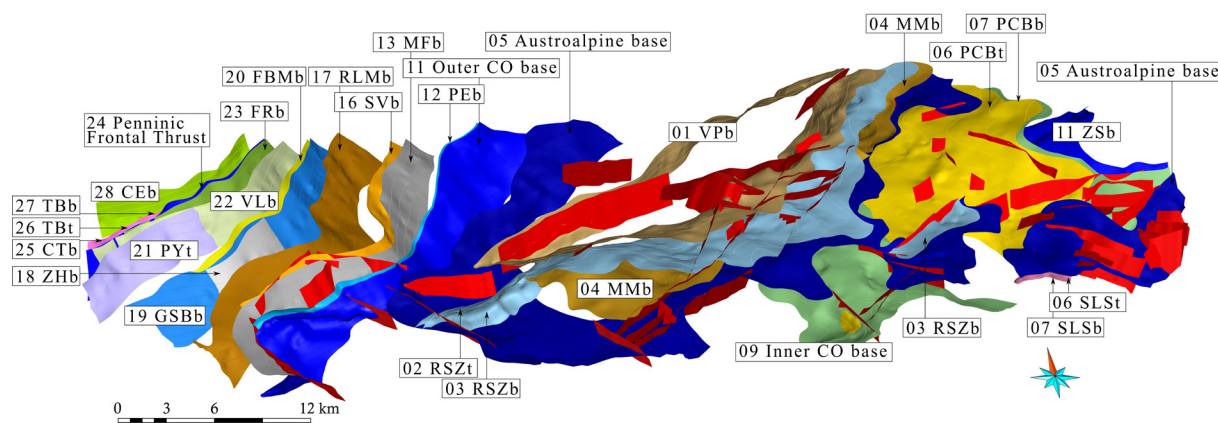
Figure 2.9. 3D structural model of the northern Aosta Valley. Tectonic map in Fig. 2.1 and tectono-metamorphic legend in Fig. 2. Detailed description of model and tectonic contacts in Sect. 2.4 of the text.

Moving towards western portions (Fig. 2.7A), the ophiolitic Combin zone overlies the European Mont Fort nappe along the western portion of the Combin Fault (named Outer Combin base in our model), defining another first order tectonic limit (Fig. 2.2). Along this tectonic contact, lenses of the Pleureur unit are discontinuously mapped (Fig. 1 and Fig. 2) and, due to the frequency and limited thickness of these lenses, we represent them by modelling a continuous volume inside which the presence of the Pleureur unit may be expected. The contacts are characterised by tight to isoclinal folds that affect the rocks of the Combin zone, the Pleureur and the Mont Fort unit. Their axial plane gently dips towards the southeast and their asymmetry can be interpreted as the result of top-to-SE extensional shear under greenschist-facies conditions (Ballèvre and Manzotti, 2019). Isoclinal folding geometries also affect the contacts of the upper Grand Saint Bernard sequence, the Siviez-Mischabel and Ruitor base. These geometries can be linked to post-nappe reactivation with top-to-SE kinematic. The mathematical problem of modelling these isoclinal folds characterised by thin limbs is the same encountered for the small-scale folds of the Cignana Lake, as discussed before. We thus apply the same geomodelling solution and we model the abovementioned tectonic contacts while maintaining only the geometries that are above the resolution limit of our 3D mesh. The 3D model hence simplifies the folds of the input tectonic map while staying true to the regional folding style.

Finally, a clear change in geometry and metamorphic conditions of the tectonic contacts is registered towards the westernmost tectonic succession. The thrust sheets of the External Penninic, Helvetic and Ultrahelvetic units constitute the youngest sequence of tectonic contacts and the easiest to model portion of the northern Aosta Valley. The sequence of thrust sheets shows frequent cross-cutting geometries that add complexity to the modelling and make up the imbricate tectonic structure. We modelled them

40

as quasi-planar tectonic surfaces, parallel to the SE-dipping greenschist facies foliation and affected by gentle folding at the regional scale.

2.5. Discussion on structural interpretation

The input data of this work is composed of the database of geological, petrographic and structural data collected in GIS and represented in the tectonic map (Fig. 2.1). Although the difficulties connected to the creation of the tectonic map are not the focus of the present work, we ought to highlight some critical steps in the process. The input map is the result of fieldwork and upscaling from previously published datasets (Geoportale Regione Valle d'Aosta, https://geoportale.regione.vda.it/). The structural model, on the other hand, is the result of the 3D interpolation of a conceptual model created from the knowledge provided by the map and by fieldwork. Although at first sight the workflow appears as a unidirectional process (i.e., the tectonic map affects the 3D model, and not vice versa), the two entities operate a process of mutual validation. For instance, an interpretation that in map view seems correct, might be discussed and improved under the light of three-dimensional reasoning.

This approach has proven instrumental in refining the tectonic map and choosing the best scenario among different interpretative possibilities in the 3D model and in the map. One notable example is provided by the reinterpretation of Gouffon's (1993) *accident col de Bard-Saint Nicolas*, an important brittle structure exposed in the southern portion of our model, east of Aosta. This fault, which puts in contact outcrops of the Combin zone with units of the Grand Saint Bernard (Fig. 2.1), was originally interpreted with reverse kinematics (Gouffon, 1993) and is instead represented in our model as a normal fault whose extension towards the south might connect to the Aosta-Ranzola fault (Bistacchi et al., 2001), outside of our 3D model, with abutting relationship. The interpretation of this fault has always been problematic due to the scarcity of available outcrops and due to its NW-SE orientation, which is sub-parallel to the interpretative profiles that are usually drawn to represent the SE-dipping nappe stack, hindering its representation in a purely two-dimensional study. The three-dimensional reasoning additionally played a crucial role in the final interpretation of the southern portion of the Outer Combin and Pleureur tectonic contacts, exposed south of Étroubles. By combining the structural database displaying sub-horizontal, NE-SW trending fold axes with the 3D topography draped with the tectonic map, the presence of large-scale recumbent folds affecting the tectonic contacts became evident and was accurately represented in both the map and the 3D structural model.

To work efficiently, this iterative process of mutual improvement between 2D and 3D interpretation requires the map and the 3D model to smoothly communicate and is the motivation for the definition of the tectono-metamorphic legend in our workflow. By representing the tectonic contacts with unique

names and clarifying their hierarchic relationships, this legend simplifies the exchange of data and interpretations between the map and the 3D model.

A fundamental bridge between the two-dimensional map and the three-dimensional model is also provided by the network of vertical cross-sections. By breaking down the 3D model into a series of smaller 2D problems, interpretation at the regional scale becomes manageable. The major downside of building a network of interpretations in vertical cross-sections is the significant interpretation workload. However, at present this is the only known way of transferring geological knowledge of complex poly-deformed structures to the 3D model at this scale.

Another critical aspect regarding the interpretation in cross-sections is the subjectivity that affects the process and the results. Two expert structural geologists, if given the same dataset, would come up with similar but not identical solutions (Bond, 2015). This is because 3D geomodelling is often an under-constrained problem and interpretations are also based on prior knowledge and structural rules issued after assuming particular deformation mechanisms and chronology. One approach to address the subjectivity issue is envisaging the creation of solutions with multiple, geologically feasible, scenarios. While in this paper we presented a single deterministic model to portray the tectonic architecture of the northern Aosta Valley, we are working on incorporating multiple solutions into the interpretation of particularly interesting subareas, as will be discussed in a future publication.

Another direction of research that could address these limitations and improve the modelling process, in terms of both efficiency and reproducibility, is the exploration of automatic modelling solutions. While a fully automated workflow for the modelling of regional-scale metamorphic settings is still to be developed, different methodologies for the upscaling of geological information to smooth high-resolution datasets to match the model's scale and eliminate the effects of parasitic deformations have been proposed (e.g., Jessell et al., 2014, 2021). In particular, we integrated in our workflow a decimation methodology aimed at averaging foliation measurements along a regular grid (Carmichael and Ailleres, 2016). Nevertheless, the process of structural interpretation on cross-sections remained necessary to interpret large-scale geometries from small-scale deformations observed in the field and registered in the tectonic map, and to achieve geological realism.

2.6.   Discussion on geomodelling methods

3D modelling of the polydeformed metamorphic units of the northwestern Alps is a challenging task. Nevertheless, by applying a model-driven workflow to leverage a rich geological, petrographic and structural dataset, it was possible to build the new 3D structural model of the northern Aosta Valley. After building a consistent conceptual model in vertical cross-sections, we exploited implicit interpolation algorithms to model the tectonic contacts outcropping in the area.
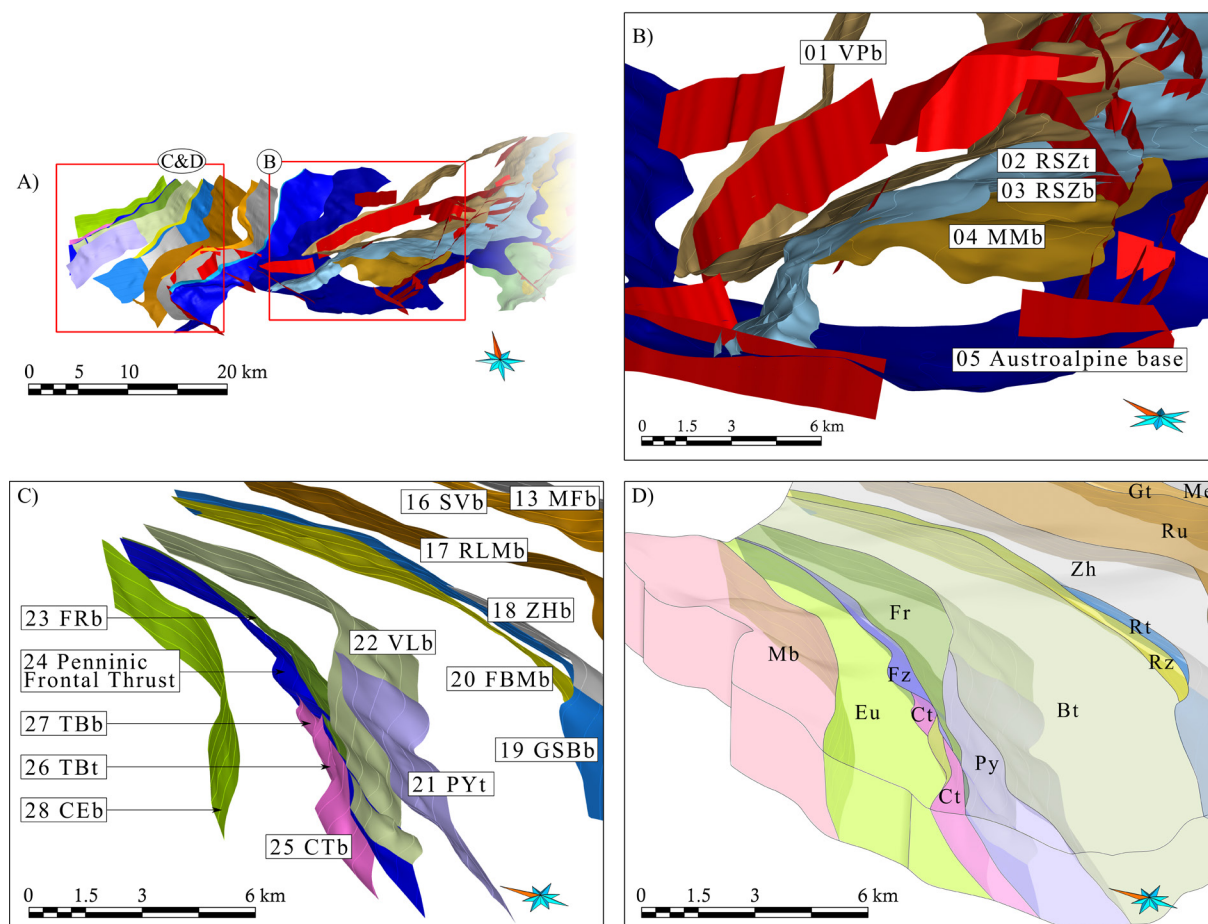
Figure 2.10. Details of the 3D model in Fig. 2.9. Tectonic map in Fig. 2.1, and scheme of the tectono-metamorphic relationships in Fig. 2.2. (A) Portion of the 3D model with highlighted subareas for (B), (C) and (D). (B) Detail of the boundary representation of the Valpelline base, Roisan-Cignana Shear Zone, Mont Mary tectonic contact and Austroalpine base. (C) Detail of the boundary representation of the westernmost portion of the 3D model (Penninic and Helvetic nappes). (D) Same subarea as in (C), displaying volumes.

In the SKUA/GOCAD environment, the integration of faults by truncated signed distance fields is particularly efficient and the modelling of gently deformed surfaces is extremely straightforward. Tapered geometries and lenses are well-represented using "unconformity" relationships in the SKUA/GOCAD *Structure and Stratigraphy* workflow, thanks to the definition of mathematical discontinuities inside the mesh.

However, when it comes to tight and/or recumbent geometries, that are in fact very frequent in the geology of the northern Aosta Valley even at a bigger scale, the software encounters difficulties. The creation of artifacts (i.e., bubbles in the surfaces or a poor fitting of the input data) is likely to happen when the spacing between data and/or the mesh resolution is of the same order of magnitude as the

wavelength of the structures. The RING Toolkit interpolator (Frank et al., 2007; Caumon et al., 2013) solves the majority of these problems by defining specific structural constraints for the interpolation. Fold axes and foliation planes guide the implicit scalar field while quantitively honouring a class of input data that holds relatively low uncertainty. The interpolator also allows for fine tuning of the relative weights between constraints in order to better account for direct field measurements vs. more uncertain structural interpretation in cross-sections.

For the modelling of large areas characterised by different deformation styles (e.g., a collisional orogenic wedge paired with a thrust sequence of semi-parallel structures as in our tectonic setting), we advise the subdivision of the model area into smaller sub-areas, where possible, to break down the interpolation of the scalar field in more manageable sectors with relatively stationary structural features.

The resolution of the mesh also has a large impact on the quality of the output, and it must be chosen in accordance with input data density, scale of the geometries to be represented and computational capacity of the machine. At the price of an increased computational cost, a finer mesh allows a more consistent representation of the geometries represented in vertical cross-section and permits smaller scale geometries to be modelled. In this project, we started by building a 3D mesh with low resolution and downsampled by a factor 2 in both vertical and horizontal directions to obtain a high quality mesh manageable by our workstation (AMD Ryzen 9 5950X Processor, 64.0 GB RAM on a Windows system) that would adequately represent the geological complexity of the northern Aosta Valley. Automatic local mesh refinement (e.g., Frank et al., 2007) could possibly be envisioned in the future to help these aspects.

Relying on structural interpretations on cross-sections for the representation of folds translates into significant subjectivity of the modelling outcome. Previous works proposed the integration of fold axes, fold axial surfaces and overprinting relationships for the modelling of folds (Maxelon et al., 2009; Laurent et al., 2016; Grose et al., 2021). While these approaches could enhance the modelling of the tectonic contacts exposed in our study area, they might not be sufficient for dealing with disharmonic and multi-scale folding, and we envision their application to subareas where more stationary patterns are exposed. Modelling efforts located in the Cignana Lake area are focused on this aspect, as will be discussed in a future publication.

Overall, this study shows that building a large-scale geological model from field data in a region of significant structural complexity remains far from full automation and still calls for significant modelling skills. In the proposed workflow, significant time was spent to interpret cross-sections, analyse and interpret the field data, experiment with the modelling parameters, the type of information to use and the 3D visualisation until an acceptable 3D geometry was obtained. This process can be seen as frustrating and found inefficient as compared to a (yet-to-be-found) fully automated solution. Nonetheless, even if new and welcome ways to translate geological knowledge into quantitative spatial

prediction methods are to be found in the future, and if the level of automation increases in future geomodelling workflows, geological reasoning (*sensu* Frodeman, 1995) will remain fundamental to judge on the geological realism of the results.

2.7.   Conclusions

We presented the new 3D structural model of the Northern Aosta Valley, built with a model-driven implicit modelling approach. Starting from a newly published 1:75,000 geological map and high resolution field structural data only, we built the conceptual model on vertical cross-sections integrating expert geological knowledge. The interpretation is performed following classic geological concepts and structural data projection techniques. The implicit interpolation of the model is performed in SKUA/GOCAD®, that implements both the Discrete Smooth Interpolator and the RING Toolkit interpolator. Together, the two interpolators allow the creation of the challenging geometries that outcrop in the Northern Aosta Valley such as hierarchical shear zones, recumbent isoclinal folds, tapered and lenticular geometries and a network of finite brittle faults whose surfaces and tip lines are internal to the 3D volume.

2.8.   Author contributions

AB conceived and supervised the project. DB acquired funding. AB, BM, GA and GDP carried out fieldwork in the study area and contributed to the tectonic legend, that was originally conceived by AB. BM and GDP managed the GIS and created the tectonic map of the study area (that will be submitted in an independent contribution), with inputs and discussion with AB. GA performed the structural data analysis, with inputs from AB and BM. AB and GA performed the structural interpretation in vertical cross-section, with feedbacks from BM and GDP. GA created the 3D structural model, with feedbacks and guidance by AB and GC. GA redacted the manuscript with inputs and contributions from AB and GC.

2.9.   Acknowledgements

unvaluable work on the tectonic map of the Northern Aosta Valley that is the synthesis of almost 70 years of fieldwork and detailed analysis.

2.10.   References

Antoine, P., 1971. La zone des brèches de Tarentaise entre Bourg-Saint-Maurice (vallée de l'Isère) et la frontière italo-suisse. Stratigraphie, Université de Grenoble 367 pp.

Argand, E., 1916. Sur l'arc des Alpes Occidentales. Eclogae Geologicae Helvetiae 14, 145–191.

Argand, E., 1911. Les nappes de recouvrement des Alpes pennines et leurs prolongements structuraux. Matériaux Pour La Carte Géologique de La Suisse 31, 1–26.

Argand, E., 1909. L'exploration géologique des Alpes pennines centrales. Bulletin de La Société Vaudoise Des Sciences Naturelles 45, 217–276.

Argand, E., 1906. Sur la tectonique du Massif de la Dent Blanche. Comptes Rendus de l'Académie Des Sciences Paris.

Ballèvre, M., Manzotti, P., 2019. Ductile shearing on top of the Eocene extruding wedge: the Combin Shear Zone. Emile Argand Conference on Alpine Geological Studies 2019. Sion, Switzerland, 4 pp.

Ballèvre, M., Merle, O., 1993. The Combin Fault: compressional reactivation of a Late Cretaceous-Early Tertiary detachment fault in the Western Alps. Schweizerische Mineralogische Und Petrographische Mitteilungen 73, 205–227. https://doi.org/https://doi.org/10/gfsjrz

Baretti, M., 1881. Apercu géologique sur la Chaine du Mont Blanc en rapport avec le traject probable d'un tunnel pour la nouvelle ligne de chemin de fer. Mem. Comité Local d'Aoste Promoteur de La Percée Du Mont Blanc, J. Candeletti Editeur-Imprimeur, Turin 38 pp.

Bearth, P., 1967. Die Ophiolithe der Zone von Zermatt-Saas Fee. Beiträge Zur Geologischen Karte Der Schweiz 132, 130 pp.

Beltrando, M., Frasca, G., Compagnoni, R., Vitale-Brovarone, A., 2012. The Valaisan controversy revisited: Multi-stage folding of a Mesozoic hyper-extended margin in the Petit St. Bernard pass area (Western Alps). Tectonophysics 579, 17–36. https://doi.org/10.1016/j.tecto.2012.02.010

Bergomi, M.A., Dal Piaz, G. V, Malusà, M.G., Monopoli, B., Tunesi, A., 2017. The Grand St Bernard-Briançonnais Nappe System and the Paleozoic Inheritance of the Western Alps Unraveled by Zircon U-Pb Dating. Tectonics 36, 2950–2972. https://doi.org/10.1002/2017TC004621

Bertrand, J.M., Aillères, L., Gasquet, D., 1996. The Pennine Front zone in Savoie (Western Alps), a review and new interpretations from the Zone Houillère Briançonnaise. Eclogae Geologicae Helvetiae 89, 298–320.

Bigi, G., Castellarin, A., Coli, M., Dal Piaz, G. V, Sartori, R., Scandone, P., Vai, G.B., 1990. Structural Model of Italy 1:500.000, Sheet 1, C.N.R. Progetto Geodinamica, SELCA Firenze. SELCA, Firenze.

Bistacchi, A., Dal Piaz, G., Massironi, M., Zattin, M., Balestrieri, M., 2001. The Aosta–Ranzola extensional fault system and Oligocene–Present evolution of the Austroalpine–Penninic wedge in the northwestern Alps. International Journal of Earth Sciences 90, 654–667. https://doi.org/10.1007/s005310000178

Bistacchi, A., Eva, E., Massironi, M., Solarino, S., 2000. Miocene to Present kinematics of the NW-Alps: evidences from remote sensing, structural analysis, seismotectonics and thermochronology. Journal of Geodynamics 30, 205–228. https://doi.org/https://doi.org/10.1016/S0264-3707(99)00034-4

Bistacchi, A., Massironi, M., 2000. Post-nappe brittle tectonics and kinematic evolution of the north-western Alps: an integrated approach. Tectonophysics 327, 267–292. https://doi.org/10.1016/S0040-1951(00)00206-7

Bistacchi, A., Massironi, M., Dal Piaz, Giorgio V, Dal Piaz, Giovanni, Monopoli, B., Schiavo, A., Toffolon, G., 2008. 3D fold and fault reconstruction with an uncertainty model: An example from an Alpine tunnel case study. Computers and Geosciences 34, 351–372. https://doi.org/10.1016/j.cageo.2007.04.002

Bond, C.E., 2015. Uncertainty in structural interpretation: Lessons to be learnt. Journal of Structural Geology 74, 185–200. https://doi.org/10.1016/j.jsg.2015.03.003

Bonetto, F., Dal Piaz, G.V., de Giusti, F., Massironi, M., Monopoli, B., Schiavo, A., 2010. Carta geologica della Valle d'Aosta alla scala 1:100.000. Regione Autonoma Valle d'Aosta, Dipartimento Difesa Del Suolo e Risorse Idriche, Tipografia Valdostana 23 pp.

Borradaile, G., 2003. Statistics of Earth Science Data. Springer Berlin Heidelberg, Berlin, Heidelberg. https://doi.org/10.1007/978-3-662-05223-5

Burri, M., 1983. Description geologique du front du St. Bernard dans les Vallees de Bagnes et d'Entremont. Eclogae Geologicae Helvetiae 76, 469–490.

Burri, M., Allimann, M., Chessex, R., Dal Piaz, G. V, Della Valle, G., Du Bois, L., Gouffon, Y., Guermani, A., Hagen, T., Krummenacher, D., Looser, M.O., 1998. Feuille 1346 Chanrion avec partie nord de la feuille 1366 Mont Vélan, Atlas géologique de la Suisse 1:25.000. Service hydrologique et géologique national, Berne.

Burri, M., Marro, C., 1993. Feuille 1345 Orsières, Atlas géologique de la Suisse 1:25.000. Service hydrologique et géologique national, Berne.

Caby, R., 1981. Le Mésozoïque de la zone du Combin en Val d'Aoste (Alpes Graies): Imbrications tectoniques entre séries issues des domaines pennique, austroalpin et océanique. Gèologie Alpine 57, 5–13.

Caby, R., 1968. Contribution à l'étude structurale des Alpes Occidentales: Subdivisions stratigraphiques et structure de la zone du Grand-Saint-Bernard dans la partie sud du Val d'Aoste (Italie). Géologie Alpine 44, 95–111.

Calcagno, P., Chilès, J.P., Courrioux, G., Guillen, A., 2008. Geological modelling from field data and geological knowledge. Part I. Modelling method coupling 3D potential-field interpolation and geological rules. Physics of the Earth and Planetary Interiors 171, 147–157. https://doi.org/10.1016/j.pepi.2008.06.013

Canepa, M., Castelletto, M., Cesare, B., Martin, S., Zaggia, L., 1990. The Austroapine Mont Mary nappe (Italian Western Alps). Memorie Scienze Geologiche 42, 1–17.

Carmichael, T., Ailleres, L., 2016. Method and analysis for the upscaling of structural data. Journal of Structural Geology 83, 121–133. https://doi.org/10.1016/j.jsg.2015.09.002

Carr, J.C., Beatson, R.K., Cherrie, J.B., Mitchell, T.J., Fright, W.R., McCallum, B.C., Evans, T.R., 2001. Reconstruction and representation of 3D objects with radial basis functions. Proceedings of the 28th Annual Conference on Computer Graphics and Interactive Techniques. Association for Computing Machinery, 67–76. https://doi.org/10.1145/383259.383266

Cartwright, I., Barnicoat, A.C., 2002. Petrology, geochronology, and tectonics of shear zones in the Zermatt-Saas and Combin zones of the Western Alps. Journal of Metamorphic Geology 20, 263–281. https://doi.org/10.1046/j.0263-4929.2001.00366.x

Caumon, G., 2010. Towards stochastic time-varying geological modeling. Math Geosci 42, 555–569. https://doi.org/10.1007/s11004-010-9280-y

Caumon, G., Collon-Drouaillet, P., Le Carlier de Veslud, C., Viseur, S., Sausse, J., 2009. Surface-Based 3D Modeling of Geological Structures. Mathematical Geosciences 41, 927–945. https://doi.org/10.1007/s11004-009-9244-2

Caumon, G., Gray, G., Antoine, C., Titeux, M.O., 2013. Three-dimensional implicit stratigraphic model building from remote sensing data on tetrahedral meshes: Theory and application to a regional model of la Popa Basin, NE Mexico. IEEE Transactions on Geoscience and Remote Sensing 51, 1613–1621. https://doi.org/10.1109/TGRS.2012.2207727

Caumon, G., Lepage, F., Sword, C.H., Mallet, J.L., 2004. Building and editing a sealed geological model. Mathematical Geology 36, 405–424. https://doi.org/10.1023/B:MATG.0000029297.18098.8a

Ceriani, S., Fügenschuh, B., Schmid, S.M., 2001. Multi-stage thrusting at the" Penninic Front" in the Western Alps between Mont Blanc and Pelvoux massifs. Int J Earth Sci 90, 685–702. https://doi.org/10.1007/s005310000188

Cita, B.M., 1953. Studi geologici sulla Valle Ferret italiana. Bollettino Del Servizio Geologico Italiano 75, 65–172.

Compagnoni, R., 2003. HP metamorphic belt of the western Alps. Episodes 26, 200–204. https://doi.org/10.18814/EPIIUGS/2003/V26I3/008

Compagnoni, R., Dal Piaz, G. V, Hunziker, J.C., Gosso, G., Lombardo, B., Williamns, P.F., 1977. The Sesia-Lanzo zone, a slice of continental crust with Alpine high pressure-low temperature assem-blages in the Western Italian Alps. Rendiconti Della Società Italiana Di Mineralogia e Petrologia 33, 281–334.

Cortiana, G., Dal Piaz, G. V, Del Moro, A., Hunziker, J.C., Martin, S., 1998. 40Ar-39Ar and Rb-Sr dating on the Pillonet klippe and frontal Sesia-Lanzo zone in the Ayas valley and evolution of the western Austroalpine nappe stack. Memorie Scienze Geologiche 50, 177–194.

Dal Piaz, G., Cortiana, G., Del Moro, A., Martin, S., Pennacchioni, G., Tartarotti, P., 2001. Tertiary age and paleostructural inferences of the eclogitic imprint in the Austroalpine outliers and Zermatt–Saas ophiolite, western Alps. International Journal of Earth Sciences 90, 668–684. https://doi.org/10.1007/s005310000177

Dal Piaz, G.V., 2001. Geology of the Monte Rosa massif: historical review and personal comments. Schweizerische Mineralogische Und Petrographische Mitteilungen 81, 273–303. https://doi.org/https://doi.org/10.5169/SEALS-61694

Dal Piaz, G.V., 1976. Il lembo di ricoprimento del Pillonet: falda della Dent Blanche nelle Alpi occidentali. Memorie Istituti Geologia Mineralogia Università Di Padova 31, 60 pp.

Dal Piaz, G.V., 1965. La formazione mesozoica dei calcescisti con pietre verdi fra la Valsesia e la Valtournanche ed i suoi rapporti strutturali con il ricoprimento del Monte Rosa e con la Zona SesiaLanzo. Bollettino Della Società Geologica Italiana 84, 67–104.

Dal Piaz, G.V., Bistacchi, A., Gianotti, F., Monopoli, B., Passeri, L., Schiavo, A., Bertolo, D., Bonetto, F., Ciarapica, G., Dal Piaz, G., Gouffon, Y., Massironi, M., Ratto, S., Toffolon, G., 2016. Foglio 070 Cervino e Note Illustrative. Carta Geologica d'Italia Alla Scala 1:50.000, ISPRA, Regione Autonoma Valle d'Aosta 432 pp.

Dal Piaz, G.V., Gianotti, F., Monopoli, B., Pennacchioni, G., Tartarotti, P., Schiavo, A., Carraro, F., Bistacchi, A., Massironi, M., Martin, S., Ratto, S., 2010. Foglio 091 Chatillon e Note Illustrative. Carta Geologica d'Italia Alla Scala 1:50.000, ISPRA, Regione Autonoma Valle d'Aosta 152 pp.

Dal Piaz, G. V, 2004. From the European continental margin to the Mesozoic Tethyan ocean: A geological map of the upper Ayas valley (Western Alps). In: Pasquarè, G., Venturini, C. (Eds.), Mapping Geology in Italy. APAT-Dip. Difesa del Suolo-Servizio Geolologico d'Italia, S.E.L.C.A., Firenze, 265–272.

Dal Piaz, G. V, 1999. The Austroalpine-Piedmont nappe stack and the puzzle of Alpine Tethys. Memorie Scienze Geologiche 53, 153–162.

Dal Piaz, G. V, Bistacchi, A., Massironi, M., 2003. Geological outline of the Alps. Episodes Journal of International Geoscience 26, 175–180. https://doi.org/10.18814/EPIIUGS/2003/V26I3/004

Dal Piaz, G. V, Sacchi, R., 1969. Osservazioni geologiche sul lembo di ricoprimento del Pillonet (Dent Blanche l.s.). Memorie Scienze Geologiche 8, 835–846.

de Kemp, E.A., 2000. 3-D visualization of structural field data: Examples from the Archean Caopatina Formation, Abitibi greenstone belt, Québec, Canada. Computers and Geosciences 26, 509–530. https://doi.org/10.1016/S0098-3004(99)00142-9

De La Varga, M., Schaaf, A., Wellmann, F., 2019. GemPy 1.0: Open-source stochastic geological modeling and inversion. Geoscientific Model Development 12, 1–32. https://doi.org/10.5194/gmd-12-1-2019

Elter, G., 1960. La zona Pennidica dell'alta e media Valle d'Aosta con carta tettonica al 1:100.000. Memorie Istituti Geologia Mineralogia Università Di Padova 22, 113 pp.

Elter, G., Elter, P., 1965. Carta geologica della regione del Piccolo S. Bernardo (versante italia-no). Note Illustrative, Memorie Istituti Geologia Mineralogia Università Di Padova 25, 53 pp.

Ernst, W.G., Dal Piaz, G. V, 1978. Mineral parageneses of eclogitic rocks and related mafic schists of the Piemonte ophiolite nappe, Breuil-St. Jacques area, Italian Western Alps. American Mineralogist 63, 621–640.

Escher, A., Masson, H., Steck, A., 1988. Coupes géologiques des Alpes occidentales suisses. Mémoires de Géologie de l'Université de Lausanne 2, 5–11.

Frank, T., Tertois, A.L., Mallet, J.L., 2007. 3D-reconstruction of complex geological interfaces from irregularly distributed and noisy point data. Computers and Geosciences 33, 932–943. https://doi.org/10.1016/j.cageo.2006.11.014

Frey, M., Hunziker, J.C., Frank, W., Bocquet, J., Dal Piaz, G.V., Jäger, E., Niggli, E., 1974. Alpine metamorphism of the Alps: a review. Schweiz. Mineral. Petrogr. Mitt. 54, 247–290.

Frezzotti, M.L., Huizenga, J.M., Compagnoni, R., Selverstone, J., 2014. Diamond formation by carbon saturation in C-O-H fluids during cold subduction of oceanic lithosphere. Geochimica et Cosmochimica Acta 143, 68–86. https://doi.org/10.1016/J.GCA.2013.12.022

Frodeman, R., 1995. Geological reasoning: Geology as an interpretive and historical science. Geological Society of America Bulletin 107, 960–0968. https://doi.org/10.1130/0016-7606(1995)107<0960:GRGAAI>2.3.CO;2

Gardien, V., Reusser, E., Marquer, D., 1994. Pre-Alpine metamorphic evolution of the gneisses from the Valpelline Series (Western Alps, Italy). Schweizerische Mineralogische Und Petrographische Mitteilungen 74, 489–502.

Giraud, J., Caumon, G., Grose, L., Ogarko, V., Cupillard, P., 2023. Integration of automatic implicit geological modelling in deterministic geophysical inversion. EGUsphere Preprint. https://doi.org/10.5194/egusphere-2023-129

Giusti, F. De, Dal Piaz, G. V, Massironi, M., Schiavo, A., 2003. Carta geotettonica della Valle d'Aosta. Memorie Scienze Geologiche 55, 129–149.

Godefroy, G., Caumon, G., Ford, M., Laurent, G., Jackson, C.A.-L., 2018. A parametric fault displacement model to introduce kinematic control into modeling faults from sparse data. Interpretation 6, B1–B13. https://doi.org/10.1190/INT-2017-0059.1

Gouffon, Y., 1993. Géologie de la" nappe" du Grand St-Bernard entre la Doire Baltée et la frontière suisse (Vallée d'Aoste-Italie). Mémoires de Géologie de l'Université de Lausanne 12, 1–147.

Grose, L., Ailleres, L., Laurent, G., Jessell, M., 2021. LoopStructural 1.0: Time-aware geological modelling. Geoscientific Model Development 14, 3915–3937. https://doi.org/10.5194/gmd-14-3915-2021

Grose, L., Laurent, G., Aillères, L., Armit, R., Jessell, M., Caumon, G., 2017. Structural data constraints for implicit modeling of folds. Journal of Structural Geology 104, 80–92. https://doi.org/10.1016/j.jsg.2017.09.013

Guillen, A., Calcagno, P., Courrioux, G., Joly, A., Ledru, P., 2008. Geological modelling from field data and geological knowledge. Part II. Modelling validation using gravity and magnetic data inversion. Physics of the Earth and Planetary Interiors 171, 158–169. https://doi.org/10.1016/j.pepi.2008.06.014

Hassen, I., Gibson, H., Hamzaoui-Azaza, F., Negro, F., Rachid, K., Bouhlila, R., 2016. 3D geological modeling of the Kasserine Aquifer System, Central Tunisia: New insights into aquifer-geometry and interconnections for a better assessment of groundwater resources. Journal of Hydrology 539, 223–236. https://doi.org/10.1016/J.JHYDROL.2016.05.034

Hillier, M., de Kemp, E., Schetselaar, E., 2013. 3D form line construction by structural field interpolation (SFI) of geologic strike and dip observations. Journal of Structural Geology 51, 167–179. https://doi.org/https://doi.org/10.1016/j.jsg.2013.01.012

Hillier, M.J., Schetselaar, E.M., de Kemp, E.A., Perron, G., 2014. Three-Dimensional Modelling of Geological Surfaces Using Generalized Interpolation with Radial Basis Functions. Mathematical Geosciences 46, 931–953. https://doi.org/10.1007/s11004-014-9540-3

Houlding, S.W., 1994. The Geological Characterization Process. 3D Geoscience Modeling. Springer Berlin Heidelberg, Berlin, Heidelberg, 7–26. https://doi.org/10.1007/978-3-642-79012-6_2

Irakarama, M., Laurent, G., Renaudeau, J., Caumon, G., 2018. Finite Difference Implicit Modeling of Geological Structures. 80th EAGE Conference and Exhibition 2018: Opportunities Presented by the Energy Transition. European Association of Geoscientists and Engineers, EAGE, 1–5. https://doi.org/10.3997/2214-4609.201800794

Irakarama, M., Thierry-Coudon, M., Zakari, M., Caumon, G., 2022. Finite Element Implicit 3D Subsurface Structural Modeling. Computer-Aided Design 149, 103267. https://doi.org/10.1016/j.cad.2022.103267

Jessell, M., Aillères, L., de Kemp, E., Lindsay, M., Wellmann, F., Hillier, M., Laurent, G., Carmichael, T., Martin, R., 2014. Next Generation Three-Dimensional Geologic Modeling and Inversion. Building Exploration Capability for the 21st Century. Society of Economic Geologists. https://doi.org/10.5382/SP.18.13

Jessell, M., Ogarko, V., de Rose, Y., Lindsay, M., Joshi, R., Piechocka, A., Grose, L., de la Varga, M., Ailleres, L., Pirot, G., 2021. Automated geological map deconstruction for 3D model construction using map2loop 1.0 and map2model 1.0. Geoscientific Model Development 14, 5063–5092. https://doi.org/10.5194/gmd-14-5063-2021

Jessell, M.W., Ailleres, L., de Kemp, E.A., 2010. Towards an integrated inversion of geoscientific data: What price of geology? Tectonophysics 490, 294–306. https://doi.org/10.1016/J.TECTO.2010.05.020

Kaufmann, O., Martin, T., 2009. Reprint of "3D geological modelling from boreholes, cross-sections and geological maps, application over former natural gas storages in coal mines" [Comput. Geosci. 34 (2008) 278-290]. Computers and Geosciences 35, 70–82. https://doi.org/10.1016/S0098-3004(08)00227-6

Kroeger, K.F., Crutchley, G.J., Kellett, R., Barnes, P.M., 2019. A 3-D Model of Gas Generation, Migration, and Gas Hydrate Formation at a Young Convergent Margin (Hikurangi Margin, New Zealand). Geochemistry, Geophysics, Geosystems 20, 5126–5147. https://doi.org/10.1029/2019GC008275

Lajaunie, C., Courrioux, G., Manuel, L., 1997. Foliation fields and 3D cartography in geology: Principles of a method based on potential interpolation. Mathematical Geology 29, 571–584. https://doi.org/10.1007/BF02775087

Lapen, T.J., Johnson, C.M., Baumgartner, L.P., Dal Piaz, G. V, Skora, S., Beard, B.L., 2007. Coupling of oceanic and continental crust during Eocene eclogite-facies metamorphism: evidence from the Monte Rosa nappe, western Alps. Contributions to Mineralogy and Petrology 153, 139–157. https://doi.org/10.1007/s00410-006-0144-x

Lardeaux, J.M., Spalla, M.I., 1991. From granulites to eclogites in the Sesia zone (Italian Western Alps): a record of the opening and closure of the Piedmont ocean. Journal of Metamorphic Geology 9, 35–59. https://doi.org/10.1111/j.1525-1314.1991.tb00503.x

Laurent, G., 2016. Iterative Thickness Regularization of Stratigraphic Layers in Discrete Implicit Modeling. Mathematical Geosciences 48, 811–833. https://doi.org/10.1007/s11004-016-9637-y

Laurent, G., Ailleres, L., Grose, L., Caumon, G., Jessell, M., Armit, R., 2016. Implicit modeling of folds and overprinting deformation. Earth and Planetary Science Letters 456, 26–38. https://doi.org/10.1016/j.epsl.2016.09.040

Laurent, G., Caumon, G., Bouziat, A., Jessell, M., 2013. A parametric method to model 3D displacements around faults with volumetric vector fields. Tectonophysics 590, 83–93. https://doi.org/10.1016/j.tecto.2013.01.015

Liang, Z., Wellmann, F., Ghattas, O., 2023. Uncertainty quantification of geologic model parameters in 3D gravity inversion by Hessian-informed Markov chain Monte Carlo. Geophysics 88, G1–G18. https://doi.org/10.1190/geo2021-0728.1

Loprieno, A., Bousquet, R., Bucher, S., Ceriani, S., Dalla Torre, F.H., Fügenschuh, B., Schmid, S.M., 2011. The Valais units in Savoy (France): a key area for understanding the palaeogeography and the tectonic evolution of the Western Alps. International Journal of Earth Sciences 100, 963–992. https://doi.org/https://doi.org/10.1007/s00531-010-0595-1

Mallet, J.-L., 2014. Elements of Mathematical Sedimentary Geology: the GeoChron Model. EAGE Publications 374 pp. https://doi.org/10.3997/9789462820081

Mallet, J.-L., 2004. Space – Time Mathematical Framework for Sedimentary Geology. Math. Geol. 36, 1–32.

Malusà, M.G., Polino, R., Martin, S., 2005. The Gran San Bernardo nappe in the Aosta valley (western Alps): a composite stack of distinct continental crust units. Bulletin de La Société Géologique de France 176, 417–431. https://doi.org/10.2113/176.5.417

Manzotti, P., Ballèvre, M., Dal Piaz, G.V., 2017. Continental gabbros in the Dent Blanche Tectonic System (Western Alps): from the pre-Alpine crustal structure of the Adriatic palaeo-margin to the geometry of an alleged subduction interface. Journal of the Geological Society 174, 541–556. https://doi.org/10.1144/jgs2016-071

Manzotti, P., Ballèvre, M., Pitra, P., Schiavi, F., 2021. Missing lawsonite and aragonite found: P–T and fluid composition in meta-marls from the Combin Zone (Western Alps). Contributions to Mineralogy and Petrology 176, 60. https://doi.org/10.1007/s00410-021-01818-0

Manzotti, P., Ballèvre, M., Zucali, M., Robyr, M., Engi, M., 2014a. The tectonometamorphic evolution of the Sesia-Dent Blanche nappes (internal Western Alps): review and synthesis. Swiss Journal of Geosciences 107, 309–336. https://doi.org/10.1007/s00015-014-0172-x

Manzotti, P., Zucali, M., Ballèvre, M., Robyr, M., Engi, M., 2014b. Geometry and kinematics of the Roisan-Cignana Shear Zone, and the orogenic evolution of the Dent Blanche Tectonic System (Western Alps). Swiss Journal of Geosciences 107, 23–47. https://doi.org/10.1007/s00015-014-0157-9

Maxelon, M., Mancktelow, N.S., 2005. Three-dimensional geometry and tectonostratigraphy of the Pennine zone, Central Alps, Switzerland and Northern Italy. Earth-Science Reviews 71, 171–227. https://doi.org/10.1016/j.earscirev.2005.01.003

Maxelon, M., Renard, P., Courrioux, G., Brändli, M., Mancktelow, N., 2009. A workflow to facilitate three-dimensional geometrical modelling of complex poly-deformed geological units. Computers & Geosciences 35, 644–658. https://doi.org/10.1016/j.cageo.2008.06.005

Milicich, S.D., Pearson-Grant, S.C., Alcaraz, S., White, P.A., Tschritter, C., 2018. 3D Geological modelling of the Taupo Volcanic Zone as a foundation for a geothermal reservoir model. New Zealand Journal of Geology and Geophysics 61, 79–95. https://doi.org/10.1080/00288306.2017.1407346

Milnes, A.G., Greller, M., Müller, R., 1981. Sequence and style of major post-nappe structures, Simplon—Pennine Alps. Journal of Structural Geology 3, 411–420. https://doi.org/10.1016/0191-8141(81)90041-9

Nicolas, A., Polino, R., Hirn, A., Nicolich, R., 1990. ECORS-CROP traverse and deep structure of the western Alps: a synthesis. Mem. Soc. Geol. Fr 156, 15–27.

Pantet, A., Epard, J.L., Masson, H., 2020. Mimicking Alpine thrusts by passive deformation of synsedimentary normal faults: a record of the Jurassic extension of the European margin (Mont Fort nappe, Pennine Alps). Swiss Journal of Geosciences 113, 1–25. https://doi.org/https://doi.org/10.1186/s00015-020-00366-2

Perello, P., Gianotti, F., Monopoli, B., Carraro, F., Venturini, G., Fontan, D., Schiavo, A., Bonetto, F., 2011. Foglio 089 Courmayeur e Note Illustrative. Carta Geologica d'Italia Alla Scala 1:50.000, ISPRA, Regione Autonoma Valle d'Aosta 152 pp.

Perrin, M., Zhu, B., Rainaud, J.F., Schneider, S., 2005. Knowledge-driven applications for geological modeling. Journal of Petroleum Science and Engineering 47, 89–104. https://doi.org/10.1016/J.PETROL.2004.11.010

Pfiffner, O.A., Lehener, P., Heitzmann, P., Mueller, S., Steck, A., 1997. Deep Structure of the Swiss Alps: Results from NRP 20. Birkhäuser, Basel.

Philippon, M., de Veslud, C.L.C., Gueydan, F., Brun, J.P., Caumon, G., 2015. 3D geometrical modelling of post-foliation deformations in metamorphic terrains (Syros, Cyclades, Greece). Journal of Structural Geology 78, 134–148. https://doi.org/10.1016/j.jsg.2015.07.002

Pizzella, L., Alais, R., Lopez, S., Freulon, X., Rivoirard, J., 2022. Taking Better Advantage of Fold Axis Data to Characterize Anisotropy of Complex Folded Structures in the Implicit Modeling Framework. Mathematical Geosciences 54, 95–130. https://doi.org/10.1007/s11004-021-09950-0

Polino, R., Malusà, M.G., S, M., Carraro, F., Gianotti, F., Bonetto, F., Perello, P., Schiavo, A., Gouffon, Y., 2015. Foglio 090 Aosta e Note Illustrative. Carta Geologica d'Italia Alla Scala 1:50.000, ISPRA, Regione Autonoma Valle d'Aosta 144 pp.

Reddy, S.M., Wheeler, J., Butler, R.W.H., Cliff, R.A., Freeman, S., Inger, S., Pickles, C., Kelley, S.P., 2003. Kinematic reworking and exhumation within the convergent Alpine Orogen. Tectonophysics 365, 77–102. https://doi.org/10.1016/S0040-1951(03)00017-9

Reinecke, T., 1991. Very-high-pressure metamorphism and uplift of coesite-bearing metasediments from the Zermatt-Saas zone, Western Alps. European Journal of Mineralogy 3, 7–18.

Renaudeau, J., Malvesin, E., Maerten, F., Caumon, G., 2019. Implicit Structural Modeling by Minimization of the Bending Energy with Moving Least Squares Functions. Mathematical Geosciences 51, 693–724. https://doi.org/10.1007/s11004-019-09789-6

Sartori, M., Gouffon, Y., Marthaler, M., 2006. Harmonisation et définition des unités lithostra-tigraphiques briançonnaises dans les nappes penniques du Valais. Eclogae Geologicae Helvetiae 99, 363–407.

Sides, E.J., 1997. Geological modelling of mineral deposits for prediction in mining. Geologische Rundschau 86, 342–353. https://doi.org/https://doi.org/10.1007/s005310050145

Soldo, L., Arienti, G., Bistacchi, A., Mezzanzanica, M., Regondi, L., Pizzarotti, E.M., 2022. Modellazione Geologica digitale e sua integrazione nelle moderne metodologie di progetto di opere infrastrutturali - Digital Geological Modelling within the modern infrastructure design methodologies. Gallerie e Grandi Opere Sotterranee 142, 27–40.

Steck, A., Masson, H., Robyr, M., 2015. Tectonics of the Monte Rosa and surrounding nappes (Switzerland and Italy): Tertiary phases of subduction, thrusting and folding in the Pennine Alps. Swiss Journal of Geosciences 108, 3–34. https://doi.org/10.1007/s00015-015-0188-x

Sue, C., Delacou, B., Champagnac, J.D., Allanic, C., Tricart, P., Burkhard, M., 2007. Extensional neotectonics around the bend of the Western/Central Alps: An overview. International Journal of Earth Sciences 96, 1101–1129. https://doi.org/10.1007/S00531-007-0181-3

Thanh, H.V., Sugai, Y., Nguele, R., Sasaki, K., 2019. Integrated workflow in 3D geological model construction for evaluation of CO2 storage capacity of a fractured basement reservoir in Cuu Long Basin, Vietnam. International Journal of Greenhouse Gas Control 90, 102826. https://doi.org/10.1016/J.IJGGC.2019.102826

Thornton, J.M., Mariethoz, G., Brunner, P., 2018. A 3D geological model of a structurally complex alpine region as a basis for interdisciplinary research. Scientific Data 5, 180238. https://doi.org/10.1038/sdata.2018.238

Trümpy, R., 1955. Remarques sur la correlation des unites penniques externes entre la Savoie et le Valais et sur l'origine des nappes pre´alpines. Bulletin De La Societe Geologique De France 5, 217–231.

Trümpy, R., 1954. La zone de Sion-Courmayeur dans le haut Val Ferret valaisan. Eclogae Geologicae Helvetiae 47, 317–359.

Trümpy, R., 1952. Sur les racines helvétiques et les «Schistes lustrés» entre le Rhône et la Vallée de Bagnes (Région de la Pierre Avoi). Eclogae Geologicae Helvetiae 44, 338–347.

Vollgger, S.A., Cruden, A.R., Ailleres, L., Cowan, E.J., 2015. Regional dome evolution and its control on ore-grade distribution: Insights from 3D implicit modelling of the Navachab gold deposit, Namibia. Ore Geology Reviews 69, 268–284. https://doi.org/https://doi.org/10.1016/j.oregeorev.2015.02.020

Vollmer, F.W., 1995. C program for automatic contouring of spherical orientation data using a modified Kamb method. Computers and Geosciences 21, 31–49. https://doi.org/10.1016/0098-3004(94)00058-3

von Raumer, J.F., Bussy, F., 2004. Mont Blanc and Aiguilles Rouges; geology of their polymetamorphic basement (External massifs, Western Alps, France-Switzerland). Mémoires de Géologie (Lausanne) 42, 1–203.

Wellmann, F., Caumon, G., 2018. 3-D Structural geological models: Concepts, methods, and uncertainties. Advances in Geophysics 59, 1–121. https://doi.org/10.1016/bs.agph.2018.09.001

Wheeler, J., Butler, R.W.H., 1993. Evidence for extension in the western Alpine orogen: the contact between the oceanic Piemonte and overlying continental Sesia units. Earth and Planetary Science Letters 117, 457–474. https://doi.org/10.1016/0012-821X(93)90097-S

Xiong, Z., Guo, J., Xia, Y., Lu, H., Wang, M., Shi, S., 2018. A 3D Multi-scale geology modeling method for tunnel engineering risk assessment. Tunnelling and Underground Space Technology 73, 71–81. https://doi.org/10.1016/J.TUST.2017.12.003

Zanchi, A., Francesca, S., Stefano, Z., Simone, S., Graziano, G., 2009. 3D reconstruction of complex geological bodies: Examples from the Alps. Computers and Geosciences 35, 49–69. https://doi.org/10.1016/j.cageo.2007.09.003

<div align="right">Chapter 3</div>

3D structural implicit modelling of folded metamorphic units at Lago di Cignana with uncertainty assessment

Gloria Arienti[1], Andrea Bistacchi[1], Guillaume Caumon[2.3], Giovanni Dal Piaz[4], Bruno Monopoli[4]

[1]Dipartimento di Scienze dell'Ambiente e della Terra, Università degli Studi di Milano-Bicocca, 20126 Italy
[2]RING, GeoRessources – ENSG, Université de Lorraine - CNRS, 54000 France
[3]Institut Universitaire de France (IUF), 75000 France
[4]LTS s.r.l., Treviso, 31020 Italy

Abstract

We present a modelling workflow for the creation of a small-scale, three-dimensional representation of the tectonic architecture exposed in the Lago di Cignana region within the Italian Pennine Alps. The model portrays notable tectonic boundaries such as the Dent Blanche Basal Thrust, the Combin Fault and the Roisan-Cignana Shear Zone. Our approach employs the implicit Discrete Smooth Interpolator, which represents the tectonic sequence as a volumetric scalar field generalising a relative distance function. The interpolation process is constrained by geological and structural data collected during fieldwork. To model the folds that outcrop in the region, we perform three-dimensional interpolation of fold axes, and we enforce these interpolated directions on the folded geometries through the imposition of tangent constraints. Furthermore, we integrate structural uncertainties through stochastic simulations of fold axes away from direct observations, by mirroring the spherical distributions derived from primary observations. We employ the uncertainty analysis on isoclinal recumbent folds exposed in the area, and the outcomes indicate partial rotation within segments of the folds, the possibility of closures along the axial plane, and higher uncertainties localised at the fold hinges.

3.1. Introduction

Three-dimensional structural models are numerical representations of the geological subsurface. When depicting metamorphic terrains, their creation is a challenging task that requires understanding of both the ductile and brittle deformation and metamorphic processes responsible for the progressive development of the tectonic architecture, and the utilisation of geomodelling workflows for their

representation (e.g., Maxelon and Mancktelow, 2005). Geomodelling algorithms therefore require the ability to handle structures such as isoclinal and/or recumbent folds, organised with disharmonic and multi-scale patterns, shear zones with hierarchical relationships that define large thickness variations, and networks of faults.

The implicit geomodelling approach, which represents geological boundaries as isovalue surfaces inside a three-dimensional scalar field (Lajaunie et al., 1997), constitutes an effective method for addressing these challenges (e.g., Maxelon and Mancktelow, 2005; Bistacchi et al., 2008; Maxelon et al., 2009; Hillier et al., 2013; Philippon et al., 2015; Vollgger et al., 2015; de Kemp et al., 2016; Schneeberger et al., 2017; Thornton et al., 2018; Arienti et al., 2024 – Chapter 2). The approach is based on modelling principles first theorised by Houlding (1994) and Lajaunie et al. (1997), and it is also known as scalar potential field method (Chilès et al., 2004). Constrained by geological data, the method builds an analogy between a volumetric scalar field and the relative distance among geological boundaries, enabling the simultaneous integration of geological information, fault data and unconformities to build a model that is consistent with field observation.

The interpolation of implicit 3D models can be controlled by structural information (e.g., foliation measurements, fold axes and mineralogical lineation data), by imposing orientation constraints on the gradient of the scalar field (Frank et al., 2007; Calcagno et al., 2008; Caumon et al., 2013; Hillier et al., 2013, 2014; Laurent et al., 2016; Grose et al., 2017). This ability can be further extended to the interpolation of vectorial fields for the propagation of structural data in the three-dimensional space. Such approach has been employed for the modelling of complexly folded terrains by Hillier et al. (2013) through the interpolation of strike and dip data, and by Laurent et al. (2016) and Grose et al. (2017) through the definition and propagation of fold parameters, enhancing geological knowledge and realism.

The implicit geomodelling approach moreover offers swift adaptability to changes in the input constraining database. The efficiency in updating the interpretation when new data becomes available paves the way to the incorporation of uncertainty analysis and stochastic simulations in the geomodelling workflows (Chilès et al., 2004; Caumon et al., 2007; Wellmann et al., 2010; Lindsay et al., 2012; Wellmann and Regenauer-Lieb, 2012; Cherpeau and Caumon, 2015; Grose et al., 2018, 2019; Pakyuz-Charrier et al., 2018), strengthening the robustness of the outcomes and capturing uncertainties related to the modelling framework (i.e., structural input database, geological knowledge and modelling algorithm).

The northwestern Alps, with a complex architecture shaped by processes of metamorphic nappe emplacement (Schmid et al., 2004) and a history of more than two centuries of geological investigations (Dal Piaz, 2001), serve as an ideal natural laboratory to further explore the application of implicit geomodelling algorithms to mountainous settings. In this study, we employ the implicit approach for

the representation of the metamorphic units exposed in the vicinity of the Lago di Cignana (Cignana Lake, 2,149 m a.s.l.), Becca di Salè (Mount Salè, 3,107 m a.s.l.) and Mont Pancherot (Mount Pancherot, 2,614 m a.s.l.). This area has recently been the subject of a regional-scale 3D modelling project covering ca. 1,500 km^2, extending from the Mont Blanc to the Monte Rosa (Arienti et al., 2024 – Chapter 2). In the present work we revisit and enhance the three-dimensional representation of the Cignana area by significantly improving the model's resolution and detailing the fold geometries that could not appear in the previous regional interpretation because sub-scale compared to the regional model's resolution. After summarising the geological context and the tectonic history of the rock units exposed within the study area, we introduce the geomodelling workflow and present the modelled outcomes.

3.2.   Geological and tectonic setting

The northwestern Alps occupy a central position within the tectonic framework of the Alpine belt and are noteworthy for exposing the remnants of the fossil oceanic-continental suture between the European and Adriatic plates (Steck et al., 1999; Dal Piaz et al., 2003). This tectonic suture can be traced following the ophiolitic units of the Piedmont nappe system, which are now interleaved between the juxtaposed Austroalpine nappe system and the underlying Penninic units, respectively associated with rocks from the Adriatic and European passive margins (Dal Piaz et al., 2003). Collectively, this tectonic sequence forms the Austroalpine-Penninic collisional wedge (Dal Piaz and Ernst, 1978), marked by a blueschist-to-eclogite-facies imprint of Cretaceous-Eocene age and a Barrovian overprint (Dal Piaz et al., 2003). Within this collisional wedge, we recognise different tectono-metamorphic units as discrete crustal elements characterised by specific associations of lithology, metamorphic conditions and tectonic evolution, stacked along tectonic boundaries that underwent a complex history of both contractional and extensional events (e.g., Reddy et al., 2003; Manzotti et al., 2014a) that also reworked and transposed fabrics internal to the tectonic units.

The Cignana area, which exposes rock units from both the Austroalpine and Piedmont systems, is situated within the Austroalpine-Penninic collisional wedge. The continental component is represented by the Dent Blanche-Sesia Lanzo system (Argand, 1909, 1911; Manzotti et al., 2014a), a major composite system of thrust sheets of which only the Dent Blanche system, Argand's (1906) Dent Blanche nappe *sensu lato* (DB s.l.), outcrops in our study area. This tectonic stack is in turn distinguished into two subnappes, the overlying Dent Blanche nappe *sensu stricto* (DB s.s.) and the underlying Mont Mary superunit. These are separated by the Roisan-Cignana Shear Zone (RCSZ), a corridor of metasediments and basement rocks that experienced high localised deformation (Manzotti et al., 2014b). The spatial and structural relationships among these tectonic units are represented in Fig. 3.1, using the same acronyms employed in this section.

Within the portion of the DB s.s. nappe exposed in our model, we identify the Arolla unit (AR),

composed of Permian-age intrusive bodies that underwent Alpine blueschist to greenschist facies metamorphism (Compagnoni et al., 1977). The RCSZ, which demarcates the lower boundary of the DB s.s., is composed of metasediments from Mesozoic non-oceanic sequences (traditionally called Roisan zone; Diehl, 1952) and slivers of basement rocks from AR and the Mont Mary superunit. According to Manzotti et al. (2014a), the tectonic amalgamation within the RCSZ occurred under blueschist facies metamorphic conditions during the Alpine subduction process. This was coupled with isoclinal folding under top-to-NW sense of shear kinematics. Subsequent greenschist facies re-equilibration took place during nappe exhumation and large-scale folding of the units.

Bounding RCSZ in lower tectonic positions we recognise the Mont Mary superunit, which is further distinguished into two tectono-metamorphic units that share strong similarities with the DB s.s. (Dal Piaz et al., 2016). The upper unit (MM), akin to the upper unit of the DB s.s. which is however not comprised in our model area, consists of mainly high-grade paragneisses (kinzigites and migmatites). It is tectonically juxtaposed with the lower Mont Mary unit (MY), which includes gneisses and meta-pelites that experienced Alpine blueschist peak metamorphism (Canepa et al., 1990). Both units underwent Alpine greenschist facies metamorphism during nappe exhumation (Diehl et al., 1952; Manzotti, 2011; Dal Piaz et al., 2016).

The basal tectonic contact of the DB s.l. is marked by the Dent Blanche Basal Thrust (DBBT; Wust and Silverberg, 1989). In lower structural positions lies the ophiolitic Combin zone (CO), which is part of the Piedmont nappe system, the remnant of the Mesozoic Piedmont-Ligurian ocean. The DBBT is believed to have served as the subduction interface and it records multiple Eocene-age reactivations under decreasing greenschist facies conditions, with both reverse- and normal-sense kinematics (Wust and Silverberg, 1989; Kirst, 2017).

CO displays an ophiolitic succession of terrigenous metasediments, metabasalts, metagabbros and serpentinites (Ernst and Dal Piaz, 1978). Within our study area, it can be further subdivided into an upper and lower unit, separated by the Pancherot-Cime Bianche-Bettaforca unit (PCB; Passeri et al., 2018). PCB is a decollement cover unit, detached from an uncertain basement, showing affinities with the sedimentary succession of the Austroalpine nappe system (Dal Piaz, 1999). It is interpreted as a remnant of the sedimentary cover of extensional allochtons positioned along the ocean-continent transition, in proximity of Adria (Passeri et al., 2018). CO underwent metamorphism peaking at blueschist facies conditions (Caby, 1981; Manzotti et al., 2021), and both CO and PCB experienced metamorphism under greenschist facies conditions during post-collisional times (Ernst and Dal Piaz, 1978).
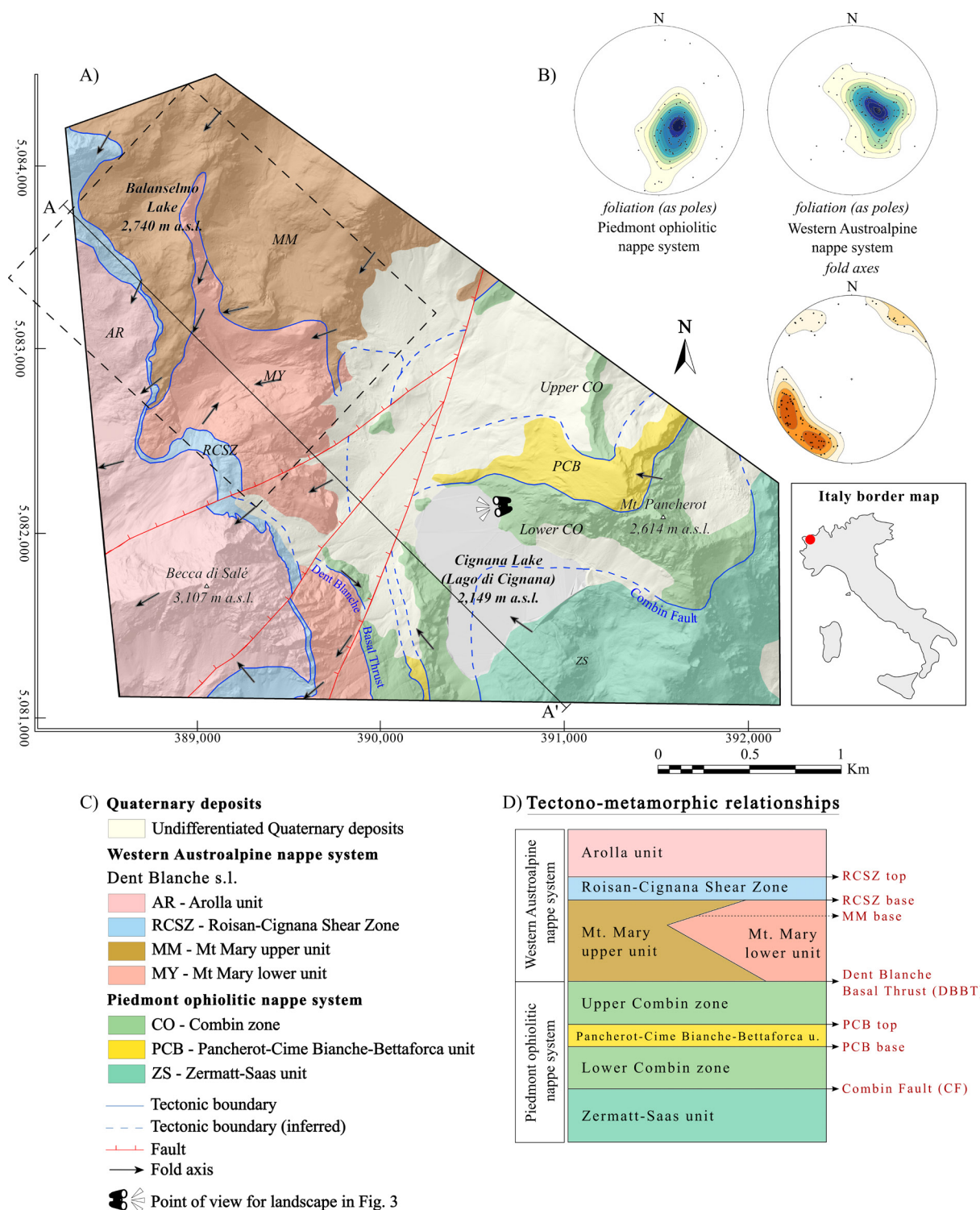
Figure 3.1. Surface input data of the Cignana Lake region. A) structural map, coordinates as WGS 1984 UTM Zone 32N. Black dashed rectangle represents the subarea for the uncertainty analysis detailed in Sect. 3.3.6. B) Normal to foliation planes are plotted as dot in stereograms, with Kamb contouring interval 1 σ (Cardozo and Allmendinger, 2013; Allmendinger et al., 2015). Fold axes measured in the field represented as dots in stereogram, with Kamb contouring interval 1.5 σ. C) Tectonic legend. D) Scheme of the tectono-metamorphic relationships.

The Combin Fault (CF; Ballèvre and Merle, 1993), the second major Alpine contact exposed within the Cignana area, forms the lower boundary of CO and separates it from the underlying Zermatt-Saas unit (ZS). ZS is an ophiolitic sequence comprising serpentinites, peridotites, metagabbros and metabasalts (Dal Piaz and Ernst, 1978). This unit experienced eclogite facies metamorphism (Ernst and Dal Piaz, 1978; Bucher, 2005) and exceptionally ultra-high-pressure (UHP) metamorphic conditions registered in coesite- and microdiamond-hosting metasediments outcropping on the shore of the Cignana Lake (Reinecke, 1998; Forster et al., 2004; Groppo et al., 2009; Frezzotti et al., 2011). Given the large gap in metamorphic pressure conditions registered between CO and ZS, CF is interpreted to have accommodated exhumation of UHP rocks to shallower depths (Ballèvre and Merle, 1993; Reddy et al., 2003; Pleuger et al., 2007). This strain zone registers kinematics of both top-SE and top-NW shearing, attesting a history of reactivation and tectonic reworking since the Eocene (Reddy et al., 2003; Pleuger et al., 2007; Kirst and Leiss, 2017).

The study area also underwent post-metamorphic extensional brittle faulting since the Oligocene. This is registered in offsets of the tectonic contacts along two NE-SW and NW-SE striking sets of brittle normal faults (Bistacchi and Massironi, 2000; Bistacchi et al., 2001; Sue et al., 2007).

3.3. Methodology: from field mapping to 3D structural modelling with uncertainty assessment

Our geomodelling workflow (Fig. 3.2) is designed to build 3D structural models conditioned by surface geological and structural data collected in the field, employing the implicit Discrete Smooth Interpolator as implemented in the RING Toolkit plugin (DSI; Frank et al., 2007; Caumon et al., 2013) running on SKUA/GOCAD (https://www.aspentech.com/en/products/sse/aspen-skua). In the following we provide details on each step of the workflow.

3.3.1. Input data

Our input data are summarised in the 1:75,000 new structural map of the northern Aosta Valley, which is the result of the recent upscaling of 1:10,000 original surveys published on the Geoportale Regione Autonoma Valle d'Aosta (https://geoportale.regione.vda.it/; Dal Piaz et al., 2010, 2016; Perello et al., 2011; Polino et al., 2015). The structural map, which represents the most recent attempt at portraying the tectonic setting of the region, is accompanied by a dataset of structural measurements of metamorphic schistosity, mineral lineation, fold axes, and axial planes (Fig. 3.1B). The scheme of tectono-metamorphic relationships in Fig. 3.1D assigns unique names to the tectonic contacts and boundaries and illustrates their hierarchical relationships. This scheme is crucial in facilitating the transfer of information between the 2D structural map and the 3D model.
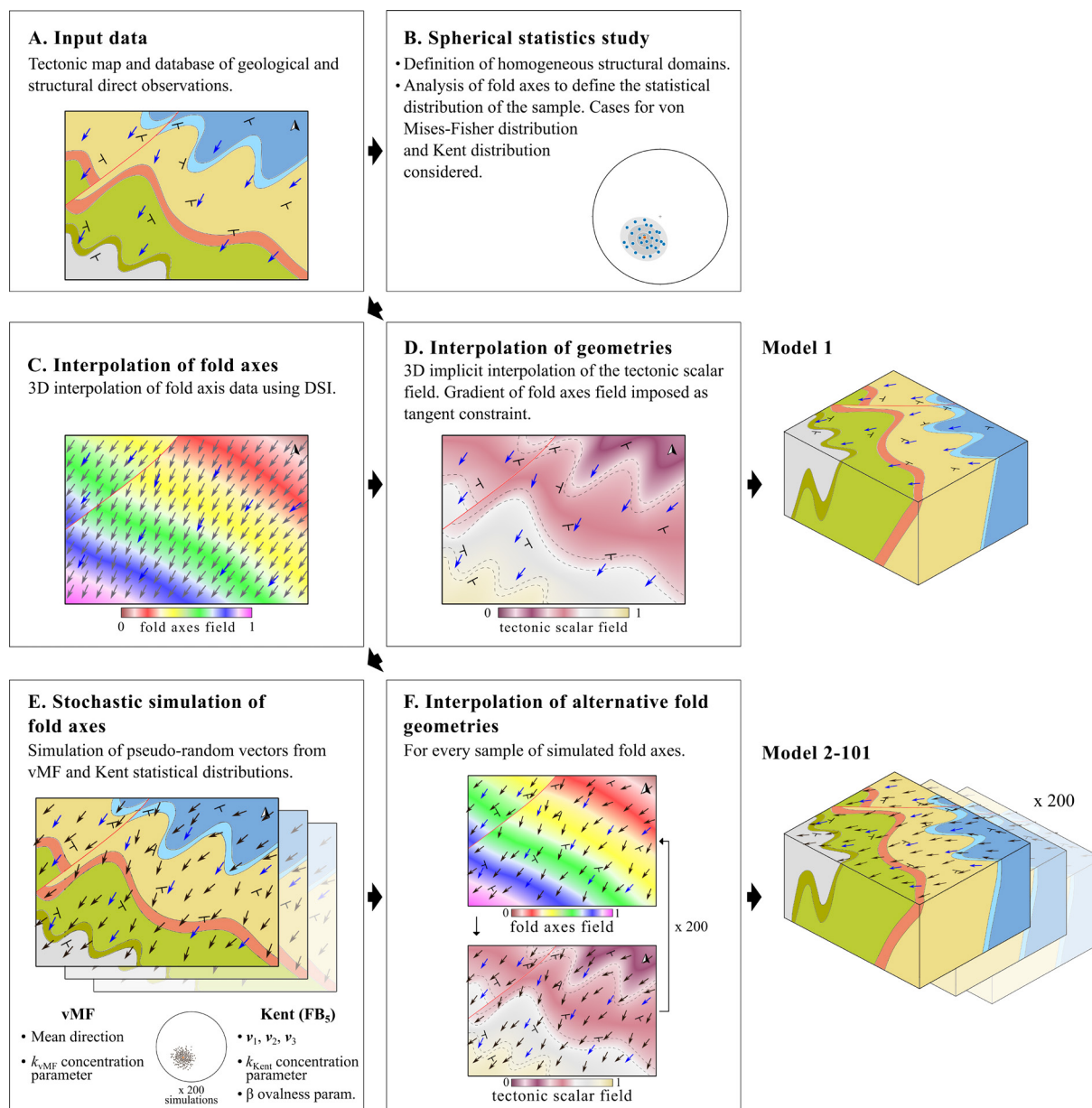
Figure 3.2. Geomodelling workflow, detailed in Sect. 3.3 of the text. A) Input data. B) Spherical statistics analysis on the structural database. C) 3D interpolation of direct measurements of fold axes. D) Interpolation of geometries. E) Stochastic simulation of fold axes derived by von Mises-Fisher and Kent distributions. F) Interpolation of alternative scenarios.

The entirety of surface data is organised in a GIS (Geographic Information System) environment and complemented by a high resolution 2 m/pixel DEM (Digital Elevation Model), obtained from a LIDAR survey, and 20 cm/pixel aerial orthophotos. The rugged topography of our study area results in a truly three-dimensional geological dataset, spanning over 1,300 m in elevation from the highest peak (Becca di Salè, 3,107 m a.s.l.) to the Cignana Valley, covering an area of ca. 9 km². Fig. 3.3 displays landscape

views of the study area with interpreted tectonic boundaries and units.

3.3.2. Structural data analysis

The structural analysis step is aimed at (i) identifying subareas governed by homogeneous structural behaviour (e.g., showing consistent foliation data or folding styles) and (ii) defining the spherical statistics distributions for the stochastic simulation of fold axes data. Results are in Sect. 3.4.

The structural analysis is performed on the three-component unit vectors ($easting, northing, elevation$) of the structural measurements, computed using the standard transformation from spherical to cartesian coordinates:

$$easting = L_i = cos(plunge)sin(trend), \tag{1}$$

$$northing = M_i = cos(plunge)cos(trend), \tag{2}$$

$$elevation = N_i = -sin(plunge). \tag{3}$$

Firstly, we identify subareas displaying homogeneous structural behaviour, such as consistent foliation attitude or folding styles. This step also implies detecting boundaries that mark abrupt shifts in deformation styles, which often correspond to tectonic contacts separating different domains.

We then proceed to analyse the statistical distribution of the database of fold axes falling within the area in which the uncertainty analysis will be performed (methodology in Sect. 3.3.6). First, we perform a preliminary exploratory step to examine the orientation, clustering and shape of the data sample (composed of n measurements) through eigenanalysis. By computing the orientation tensor A (Woodcock, 1977):

$$a = \begin{bmatrix} \sum_{i=1}^{n} L_i^2 & \sum_{i=1}^{n} L_i M_i & \sum_{i=1}^{n} L_i N_i \\ \sum_{i=1}^{n} M_i L_i & \sum_{i=1}^{n} M_i^2 & \sum_{i=1}^{n} M_i N_i \\ \sum_{i=1}^{n} N_i L_i & \sum_{i=1}^{n} N_i M_i & \sum_{i=1}^{n} N_i^2 \end{bmatrix} \quad \text{and} \tag{4}$$

$$A = \frac{a}{n}, \tag{5}$$

we obtain information on the three eigenvectors ($\boldsymbol{v}_1, \boldsymbol{v}_2, \boldsymbol{v}_3$) that describe the orthogonal principal axes of the sample, with $\boldsymbol{v}_1$ being the major axis (and often an estimate of the mean direction), $\boldsymbol{v}_2$ the intermediate and $\boldsymbol{v}_3$ the minor axis. We also compute the corresponding eigenvalues (S_1, S_2, S_3) in their normalised form, obtaining a first statistical characterisation of the data sample. The eigenvalues are directly related to fabric shape, which can be quantified computing the shape parameter K (Woodcock, 1977):

$$K = \frac{\ln(S_1/S_2)}{\ln(S_2/S_3)}. \tag{6}$$

Low values of K ($0 \leq K < 1$) indicate data samples with girdle tendencies, while clusters are indicated by high values of K ($1 < K \leq \infty$; Woodcock, 1977). Eigenanalysis additionally allows to quantify the strength of the preferred orientation by computing the parameter C (Woodcock, 1977):

$$C = ln\,(S_1/S_3)\,. \tag{7}$$

After eigenanalysis, we proceed by characterising the statistical distribution of the data sample by computation of parameters such as mean direction and concentration of the sample. Here we present the cases for von Mises-Fisher (vMF; Fisher, 1953) and Kent (Kent, 1982) distributions in order to perform simulations of both distributions in the uncertainty analysis step of our work, as we will see in Sect. 3.4.2. The vMF distribution on the sphere is the analogue of the isotropic bivariate normal distribution, characterised by circular contours, while the Kent distribution (also called Fisher-Bingham, or FB$_5$) is the analogue for the general bivariate normal distribution and it draws oval contours on the sphere (Kent, 1982). Both distributions characterise uniaxial sample datasets.

The vMF distribution is parameterised using the mean direction and concentration parameter k_{Fisher} of the sample. For samples of n measurements, the mean direction is computed by defining the orientation $(\bar{x}, \bar{y}, \bar{z})$ of the resultant vector R (Borradaile, 2003):

$$R^2 = (\sum_{i=1}^{n} L_i)^2 + (\sum_{i=1}^{n} M_i)^2 + (\sum_{i=1}^{n} N_i)^2, \tag{8}$$

$$\bar{x} = \frac{1}{R}\sum_{i=1}^{n} L_i, \qquad \bar{y} = \frac{1}{R}\sum_{i=1}^{n} M_i, \qquad \bar{z} = \frac{1}{R}\sum_{i=1}^{n} N. \tag{9}$$

The concentration parameter k_{Fisher}, which quantifies the degree of clustering of the sample around the mean direction, can be approximated by (Fisher, 1953):

$$\begin{cases} k_{Fisher} = \frac{n-1}{n-R} & when\ n \geq 16 \\ k_{Fisher} = \frac{n}{n-R} & when\ n < 16. \end{cases} \tag{10}$$

On the other hand, the Kent distribution is described by a concentration parameter k_{Kent}, an ovalness parameter β and the orientation matrix. The parameterisation of this distribution, which relies on the computation of maximum likelihood estimates, is not as straightforward as for the vMF case, however libraries that deal with this problematic have been recently published (e.g., Yuan, 2021). The Kent distribution requires the relation $k_{Kent} > 2\beta$ to be met for its interpretation as an analogue of the general bivariate normal distribution, while the case with $\beta = 0$ corresponds to the vMF distribution (Kent, 1982).

3.3.3.   The Discrete Smooth Interpolator: an overview

Following data analysis and preparation, we perform interpolation in 3D using implicit DSI interpolation

(Frank et al., 2007; Caumon et al., 2013). First implemented to represent sedimentary sequences, implicit methods model the stratigraphic (or tectonic) sequence as a continuous, derivable (at exclusion of faults and unconformities) scalar field representing the age of rock units throughout the model volume (Houlding, 1994; Lajaunie et al., 1997). Stratigraphic (or tectonic) boundaries such as top of formations are extracted a posteriori as isovalue surfaces of the scalar stratigraphic field and can be used to obtain a classical boundary representation.
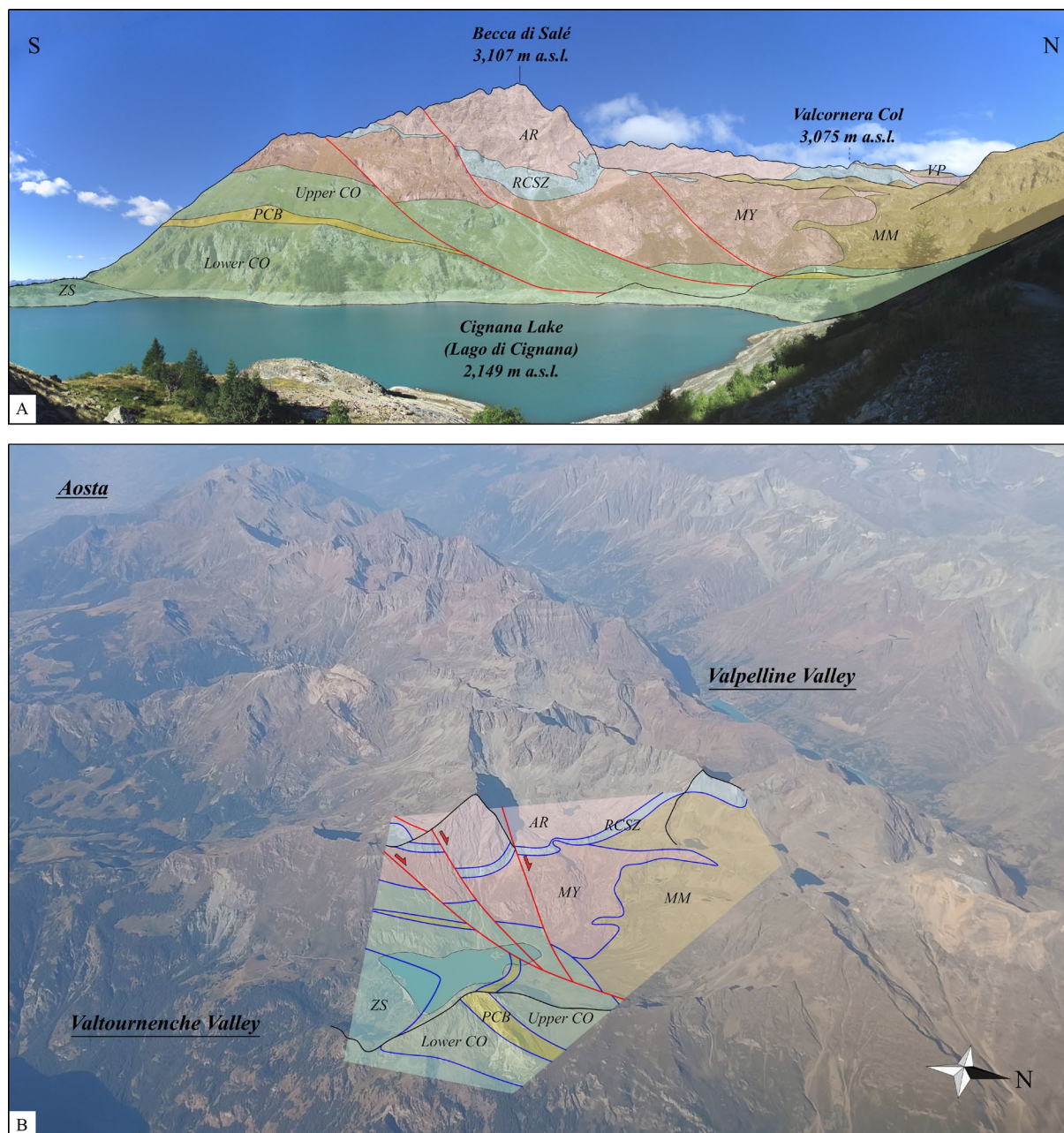

Figure 3.3. Interpreted landscape views of the Cignana Lake area. Colours and names of tectonic units as in the structural map in Fig. 3.1, except for VP (Valpelline unit), not considered in this study. A) Terrestrial landscape view. Point of view indicated by binoculars icon in Fig. 3.1A. B) View from commercial plane.

In the workflow presented in this work we employ the DSI of SKUA/GOCAD as implemented in the RING Toolkit (Frank et al., 2007; Caumon et al., 2013), which solves the mathematical problem at the nodes of a tetrahedral mesh with a least-squares weighted approach.

Different types of constraints, each one with customisable weights, control the interpolation process. Firstly, position constraints are defined based on geological information (i.e., mapped boundaries or interpolations in vertical cross-sections) that constrain the value of the scalar field at specific locations. Other constraints can be imposed that influence the gradient of the scalar field, which by definition is orthogonal to the isovalue surfaces, in different ways. Foliation attitude data can be used to align the gradient with the normal direction to the dip-dip direction plane, while the "stacking direction of the succession holds the polarity information of the constraining vector. Moreover, vectors such as fold axes or lineations can be imposed as tangent constraints to bind isovalue surfaces of the implicit scalar field to the tangent vector (Frank et al., 2007; Caumon et al., 2013). This enforces a gradient that is maintained perpendicular to the tangent vector and, as we will see in the next section, is particularly useful for modelling complex structures such as isoclinal recumbent folds.

The gradual transition of the scalar field between two points is ensured by a continuity (smoothness) constraint imposed at faces of the tetrahedra (Frank et al., 2007; Caumon et al., 2013). This constraint also guarantees the well-posedness of the mathematical interpolation problem and is responsible for the creation of continuous and derivable scalar fields. The continuity is interrupted only at the intersection with fault surfaces and unconformities, which are therefore represented as mathematical – in addition to geological - discontinuities. This approach allows modelling both infinitely extended and finite faults (i.e., faults with tip line falling within the modelling domain).

However, hierarchical relationships such as stratigraphic or tectonic discontinuities are not handled by the RING Toolkit interpolator (Frank et al., 2007; Caumon et al., 2013) used in the present study. We solve this issue by applying mesh cutting tools, as implemented in SKUA/GOCAD, to the boundary representation surfaces extracted from the implicit scalar field.

3.3.4. Interpolation of the fold axes field

Fold axes measurements collected in the field are relatively sparse and heterogeneously distributed. These are axes of outcrop-scale parasitic folds (with respect to folded major tectonic contacts), and before using them as constraints to interpolate larger-scale model of major tectono-metamorphic units, their meaning must be assessed in terms of tectonic phases and cylindricity of large-scale folds (at least within subdomains of the study area), which is a fundamental precondition for upscaling fold geometry (Ramsay, 1967). We will discuss these topics in the results and we will show that we are able, with some caution, to adopt a fold axes interpolation strategy inspired by the work of Laurent et al. (2016).

Fold axes represented as unit vectors (equations 1-3) are used in the interpolation with DSI of a three-dimensional scalar field, that we here refer to as "fold axes field" (F_{fa}; Fig. 3.2C). Within this field, the fold axes are parallel to the gradient, and the scalar value itself represents just a dummy variable that increases along the fold axes direction. The advantage of this approach is that it honours the direct measurements of fold axes (in a least-squares sense) while performing a smoothing (Frank et al., 2007; Caumon et al., 2013). The gradient of F_{fa} (i.e., upscaled fold axes) is then enforced as tangent constraint for the interpolation of the "tectonic scalar field" (F_t; Fig. 3.2C) that describes the tectono-metamorphic units and their boundaries.

We will show that this strategy allows accurately modelling isoclinal recumbent folds (Sect. 3.4.1) and paves the way for stochastic modelling of the associated uncertainty (Sect. 3.3.6 and applications in Sect. 3.4.2).

3.3.5. Using fold axes field for densification of mapped boundaries constraints

In this section, we show how we exploit the geometric properties of the fold axes field F_{fa} to densify the constraints represented by the mapped tectonic boundaries. In analogy to "manual" geomodelling workflows, which often involve building a conceptual model on vertical cross-sections and using it to constrain the 3D interpolation (Kaufmann and Martin, 2009; Arienti et al., 2024 – Chapter 2), and inspired to the "plunge model" of Stockwell (1950) and de Kemp (2000), we introduce a quantitative approach to densify polylines representing mapped tectonic boundaries by multiple projection along the gradient of F_{fa} (i.e., along upscaled fold axes). This approach has the advantages, with respect to manual methods, of being fast and not subject to interpretation bias (Bond, 2015).

In an iterative workflow, we project for a finite distance the mapped tectonic boundary polylines along the direction defined by the gradient of F_{fa} at each polyline node. The local F_{fa} gradient is then transferred on the nodes of the projected polyline, and the projection is repeated a number of times. The product of projection distance with the number of iterations yields the distance covered by the additional constraints. Lastly, the projected tectonic lines are used as position constraints for the interpolation of the tectonic scalar field F_t. This strategy is demonstrated in Sect. 3.4.1, where we apply it to model the recumbent isoclinal fold deforming the Mont Mary inner tectonic contact. Noteworthy, since the local F_{fa} gradient is transferred at each step to be used for projecting the polylines, this approach allows modelling folds with smoothly curved fold hinges, and not only perfectly cylindrical folds.

3.3.6. Stochastic simulation of fold axes for uncertainty analysis

The geomodelling workflow described above is aimed at creating deterministic models that represent the "best guess" interpretation compatible with field data and their interpretation in terms of expert geological knowledge. In this section we expand the workflow by introducing stochastic simulation of

fold axes data that will be perturbed according to a suitable orientation distribution. In the following we will discuss the case for both von Mises-Fisher (Fisher, 1953) and Kent (Kent, 1982) distributions.

Our simulation algorithm proceeds in three steps: (i) simulation of fold axes perturbed with a suitable orientation distribution; (ii) interpolation of the tectonic field using both perturbed and original axes; (iii) quantitative analysis of the results in terms of information entropy (Shannon, 1948; Wellmann and Regenauer-Lieb, 2012).

To generate pseudorandom fold axes vectors distributed according to the parameters of vMF distributions on a sphere, we employ a methodology initially introduced by Fisher et al. (1981), also applied by Wood (1994), and as presented in Appendix A in Pakyuz-Charrier et al. (2018). Given a mean vector and a concentration parameter k_{Fisher} (Fisher, 1953), the methodology creates samples of unit vectors that mirror the vMF distribution. We select the mean vector and the concentration parameter k_{Fisher} based on the results of the orientation analysis presented in Sect. 3.3.2, aiming to replicate the distribution observed in the input fold axes database with a larger sample size. Each simulated sample is composed of 1,000 vectors, whose positions are randomly distributed within the 3D model volume.

On the other hand, to simulate pseudo-random vectors belonging to Kent distributions, we leverage the library developed by Yuan (2021) for analysis of n-parameter Fisher-Bingham distributions on the sphere. Similarly to the vMF simulations, we simulate 100 samples of vectors (1,000 vectors per data sample, randomly distributed in the model volume) that follow the parameters of the Kent distribution derived from the dataset of field fold axes.

The second step of the uncertainty assessment workflow expects the implicit interpolation of folded geometries, following the approach outlined in Sect. 3.3.4, for each set of simulated fold axes. For the interpolation of the new fold axes fields F_{fa}, we consider both direct field observations and simulated fold axes as constraining data, assigning higher weights (10 times higher) to the former. We proceed with the interpolation of the implicit F_t following the general workflow (Sect. 3.3.4) and enforce the gradient of the newly generated F_{fa} as tangent constraint. This results in the generation of multiple plausible tectonic contact geometries that conform to both observed and simulated data.

We measure the degree of model consistency by employing the notion of information entropy H (Shannon, 1948; Wellmann and Regenauer-Lieb, 2012), which computes the probability p_i of every node of the tetrahedral mesh of belonging to a given tectono-metamorphic unit. Higher values of entropy in the system indicate higher uncertainty on the value of the scalar field at the node. After a number of simulations (S) have been performed, information entropy is computed with the following equation (Shannon, 1948; Wellmann and Regenauer-Lieb, 2012):

$$H = -\sum_{i=1}^{S} p_i \log p_i. \tag{11}$$

67
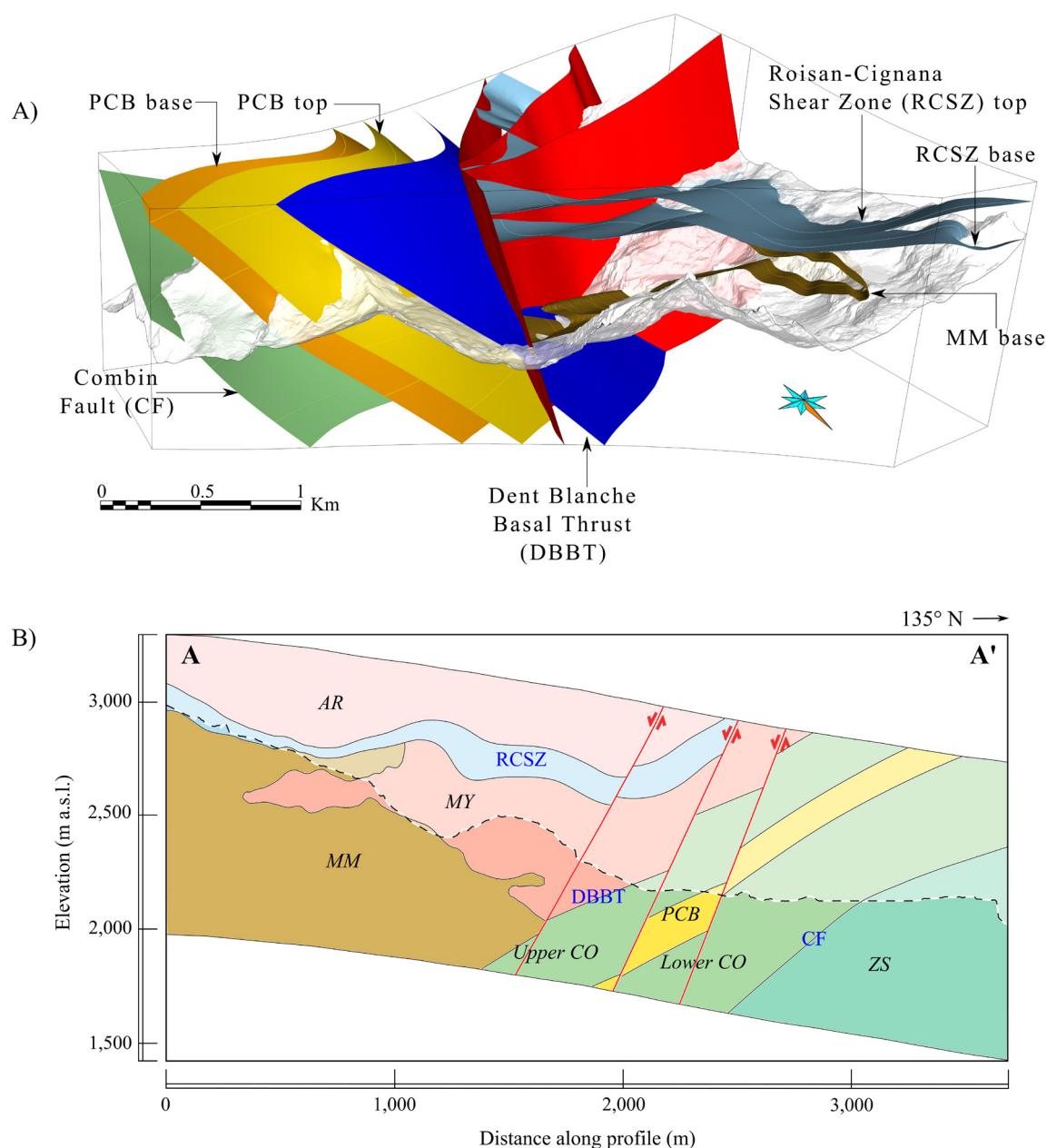
Figure 3.4. 3D structural model of the Cignana Lake. Description of the model in Sect 3.4.1 of the text. A) 3D view of the boundary representation with semi-transparent DEM. Names as in the scheme of tectono-metamorphic relationships in Fig. 3.1D. B) Vertical cross-section of the model. Trace of the cross-section and legend in Fig. 3.1.

3.4.   Results

In this section we present the deterministic 3D structural model of the Cignana Lake area and we then apply the uncertainty workflow, as described in the previous section, to the isoclinal recumbent fold formed by the Mont Mary inner tectonic contact (highlighted in Fig. 3.1A).

3.4.1.   The 3D structural model of the Cignana Lake area

The 3D model has been interpolated along the nodes of a tetrahedral mesh with roughly uniform horizontal and vertical resolution of approximately 26 meters, corresponding to the average tetra edge length. This results in ca. 8.3×10^5 nodes and ca. 4.8×10^6 tetrahedra, which allows for practical execution times, around 10 minutes for interpolation of a single model, on a desktop workstation (AMD Ryzen 9 5950X Processor, NVIDIA GeForce RTX 3080 GPU, 64.0 GB RAM on a Windows system). This resolution also provides a good balance between computational efficiency and sufficient detail to model the geological features accurately. The model's vertical extent covers a range of 1,300 meters, and the upper and lower boundaries conform to the topography. Consistently with the Alpine tradition of interpreting both subsurface and eroded spaces, the interpolated tectonic contacts extend both above and below the topographic surface to account for a continuous representation of the tectonic structures and prevent edge effects. 3D and cross-section views of our structural model are shown in Fig. 3.4.

The 3D model also takes into consideration a system of three normal faults, which are attributed to normal faulting events that took place in brittle post-nappe conditions (Bistacchi and Massironi, 2000). Faults are integrated in the modelling workflow at an early stage, and the implicit mesh is built conformable to their surfaces. Since the faults traverse the entire model domain, they limit four independent fault blocks (Fig. 3.5B). According to the DSI's implementation, each of these fault blocks yields independent scalar fields and this implies that constraints whose geographical coordinates are situated between two fault surfaces solely affect the corresponding fault block and are disregarded by the others. However, the interpolation function typically requires at least two position constraints with different values and orientation data for geologically feasible geometries, and this might call for artificial constraints in fault blocks lacking outcrops, as we will see in the next paragraphs.

The fault surfaces are arranged in a set of synthetic normal faults, all dipping to the northwest with high angles ranging between 60° and 70° (Fig. 3.4). This set is composed of a master fault and two branching faults in its hanging wall. According to fault kinematics data collected in the field, we have modelled them as purely dip-slip normal faults, with displacements ranging from 50 to 250 meters.
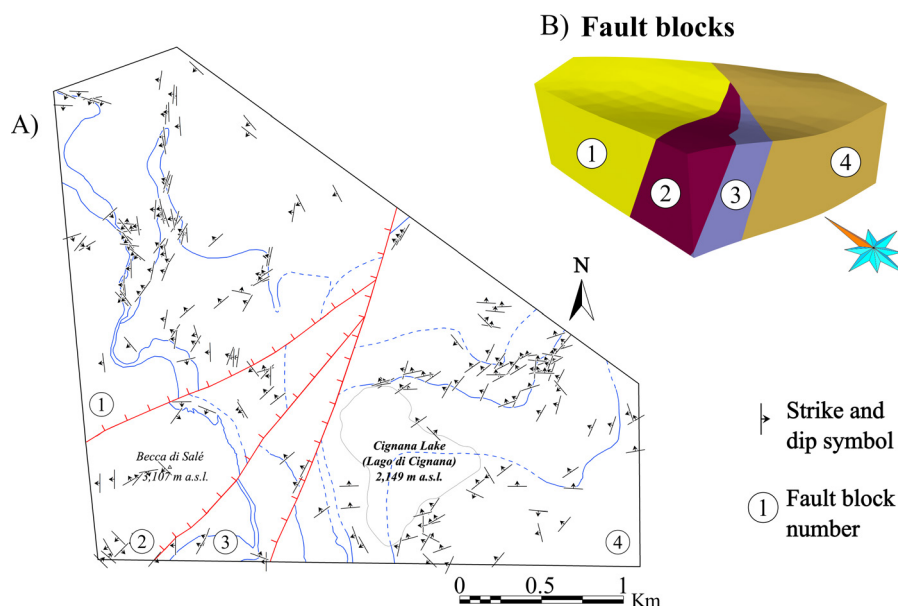
Figure 3.5. Foliation data. A) Direct observations of foliation planes. B) 3D view of independent fault blocks defined by the system of synthetic normal faults.

The rock units and tectonic contacts of the Austroalpine nappe system, in the hanging wall of the DBBT, are folded along a generally NE-SW trending system and foliation data display moderate dispersion (Fig. 3.1B). Several outcrop-scale folds are exposed, forming parasitic structures with respect to the large-scale folding of the tectonic contacts, and displaying isoclinal and close geometries. Folding patterns are disharmonic, non-cylindrical and result in geometries that are often challenging to trace as the scale increases beyond the outcrops scale. These geometries are also recognised at the larger scale, where they affect tectonic contacts folded with km-large isoclinal to open geometries (Fig. 3.1). The structural database for this subarea is composed of 84 direct observation of fold axes and 327 observations of schistosity planes (Fig. 3.5A). In contrast, in the Piedmont nappe system the structural behaviour is governed by NW-dipping foliation, and small scale undulations within the units are attributed to NW-SE trending parasitic folds (Fig. 3.1B). The structural database for these units includes 12 fold axes and 124 schistosity plane measurements.

For the modelling of the RCSZ and the Mont Mary internal boundary (Fig. 3.1), we employed the methodology described in Sect. 3.3.4, which interpolates direct fold axes measurements (Fig. 3.6A) into a fold axes field F_{fa} (Fig. 3.6B) using the RING Toolkit interpolator (Frank et al., 2007; Caumon et al., 2013). The gradient of this generated field, continuous across the model volume, is then imposed as tangent constraint on the interpolation of a second tectonic scalar field F_t that describes the geometries of the folded tectonic contacts (Fig. 3.6C). This approach allows propagating the vectorial information of the field fold axes measurements (collected at the outcrop-scale) to build a constraining field for the

interpolation of the model-scale folded geometries. In addition to this, we constrained the Mont Mary boundary, whose geometry is particularly complex with limbs that are locally less than 100 meters apart, by applying the methodology described in Sect. 3.3.5 that allows the creation of additional constraining lines through projection of surface information along the F_{fa}'s gradient (Fig. 3.7). As a result, at the scale of the 3D model, the RCSZ is characterised by upright open folds, while the Mont Mary internal boundary displays recumbent isoclinal folds.

In the southeastern portion of the model, the sequence of tectonic contacts of the oceanic Piedmont domain, together with the DBBT, forms a conformable sequence with a NW-dipping attitude affected by brittle normal faulting (Fig. 3.1). The interpolation of these geometries is guided by the foliation measurements (Fig. 3.5A) imposed as gradient constraints. However, as shown in Fig. 3.5, fault blocks number 1 and 2 lack outcrops of these tectono-metamorphic units, resulting in absence of strike and dip measurements to guide the implicit interpolation. To resolve these cases, we employ geomodelling solutions informed by structural knowledge and we assign to blocks number 1 and 2 an artificial constraining value, result of the average foliation of the measurements collected in blocks number 3 and 4.

Lastly, the implicit isosurfaces generated from the scalar fields for both the Austroalpine and Piedmont systems are saved independently as triangulated meshes, creating the boundary representation of the 3D structural model (Fig. 3.4A).
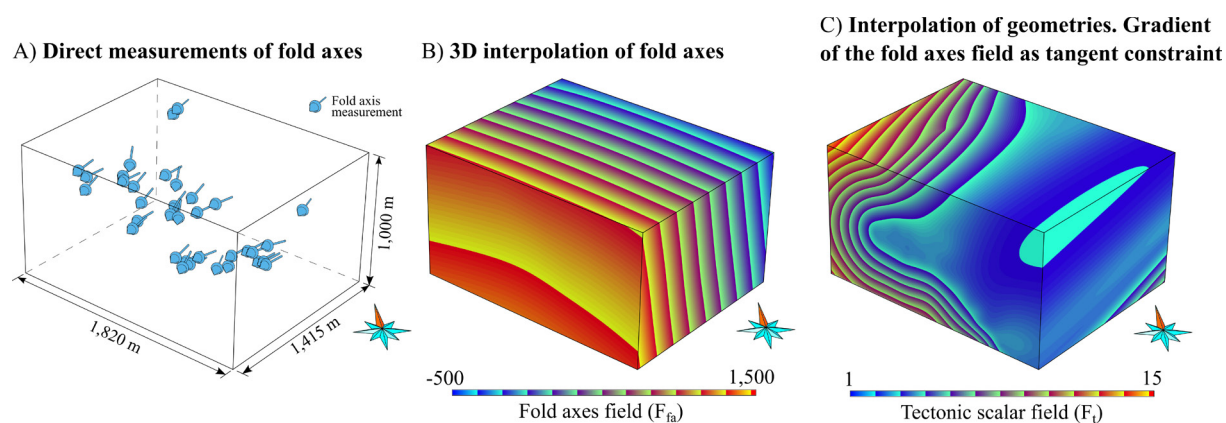

Figure 3.6. Implicit interpolation steps, as detailed in Sect. 3.3.4 and 3.4.1 of the text. Location of the investigated volume is indicated in Fig. 3.1A by the dashed rectangle. A) Direct measurements of fold axes. B) 3D interpolation of fold axes. C) Interpolation of geometries constrained by the gradient of the fold axes field imposed as tangent constraint.
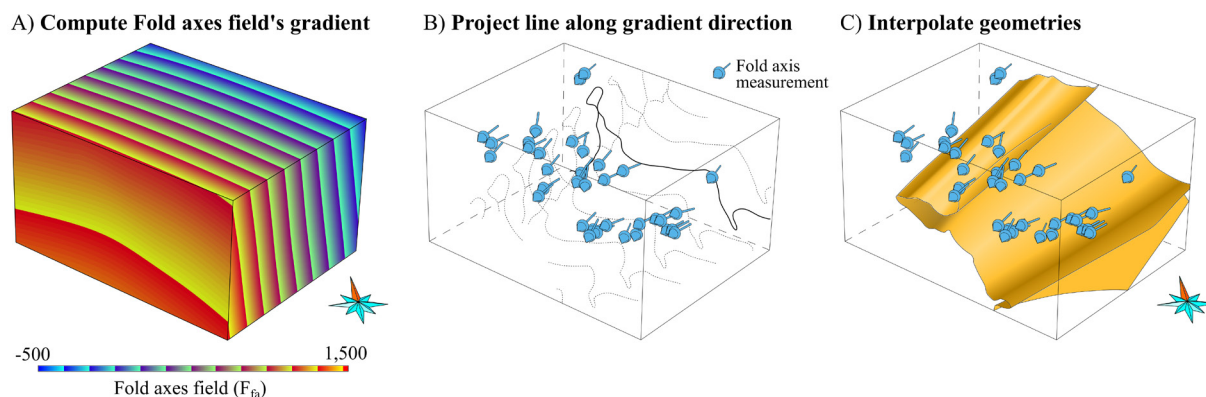
Figure 3.7. Densification of position constraints by projection of mapped polyline. Methodology in Sect. 3.3.5. A) Computation of the fold axes field's gradient (Fig. 3.6). B) Iterative process of projection of the mapped tectonic contact along the gradient computed from (A). Only a few representative polylines are represented here. C) Interpolation of the new geometry using original and projected constraints.

3.4.2. Simulation of fold axes for uncertainty assessment

The uncertainty analysis was carried out in the subarea of the DB s.l. system highlighted in Fig. 3.8A, covering an area of about 2.6 km^2. This area is of particular interest because it shows an isoclinal recumbent fold of the Mont Mary inner tectonic contact.

The subarea includes 44 measured fold axes with sub-horizontal plunge and NE-SW trend. In the stereogram of Fig. 3.8B, if analysed as a whole, the fold axes seem to show a multimodal girdle pattern that extends across the NE and SW quadrants. However, upon closer examination of the map, it becomes evident that the orientation of fold axes is not spatially uniform. Instead, we recognise two sub-areas (Sector 1 and 2) that, if analysed separately, show distributions with a more concentrated axial symmetry. The dashed black and white line in Fig. 3.8A delineates the boundary between the two sectors. This line does not correspond to a particular structure or lithological boundary mapped in the field and we assume that it is related either to a refraction of strain getting closer to the Mont Mary tectonic boundary or to a younger open fold.

Fold axes belonging to Sectors 1 and 2 have been independently examined through eigenanalysis, following the methodology in Sect. 3.3.2. The results of the K and C parameters (Fig. 3.8B), if plotted in the two-axis plot of Woodcock (1977), show uniaxial clustering behaviour and non-isotropic axial symmetries. We proceed with the independent analysis of the two sectors, and we perform the parameterisation assuming two different scenarios. For the sake of simplicity, in the first scenario we assume that the two Sectors have been sampled from two vMF distributions (Fisher, 1953), and we therefore perform the sample parameterisation and later vector simulation following this statistics. In the second scenario, we instead assume that the two Sectors have been collected from Kent distributions

(Kent, 1982) and perform the uncertainty analysis under this assumption. This choice allows us to compare the outcomes of the two scenarios and propose reasonings on how the uncertainty analysis is influenced by the assumption of different spherical statistics.

First, we assume that the two samples are derived from vMF distributions, and we parameterise the sample with mean direction and k_{Fisher} using equations (9) and (10). We obtain mean fold axes of respectively 213/08 and 251/19 (trend/plunge), and concentration parameters k_{Fisher} of values 19.0 and 110.9 (Fig. 3.8C). Successively, we assume Kent distributions for the two data samples and compute the spherical parameters as presented in Sect. 3.3.2, resulting in mean directions (corresponding to the first eigenvector) of respectively 212/08 and 251/19 (trend/plunge) for Sectors 1 and 2, concentration parameters k_{Kent} of values 20.9 and 177.8, and ovalness parameter β of 2.84 and 46.21 (Fig. 3.8D).

While it is evident that the two parameterisations show aligned mean directions for both samples, it can also be noticed that the assumption of Kent distribution allows detecting high ovalness for Sector 2 and only mild for Sector 1, in accordance with the computed shape parameters K, higher for Sector 1 (Fig. 3.8B and 3.8D). Moreover, as already suggested by the higher parameter C for Sector 2 (Fig. 3.8B), the Kent distributions that describe fold axes falling into Sector 2 are characterised by a high concentration parameter k_{Kent}.

To perform the interpolation of 200 geologically plausible alternative folded geometries (100 under the assumption of vMF distribution, and other 100 for the Kent scenario), we build a three-dimensional tetrahedral mesh that covers the subarea used for the uncertainty study (Fig. 3.8A). The mesh has a vertical extension of 1,000 meters, spanning from 2,015 m a.s.l. to 3,015 m a.s.l. With a resolution of 20 meters (corresponding to the average distance between nodes), the mesh totals ca. 7.0×10^5 nodes and 4×10^6 cells. To maintain separation between the two homogeneous sectors in the investigated volume, the tetrahedral mesh is divided in two sub-volumes, obtained by projection of the boundary line that divides the two sectors (Fig. 3.8A) following the methodology of Sect. 3.3.5.

We generate a total of 200 realisations (100 per scenario), each containing 1,000 simulated fold axes, using the spherical parameters derived from the input data. Example of stereograms of simulated fold axes, one for each distribution (vMF and Kent), are shown in Fig. 3.8C and 3.8D. These simulated vectors are randomly distributed throughout the 3D tetrahedral mesh, covering the whole investigated volume. Finally, we impose both original and simulated fold axes as constraints on the implicit interpolation, resulting in the computation of 100 realisations of F_{fa} and F_t (Fig. 3.9) per statistical distribution, following the method discussed above (Sect. 3.3.6). The interpolation time, considering both the simulation of the new fold axes and the interpolation of the scalar field describing the fold, is in the range of 15 minutes per realisation.

B) Original fold axes

▲ 29 primary observations
⬤ 15 primary observations
⊗ (of which 3 outliers)

	Sector 1	Sector 2
Shape p. *K*	5.50	3.95
C	3.19	5.59

C) scenario with vMF distributions

▲ 820 simulated vectors
⬤ 180 simulated vectors

▲⬤ Mean directions

	Sector 1	Sector 2
Mean direction	213/08	251/19
k_{Fisher}	19.0	110.9

D) scenario with Kent (FB₅) distributions

▲ 820 simulated vectors
⬤ 180 simulated vectors

▲⬤ Mean directions (v_1)

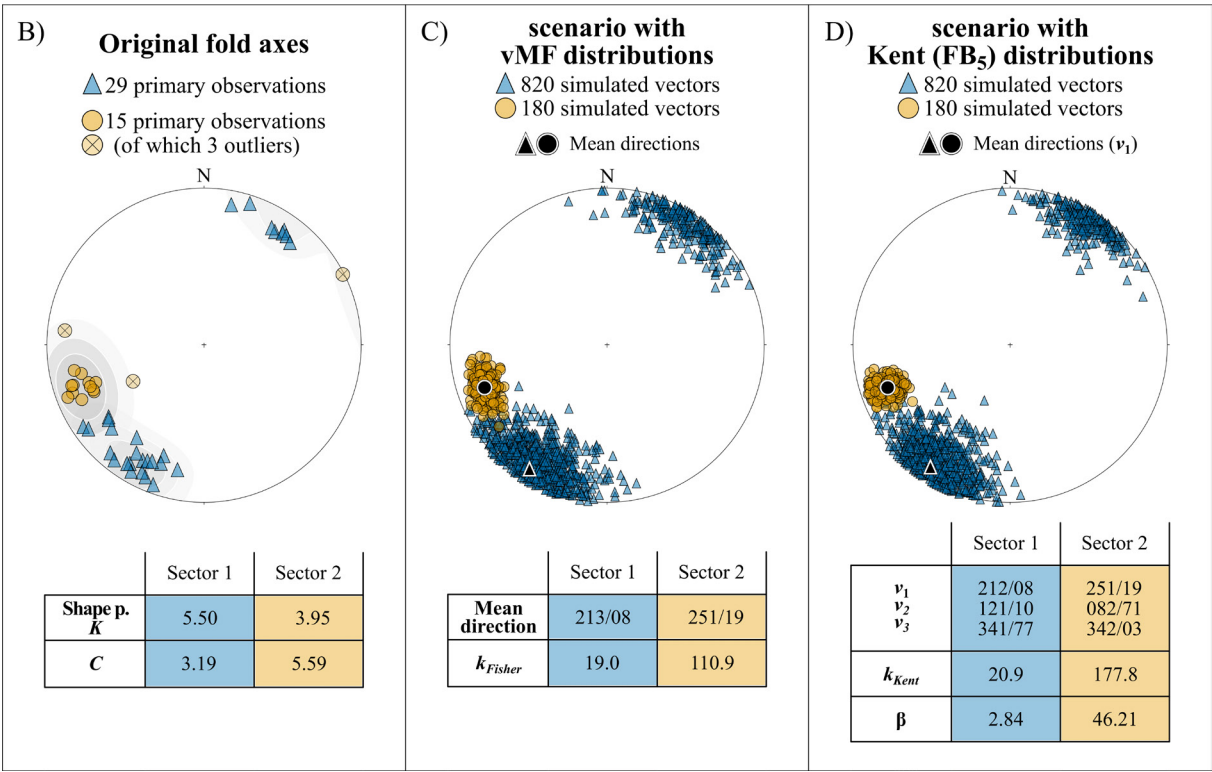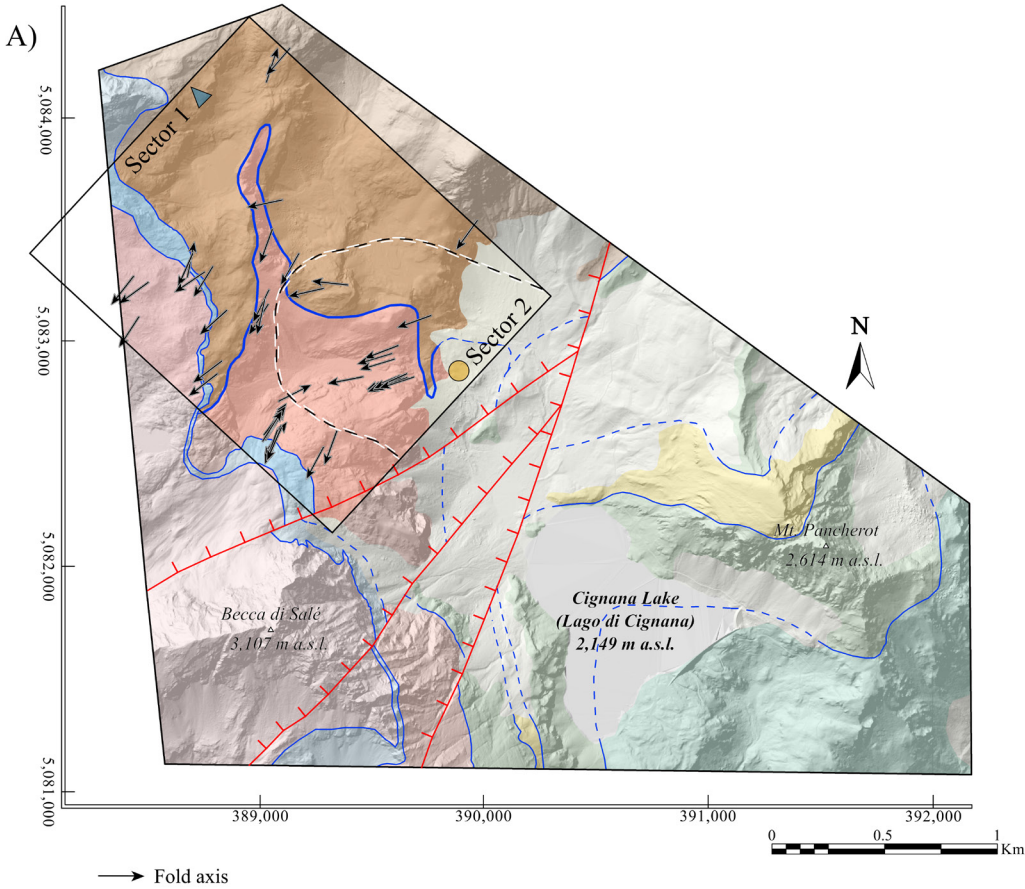|	Sector 1	Sector 2
v_1 v_2 v_3	212/08 121/10 341/77	251/19 082/71 342/03
k_{Kent}	20.9	177.8
β	2.84	46.21

Figure 3.8 (previous page). Choice of simulation parameters for stochastic simulation of fold axes. Methodology detailed in Sect. 3.4.2 of the text. A) Structural map, with colours and names as in Fig. 3.1. Black rectangle bounds the analysed area. Location of direct observations of fold axes in map view. Black and white dashed line separates the two structurally distinct sectors. B) Stereogram of original fold axes with results of eigenanalysis. C) Stereogram of 1,000 simulated fold axes, mirroring the von Mises-Fisher distribution parameterised from data in (B). vMF parameters in the table. D) Stereogram of 1,000 simulated fold axes, mirroring the Kent distribution parameterised from data in (B). Kent parameters in the table. In (B), (C) and (D), Sector 1 is represented by blue triangles, Sector 2 by light orange circles. Mean vectors as black symbols.

Results of the simulations are shown in cross-sections across the simulation volume (Fig. 3.10 and 3.11), where both boundaries generated by different realisations and information entropy are displayed. In Fig. 3.11 we also display the difference between the information entropies obtained for the vMF and Kent scenarios ($H_{vMF} - H_{Kent}$), in order to highlight how the assumption of different spherical distributions affect the uncertainty analysis.

Larger deviations in the simulated boundaries are always observed moving away from the topographic surface, where outcrops and hence constraints are present. For instance, section D-D' exhibits well-constrained results for the isoclinal fold, as the cross-section intersects the mapped tectonic contact multiple times, providing strong constraints. Conversely, as we move farther from the topographic surface, both in the eroded and in the subsurface space, higher levels of uncertainty become evident.

A) **3D interpolation of simulated fold axes**   B) **Interpolation of new geometries**   C) **Visualisation of results**

-500	1,500
Fold axes field (F_{fa})	

1	15
Tectonic scalar field (F_t)	

0	1
Information entropy	
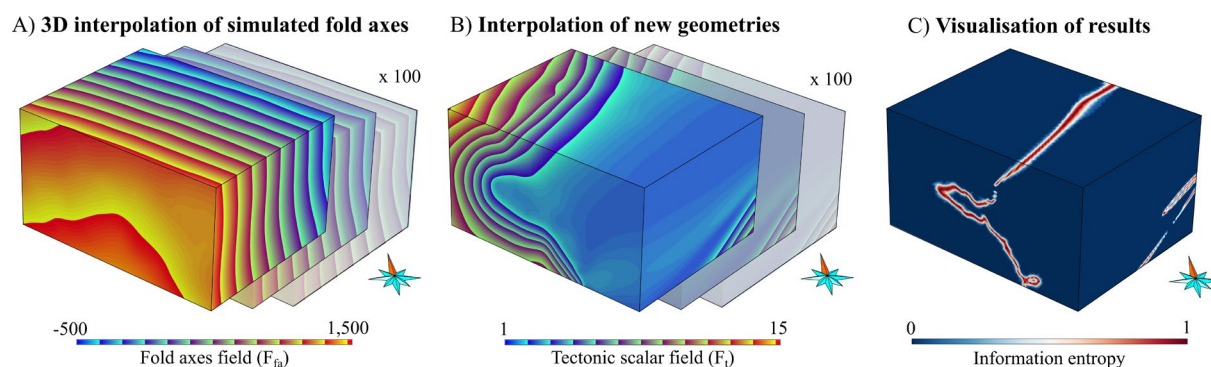
Figure 3.9. Uncertainty workflow, as detailed in Sect. 3.3.6 and 3.4.2 of the text. Location of the investigated volume is indicated in Fig. 3.1A by the dashed rectangle. A) Interpolation of 100 fold axes fields from original and simulated fold axes (considering a single statistical scenario). B) Interpolation of 100 new geometries. C) Visualisation of results with information entropy (Wellmann and Regenauer-Lieb, 2012).

Figure 3.10. Result of the 200 realisations displayed on vertical cross-sections (100 for the scenario with vMF distribution on the left, and 100 for Kent distribution on the right). Intersection lines between the generated geometries and the cross-sections planes. The area of investigation is shown in map view at the bottom of the figure (location is indicated in Fig. 3.1A by the dashed rectangle). Description of the results in Sect. 3.4.2 of the text.

We moreover notice higher uncertainties at the hinge of the isoclinal folds in sections B-B' and C-C' (Fig. 3.10 and 3.11). Specifically, in section B-B' the positions of the hinges exhibit a vertical oscillation of approximately 100 meters and a horizontal shift of about 70 meters. The results also indicate that the minor southeastern isoclinal fold tends to close along the axial plane (Fig. 3.11, B-B' section), and portions of the folds also undergo counterclockwise and clockwise rotations, ultimately adopting inclined NW-dipping and SE-dipping geometries (Fig. 3.11, B-B' section). The series of parallel cross-sections also underlines the non-cylindrical nature of the fold since, moving from section E-E' to section B-B', it is evident how the fold hinges get closer due to converging mean fold axes.

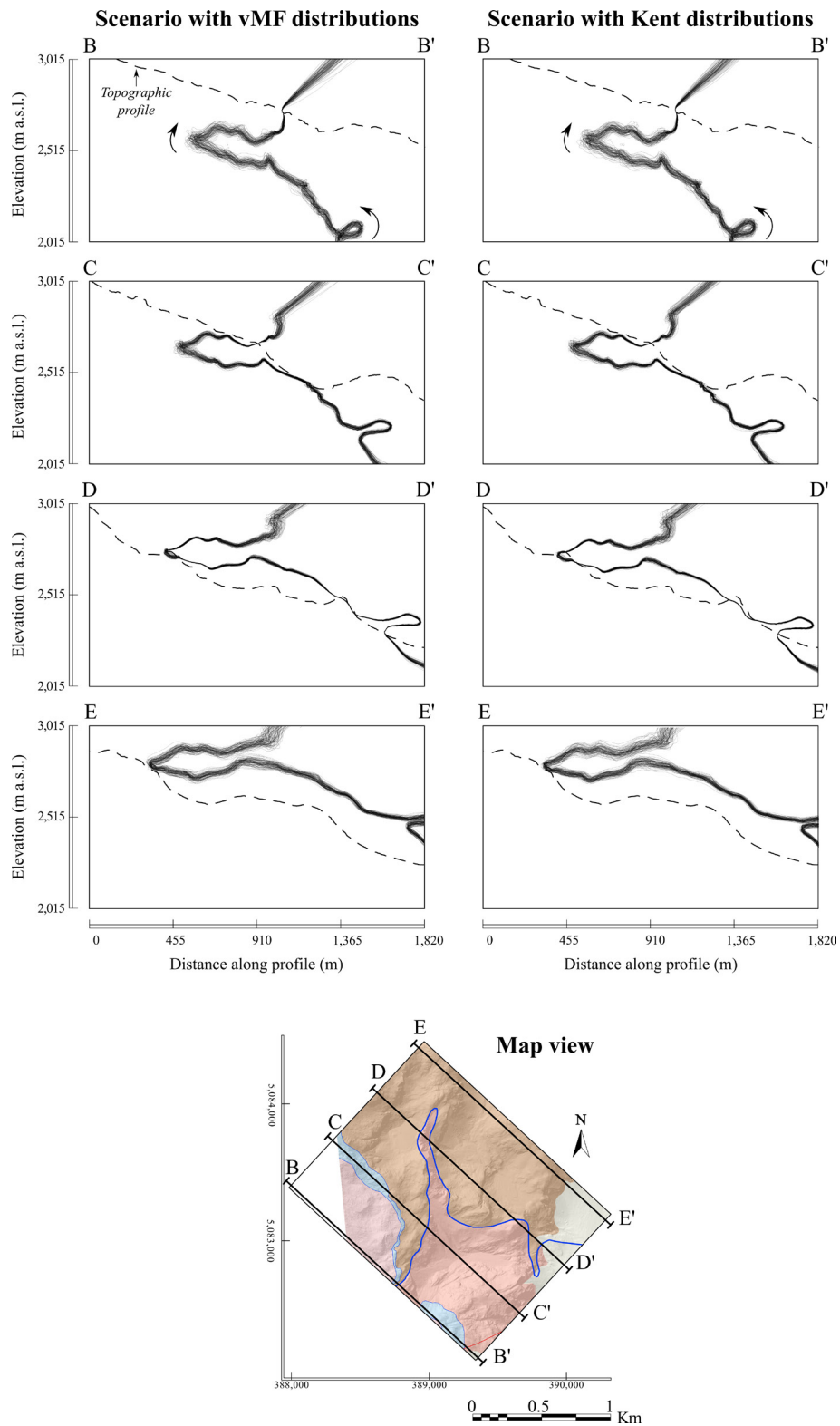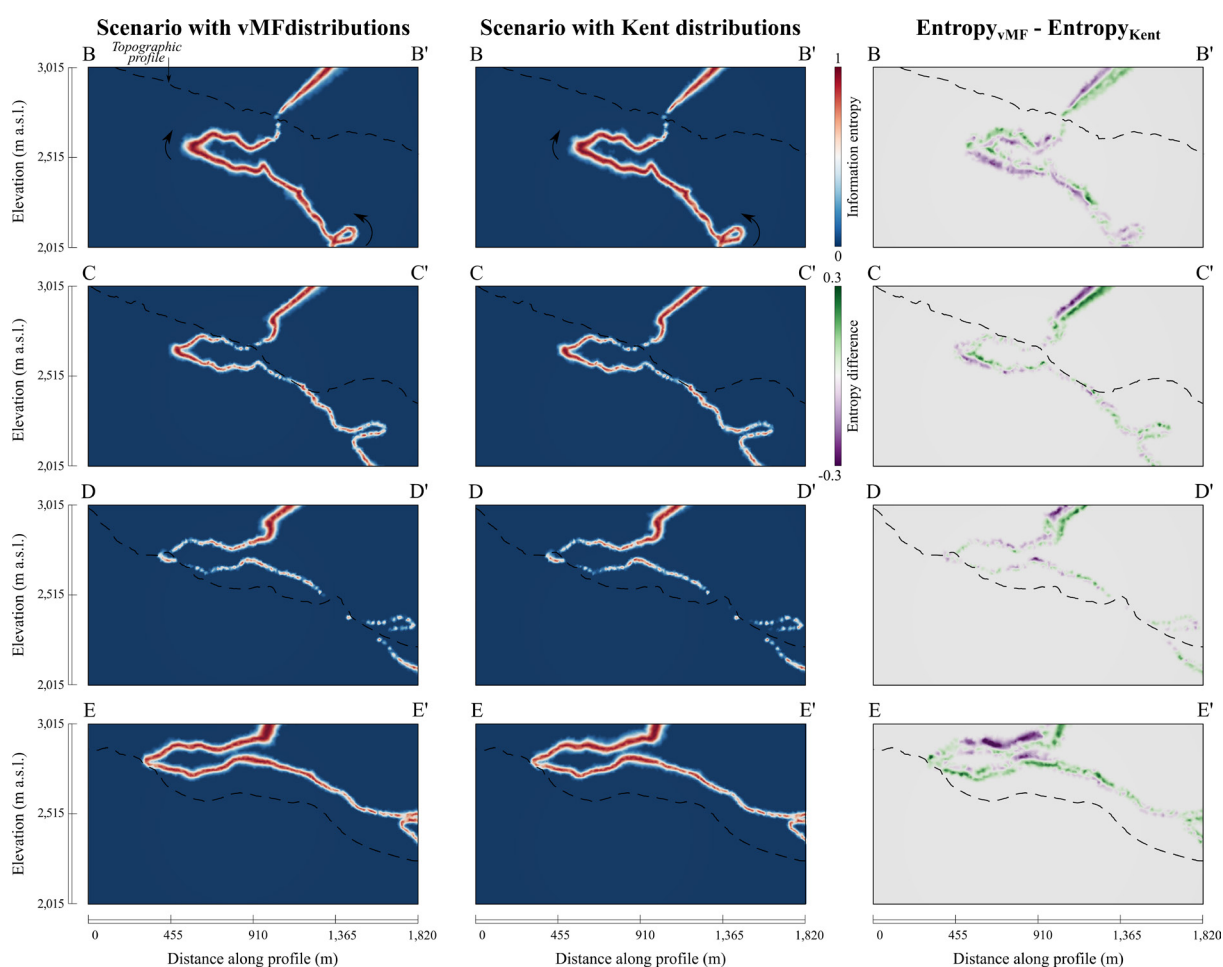Figure 3.11. Result of the 200 realisations displayed on vertical cross-sections (100 for the scenario with vMF distribution on the left, and 100 for Kent distribution in the middle column): information entropy at cross-section's locations. On the right, difference between entropies. The area of investigation is shown in map view at the bottom of Fig. 3.10. Description of the results in Sect. 3.4.2 of the text.

As highlighted in Fig. 3.11, the assumption of vMF against Kent distributions generate different models. While the general behaviours just described such as the partial rotation of sectors of the folds and possible closure along the axial plane are common, the comparison between entropies indicate shifts in the location of portion of the folds (in the order of ca. 100 meters). In section B-B', higher entropy values for the vMF scenario are concentrated at shallower depths for the limbs of the north-western portion of the fold, behaviour that instead results reversed for the south-eastern smaller fold. As expected, higher differences in entropies between scenarios are registered away from constraining data.

Finally, while interpolating or extrapolating in the subsurface or the eroded part of the simulated volume (see Fig. 3.10 and 3.11) may have different practical applications, our simulations indicate that, from a mathematical perspective, they are equivalent.

3.5. Discussion

We have applied the implicit modelling approach for the representation of a 9 km^2 portion of the Pennine Italian Alps situated on the right bank of the Valtournenche valley, around the Cignana Lake area. This area is within the scope of a previously developed regional 3D structural model presented by Arienti et al. (2024 – Chapter 2) which covers the entire transect from Mont Blanc to Monte Rosa. In the larger regional model, the geometry of tectonic boundaries relied heavily on structural interpretations drawn on vertical cross-sections that played a crucial role in propagating structural and geological information from the outcrop scale to the regional scale. In contrast, given the smaller size of the Cignana Lake area and the wealth of structural measurements, in this work we avoid using interpretations on vertical cross-sections and we are able to emphasise structural constraints through the implicit approach, thus reducing the subjective contribution of the interpreter. With respect to the regional-scale model by Arienti et al. (2024 - Chapter 2), we have also improved the resolution of the model and now the reconstruction better adheres to geological and structural data collected at outcrops.

For the modelling of folds, we employ a strategy based on the work of Laurent et al. (2016) and perform 3D interpolation of fold axes' vectors to homogenise the structural control on the interpolation. Differently from Laurent et al. (2016) and Grose et al. (2021), in our work we do not introduce constraints about the axial surfaces and instead leverage the rich database of fold axes measurements, mainly due to the difficulties to trace the univocal envelopment of hinge lines (i.e., the axial surface) in our complex metamorphic setting. In fact, in our study area the folded schistosity is the result of multiple tectonic events that have transposed and obliterated the original magmatic contacts, and folds develop across various scales drawing parasitic geometries. Moreover, the absence of clear indicators of the stratigraphic polarity makes often difficult to distinguish separate fold limbs when these are sub-parallel, such as for the isoclinal folds that we model.

This modelling approach of interpolation of fold axes, in addition to the densification of position constraints through projection of the mapped tectonic contacts in the fold axes directions presented in Sect. 3.3.5, enabled the representation of non-cylindrical geometries that preserve model-resolution variability of fold axes. Due to the lack of harmony of the folding patterns, whose behaviour is strongly influenced by the rheologic characteristics of the rocks they deform, it results difficult predicting geometries that cannot be observed at surface. Therefore no assumption of harmonic behaviour was made in this study and, instead, our geomodelling workflow aims at leveraging the surface database and its components, including the rugged topography that allows the three-dimensionality of the dataset.

A limitation to the faithful representation of disharmonic, similar, and particularly isoclinal folds, arises from the difficulty of the DSI implicit interpolator to enable thickness variations, that in the implicit approach implies strong variations in the modulus of the gradient of the potential field. This is primarily due to the imposition of the constant gradient constraint (Frank et al., 2007) in the interpolation. While this constraint is essential for ensuring the well-posedness of the mathematical problem and minimising gradient variations between adjacent tetrahedra, it is most suitable to model parallel fold and/or sedimentary sequences with almost constant thicknesses of layers (Laurent et al., 2016). In contrast, when applied to disharmonic, similar, and particularly isoclinal folds like in this study, the constant gradient constraint leads to a strong smoothing and to a "rebounding" effect away from observed features at depth, to maintain constant thicknesses within the layers. In this study we minimised, as much as possible, the effect of this constraint by setting lower weights in the interpolation compared to position and orientation constraints (as low as 10^{-5}). However, to further enhance the accuracy of the interpretation, future improvements may consider introducing anisotropies in the gradient of the scalar field that models the tectonic contacts (Laurent et al., 2016; Pizzella et al., 2022), to better capture the intricacies of geological structures characterised by non-uniform lateral homogeneous thicknesses and enhancing the geological realism.

Our workflow proposes, in addition to the generation of a deterministic 3D structural model for the whole Cignana area, the incorporation of uncertainties affecting the database of fold axes measurements and the analysis of their effects on isoclinal recumbent folds exposed in the area. Since the strategies implemented in our workflow for the modelling of folds are primarily affected by fold axes vectors, our uncertainty analysis focused on the simulation of alternative suites of fold axes according to orientation distributions derived from the input database, in a workflow inspired to the work of Lindsay et al. (2012). The simulated fold axes, used as constraining data together with original field observations, are treated in our workflow to address the problem of sparse and incomplete data sampling as they represent plausible, additional measurements that we would expect to collect through hypothetic additional sampling (e.g. borehole drilling or additional fieldwork). The sources of uncertainty that affect our

uncertainty analysis are however multiple and not easily distinguishable. In fact, since for the statistical characterisation of spherical distributions and for the consequent generation of fold axes we consider input data manually collected in the field, the entropy resulting from the multiple realisations is also intrinsically affected by the instrumental uncertainty of the measurements and by the complex nature of geological structures.

Due to the difficulties inherent in defining with certainty the spherical statistical distribution of the input datasets of fold axes, in our work we presented two plausible uncertainty scenarios and analysed the data samples under the assumptions of respectively vMF and Kent distributions (Sect. 3.4.2). This allowed comparing the outcoming entropies, and therefore a quantitative analysis of the effects that the choice of different spherical distributions has on the uncertainty assessment. Results show that the two scenarios (vMF against Kent models) produce similar folded geometries. However, as presented in Sect. 3.4.2, a shift in the location of the portions of fold limbs is noticeable across the volume, caused by the different ovalness parameters of the distributions ($\beta = 0$ for vMF and $\beta \neq 0$ for Kent). This simulation approach could also be easily transferred to the simulation of multiple types of vectorial data, such as dip-dip direction datasets, and the same rationale could be employed to simulate other statistical distributions (Fisher et al., 1987).

The outcomes of the uncertainty analysis yielded important insights into the position of fold hinge sectors and potential rotations of the axial plane, which is of great importance when modelling three-dimensional structures, since fold hinges are often complex structures and can serve as focal regions for subsurface fluid or gas migration. They may also be sites where localised crenulation cleavage develops and might impact stresses distribution and mechanical behaviour in rock masses. Therefore, understanding the magnitude of uncertainty surrounding the location of fold hinges has practical implications across multiple domains, such as resource exploration endeavours, geotechnical engineering applications including tunnelling and construction projects, groundwater management strategies, and environmental impact assessments.

3.6.   Conclusions

We have successfully built a three-dimensional structural model of the Lago di Cignana area by relying on high-resolution geological mapping and an extensive dataset comprising both original and legacy structural measurements of foliation and fold axis observations. Within this model, we have represented the tectonic boundaries exposed in the area, some of which are major Alpine shear structures such as the Roisan-Cignana Shear Zone, the Dent Blanche Basal Thrust and the Combin Fault. Our interpolation workflow employs the Discrete Smooth Interpolator algorithm, allowing to impose the tectonic surfaces to align with the foliation planes and fold axes vectors. For the modelling of open and isoclinal folds, we have incorporated the 3D implicit interpolation of a fold axes and imposed the interpolated directions

as tangent constraint on the interpolation of the folded geometries. Furthermore, we have integrated stochastic simulations of fold axes following von Mises-Fisher and Kent models, and quantitatively assessed the uncertainty of isoclinal recumbent folds with this method. The outcoming 200 realisations display partial rotation of the axial plane, closure along the fold axis direction of the isoclinal fold, and higher uncertainty values at fold hinges.

3.7. Author contributions

GA, AB and GC conceptualised the workflow. BM, GDP, GA and AB carried out fieldwork in the study area. BM and GDP managed the GIS and created the structural map of the study area. GA performed the data analysis, modelling and interpretation, with input from AB and GC. GA redacted the manuscript, with inputs from AB. AB acquired funding.

3.8. Acknowledgements

3.9. References

Allmendinger, R.W., Cardozo, N., Fisher, D.M., 2015. Structural Geology Algorithms: Vectors and tensors. Cambridge University Press, Cambridge.

Argand, E., 1916. Sur l'arc des Alpes Occidentales. Eclogae Geologicae Helvetiae 14, 145–191.

Argand, E., 1911. Les nappes de recouvrement des Alpes pennines et leurs prolongements structuraux. Matériaux Pour La Carte Géologique de La Suisse 31, 1–26.

Argand, E., 1909. L'exploration géologique des Alpes pennines centrales. Bulletin de La Société Vaudoise Des Sciences Naturelles 45, 217–276.

Arienti, G., Bistacchi, A., Caumon, G., Dal Piaz, G., Monopoli, B., Bertolo, D., 2024. Regional-scale 3D modelling in metamorphic belts: An implicit model-driven workflow applied in the Pennine Alps. Journal of Structural Geology 180, 105045. https://doi.org/10.1016/j.jsg.2023.105045

Ballèvre, M., Merle, O., 1993. The Combin Fault : compressional reactivation of a Late Cretaceous-Early Tertiary detachment fault in the Western Alps. Schweizerische Mineralogische Und Petrographische Mitteilungen 73, 205–227. https://doi.org/https://doi.org/10/gfsjrz

Bistacchi, A., Dal Piaz, G., Massironi, M., Zattin, M., Balestrieri, M., 2001. The Aosta–Ranzola extensional fault system and Oligocene–Present evolution of the Austroalpine–Penninic wedge in the northwestern Alps. International Journal of Earth Sciences 90, 654–667. https://doi.org/10.1007/s005310000178

Bistacchi, A., Massironi, M., 2000. Post-nappe brittle tectonics and kinematic evolution of the north-western Alps: an integrated approach. Tectonophysics 327, 267–292. https://doi.org/10.1016/S0040-1951(00)00206-7

Bistacchi, A., Massironi, M., Dal Piaz, Giorgio V, Dal Piaz, Giovanni, Monopoli, B., Schiavo, A., Toffolon, G.,

2008. 3D fold and fault reconstruction with an uncertainty model: An example from an Alpine tunnel case study. Computers and Geosciences 34, 351–372. https://doi.org/10.1016/j.cageo.2007.04.002

Bond, C.E., 2015. Uncertainty in structural interpretation: Lessons to be learnt. Journal of Structural Geology 74, 185–200. https://doi.org/10.1016/j.jsg.2015.03.003

Borradaile, G., 2003. Statistics of Earth Science Data. Springer Berlin Heidelberg, Berlin, Heidelberg. https://doi.org/10.1007/978-3-662-05223-5

Bucher, K., 2005. Blueschists, eclogites, and decompression assemblages of the Zermatt-Saas ophiolite: High-pressure metamorphism of subducted Tethys lithosphere. American Mineralogist 90, 821–835. https://doi.org/10.2138/am.2005.1718

Caby, R., 1981. Le Mésozoïque de la zone du Combin en Val d'Aoste (Alpes Graies): Imbrications tectoniques entre séries issues des domaines pennique, austroalpin et océanique. Gèologie Alpine 57, 5–13.

Calcagno, P., Chilès, J.P., Courrioux, G., Guillen, A., 2008. Geological modelling from field data and geological knowledge. Part I. Modelling method coupling 3D potential-field interpolation and geological rules. Physics of the Earth and Planetary Interiors 171, 147–157. https://doi.org/10.1016/j.pepi.2008.06.013

Canepa, M., Castelletto, M., Cesare, B., Martin, S., Zaggia, L., 1990. The Austroapine Mont Mary nappe (Italian Western Alps). Memorie Scienze Geologiche 42, 1–17.

Cardozo, N., Allmendinger, R.W., 2013. Spherical projections with OSXStereonet. Computers & Geosciences 51, 193–205. https://doi.org/10.1016/j.cageo.2012.07.021

Caumon, G., Gray, G., Antoine, C., Titeux, M.O., 2013. Three-dimensional implicit stratigraphic model building from remote sensing data on tetrahedral meshes: Theory and application to a regional model of la Popa Basin, NE Mexico. IEEE Transactions on Geoscience and Remote Sensing 51, 1613–1621. https://doi.org/10.1109/TGRS.2012.2207727

Caumon, G., L. Tertois, A., Zhang, L., 2007. Elements for Stochastic Structural Perturbation of Stratigraphic Models. EAGE Conference on Petroleum Geostatistics. European Association of Geoscientists & Engineers. https://doi.org/10.3997/2214-4609.201403041

Cherpeau, N., Caumon, G., 2015. Stochastic structural modelling in sparse data situations. Petroleum Geoscience 21, 233–247. https://doi.org/10.1144/petgeo2013-030

Chilès, J.P., Aug, C., Guillen, A., Lees, T., 2004. Modelling the geometry of geological units and its uncertainty in 3D from structural data: the potential-field method. Proceedings of International Symposium on Orebody Modelling and Strategic Mine Planning. Perth, 313–320.

Compagnoni, R., Dal Piaz, G. V, Hunziker, J.C., Gosso, G., Lombardo, B., Williamns, P.F., 1977. The Sesia-Lanzo zone, a slice of continental crust with Alpine high pressure-low temperature assem-blages in the Western Italian Alps. Rendiconti Della Società Italiana Di Mineralogia e Petrologia 33, 281–334.

Dal Piaz, G.V., Bistacchi, A., Gianotti, F., Monopoli, B., Passeri, L., Schiavo, A., Bertolo, D., Bonetto, F., Ciarapica, G., Dal Piaz, G., Gouffon, Y., Massironi, M., Ratto, S., Toffolon, G., 2016. Foglio 070 Cervino e Note Illustrative. Carta Geologica d'Italia Alla Scala 1:50.000, ISPRA, Regione Autonoma Valle d'Aosta 432 pp.

Dal Piaz, G.V., Gianotti, F., Monopoli, B., Pennacchioni, G., Tartarotti, P., Schiavo, A., Carraro, F., Bistacchi, A., Massironi, M., Martin, S., Ratto, S., 2010. Foglio 091 Chatillon e Note Illustrative. Carta Geologica d'Italia Alla Scala 1:50.000, ISPRA, Regione Autonoma Valle d'Aosta 152 pp.

Dal Piaz, G. V, 2001. History of tectonic interpretations of the Alps. Journal of Geodynamics 32, 99–114. https://doi.org/10.1016/S0264-3707(01)00019-9

Dal Piaz, G. V, 1999. The Austroalpine-Piedmont nappe stack and the puzzle of Alpine Tethys. Memorie Scienze Geologiche 53, 153–162.

Dal Piaz, G. V, Bistacchi, A., Massironi, M., 2003. Geological outline of the Alps. Episodes Journal of International Geoscience 26, 175–180. https://doi.org/10.18814/EPIIUGS/2003/V26I3/004

Dal Piaz, G. V, Ernst, W.G., 1978. Areal geology and petrology of eclogites and associated metabasites of the Piemonte ophiolite nappe, breuil—st. Jacques area, Italian Western Alps. Tectonophysics 51, 99–126. https://doi.org/10.1016/0040-1951(78)90053-7

de Kemp, E.A., 2000. 3-D visualization of structural field data: Examples from the Archean Caopatina Formation, Abitibi greenstone belt, Québec, Canada. Computers and Geosciences 26, 509–530. https://doi.org/10.1016/S0098-3004(99)00142-9

de Kemp, E.A., Schetselaar, E.M., Hillier, M.J., Lydon, J.W., Ransom, P.W., 2016. Assessing the workflow for regional-scale 3D geologic modeling: An example from the Sullivan time horizon, Purcell Anticlinorium East Kootenay region, southeastern British Columbia. Interpretation 4, SM33–SM50. https://doi.org/10.1190/INT-2015-0191.1

Diehl, E.A., Masson, H., Stutz, A.H., 1952. Contributo alla conoscenza del ricoprimento Dent Blanche. Memorie Istituti Geologia Mineralogia Università Di Padova 17, 53 pp.

Ernst, W.G., Dal Piaz, G. V, 1978. Mineral parageneses of eclogitic rocks and related mafic schists of the Piemonte ophiolite nappe, Breuil-St. Jacques area, Italian Western Alps. American Mineralogist 63, 621–640.

Fisher, N.I., Lewis, T., Embleton, B.J.J., 1987. Statistical analysis of spherical data. Cambridge University Press.

Fisher, N.I., Lewis, T., Willcox, M.E., 1981. Tests of Discordancy for Samples from Fisher's Distribution on the Sphere. Applied Statistics 30, 230. https://doi.org/10.2307/2346346

Fisher, R.A., 1953. Dispersion on a sphere. Proceedings of the Royal Society of London 217, 295–305.

Forster, M., Lister, G., Compagnoni, R., Giles, D., Hills, Q., Betts, P., Beltrando, M., Tamagno, E., 2004. Mapping of oceanic crust with" HP" to" UHP" metamorphism: The Lago di Cignana Unit (Western Alps). In: Pasquarè, G., Venturini, C., Groppelli, G. (Eds.), Mapping Geology in Italy. APAT - Dip. Difesa del Suolo, Serv. Geol. d'Italia, Roma, 279–286.

Frank, T., Tertois, A.L., Mallet, J.L., 2007. 3D-reconstruction of complex geological interfaces from irregularly distributed and noisy point data. Computers and Geosciences 33, 932–943. https://doi.org/10.1016/j.cageo.2006.11.014

Frezzotti, M.L., Selverstone, J., Sharp, Z.D., Compagnoni, R., 2011. Carbonate dissolution during subduction revealed by diamond-bearing rocks from the Alps. Nature Geoscience 4, 703–706. https://doi.org/10.1038/ngeo1246

Groppo, C., Beltrando, M., Compagnoni, R., 2009. The P-T path of the ultra-high pressure Lago Di Cignana and adjoining high-pressure meta-ophiolitic units: insights into the evolution of the subducting Tethyan slab. Journal of Metamorphic Geology 27, 207–231. https://doi.org/10.1111/j.1525-1314.2009.00814.x

Grose, L., Ailleres, L., Laurent, G., Armit, R., Jessell, M., 2019. Inversion of geological knowledge for fold geometry. Journal of Structural Geology 119, 1–14. https://doi.org/10.1016/j.jsg.2018.11.010

Grose, L., Ailleres, L., Laurent, G., Jessell, M., 2021. LoopStructural 1.0: Time-aware geological modelling. Geoscientific Model Development 14, 3915–3937. https://doi.org/10.5194/gmd-14-3915-2021

Grose, L., Laurent, G., Aillères, L., Armit, R., Jessell, M., Caumon, G., 2017. Structural data constraints for implicit modeling of folds. Journal of Structural Geology 104, 80–92.

https://doi.org/10.1016/j.jsg.2017.09.013

Grose, L., Laurent, G., Aillères, L., Armit, R., Jessell, M., Cousin-Dechenaud, T., 2018. Inversion of Structural Geology Data for Fold Geometry. Journal of Geophysical Research: Solid Earth 123, 6318–6333. https://doi.org/10.1029/2017JB015177

Hillier, M., de Kemp, E., Schetselaar, E., 2013. 3D form line construction by structural field interpolation (SFI) of geologic strike and dip observations. Journal of Structural Geology 51, 167–179. https://doi.org/https://doi.org/10.1016/j.jsg.2013.01.012

Hillier, M.J., Schetselaar, E.M., de Kemp, E.A., Perron, G., 2014. Three-Dimensional Modelling of Geological Surfaces Using Generalized Interpolation with Radial Basis Functions. Mathematical Geosciences 46, 931–953. https://doi.org/10.1007/s11004-014-9540-3

Houlding, S.W., 1994. The Geological Characterization Process. 3D Geoscience Modeling. Springer Berlin Heidelberg, Berlin, Heidelberg, 7–26. https://doi.org/10.1007/978-3-642-79012-6_2

Kaufmann, O., Martin, T., 2009. Reprint of "3D geological modelling from boreholes, cross-sections and geological maps, application over former natural gas storages in coal mines" [Comput. Geosci. 34 (2008) 278-290]. Computers and Geosciences 35, 70–82. https://doi.org/10.1016/S0098-3004(08)00227-6

Kent, J.T., 1982. The Fisher-Bingham Distribution on the Sphere. Journal of the Royal Statistical Society 44, 71–80.

Kirst, F., 2017. Polyphase greenschist-facies reactivation of the Dent Blanche Basal Thrust (Western Alps) during progressive Alpine orogeny. Swiss Journal of Geosciences 110, 503–521. https://doi.org/10.1007/s00015-017-0264-5

Kirst, F., Leiss, B., 2017. Kinematics of syn- and post-exhumational shear zones at Lago di Cignana (Western Alps, Italy): constraints on the exhumation of Zermatt–Saas (ultra)high-pressure rocks and deformation along the Combin Fault and Dent Blanche Basal Thrust. International Journal of Earth Sciences 106, 215–236. https://doi.org/10.1007/s00531-016-1316-1

Lajaunie, C., Courrioux, G., Manuel, L., 1997. Foliation fields and 3D cartography in geology: Principles of a method based on potential interpolation. Mathematical Geology 29, 571–584. https://doi.org/10.1007/BF02775087

Laurent, G., Ailleres, L., Grose, L., Caumon, G., Jessell, M., Armit, R., 2016. Implicit modeling of folds and overprinting deformation. Earth and Planetary Science Letters 456, 26–38. https://doi.org/10.1016/j.epsl.2016.09.040

Lindsay, M.D., Aillères, L., Jessell, M.W., de Kemp, E.A., Betts, P.G., 2012. Locating and quantifying geological uncertainty in three-dimensional models: Analysis of the Gippsland Basin, southeastern Australia. Tectonophysics 546–547, 10–27. https://doi.org/10.1016/j.tecto.2012.04.007

Manzotti, P., 2011. Petro-structural map of the Dent Blanche tectonic system between Valpelline and Valtournenche valleys, Western Italian Alps. Journal of Maps 7, 340–352. https://doi.org/10.4113/jom.2011.1179

Manzotti, P., Ballèvre, M., Pitra, P., Schiavi, F., 2021. Missing lawsonite and aragonite found: P–T and fluid composition in meta-marls from the Combin Zone (Western Alps). Contributions to Mineralogy and Petrology 176, 60. https://doi.org/10.1007/s00410-021-01818-0

Manzotti, P., Ballèvre, M., Zucali, M., Robyr, M., Engi, M., 2014a. The tectonometamorphic evolution of the Sesia-Dent Blanche nappes (internal Western Alps): review and synthesis. Swiss Journal of Geosciences 107, 309–336. https://doi.org/10.1007/s00015-014-0172-x

Manzotti, P., Zucali, M., Ballèvre, M., Robyr, M., Engi, M., 2014b. Geometry and kinematics of the Roisan-Cignana Shear Zone, and the orogenic evolution of the Dent Blanche Tectonic System (Western Alps). Swiss Journal of Geosciences 107, 23–47. https://doi.org/10.1007/s00015-014-0157-9

Maxelon, M., Mancktelow, N.S., 2005. Three-dimensional geometry and tectonostratigraphy of the Pennine zone, Central Alps, Switzerland and Northern Italy. Earth-Science Reviews 71, 171–227. https://doi.org/10.1016/j.earscirev.2005.01.003

Maxelon, M., Renard, P., Courrioux, G., Brändli, M., Mancktelow, N., 2009. A workflow to facilitate three-dimensional geometrical modelling of complex poly-deformed geological units. Computers & Geosciences 35, 644–658. https://doi.org/10.1016/j.cageo.2008.06.005

Pakyuz-Charrier, E., Lindsay, M., Ogarko, V., Giraud, J., Jessell, M., 2018. Monte Carlo simulation for uncertainty estimation on structural data in implicit 3-D geological modeling, a guide for disturbance distribution selection and parameterization. Solid Earth 9, 385–402. https://doi.org/10.5194/se-9-385-2018

Passeri, L., Ciarapica, G., Dal Piaz, G.V., 2018. The problematic origin of the Pancherot-Cime Bianche-Bettaforca unit (PCB) in the Piemonte zone (Western Alps). Italian Journal of Geosciences 137, 478–489. https://doi.org/doi.org/10.3301/IJG.2018.21

Perello, P., Gianotti, F., Monopoli, B., Carraro, F., Venturini, G., Fontan, D., Schiavo, A., Bonetto, F., 2011. Foglio 089 Courmayeur e Note Illustrative. Carta Geologica d'Italia Alla Scala 1:50.000, ISPRA, Regione Autonoma Valle d'Aosta 152 pp.

Philippon, M., de Veslud, C.L.C., Gueydan, F., Brun, J.P., Caumon, G., 2015. 3D geometrical modelling of post-foliation deformations in metamorphic terrains (Syros, Cyclades, Greece). Journal of Structural Geology 78, 134–148. https://doi.org/10.1016/j.jsg.2015.07.002

Pizzella, L., Alais, R., Lopez, S., Freulon, X., Rivoirard, J., 2022. Taking Better Advantage of Fold Axis Data to Characterize Anisotropy of Complex Folded Structures in the Implicit Modeling Framework. Mathematical Geosciences 54, 95–130. https://doi.org/10.1007/s11004-021-09950-0

Pleuger, J., Roller, S., Walter, J.M., Jansen, E., Froitzheim, N., 2007. Structural evolution of the contact between two Penninic nappes (Zermatt-Saas zone and Combin zone, Western Alps) and implications for the exhumation mechanism and palaeogeography. International Journal of Earth Sciences 96, 229–252. https://doi.org/10.1007/s00531-006-0106-6

Polino, R., Malusà, M.G., S, M., Carraro, F., Gianotti, F., Bonetto, F., Perello, P., Schiavo, A., Gouffon, Y., 2015. Foglio 090 Aosta e Note Illustrative. Carta Geologica d'Italia Alla Scala 1:50.000, ISPRA, Regione Autonoma Valle d'Aosta 144 pp.

Ramsay, J.G., 1967. Folding and Fracturing of Rocks. McGraw-Hill, New York.

Reddy, S.M., Wheeler, J., Butler, R.W.H., Cliff, R.A., Freeman, S., Inger, S., Pickles, C., Kelley, S.P., 2003. Kinematic reworking and exhumation within the convergent Alpine Orogen. Tectonophysics 365, 77–102. https://doi.org/10.1016/S0040-1951(03)00017-9

Reinecke, T., 1998. Prograde high- to ultrahigh-pressure metamorphism and exhumation of oceanic sediments at Lago di Cignana, Zermatt-Saas Zone, western Alps. Lithos 42, 147–189. https://doi.org/https://doi.org/10.1016/S0024-4937(97)00041-8

Schmid, S.M., Fügenschuh, B., Kissling, E., Schuster, R., 2004. Tectonic map and overall architecture of the Alpine orogen. Eclogae Geologicae Helvetiae 97, 93–117. https://doi.org/10.1007/s00015-004-1113-x

Schneeberger, R., de La Varga, M., Egli, D., Berger, A., Kober, F., Wellmann, F., Herwegh, M., 2017. Methods and uncertainty estimations of 3-D structural modelling in crystalline rocks: a case study. Solid Earth 8,

987–1002. https://doi.org/10.5194/se-8-987-2017

Shannon, E.C., 1948. A mathematical theory of communication. Bell System Technical Journal 27, 379–423.

Steck, A., Bigioggero, B., Dal Piaz, G. V, Escher, A., Martinotti, G., Masson, H., 1999. Carta tectonique des Alpes de Suisse occidentale et des régions avoisinantes, 1:100.000. Service Hydrologique et Géologique National Carte spéc, 4 feuilles.

Stockwell, C.H., 1950. The use of plunge in the construction of cross-sections of folds. Proceedings of the Geological Society of Canada 3, 97–121.

Sue, C., Delacou, B., Champagnac, J.D., Allanic, C., Tricart, P., Burkhard, M., 2007. Extensional neotectonics around the bend of the Western/Central Alps: An overview. International Journal of Earth Sciences 96, 1101–1129. https://doi.org/10.1007/S00531-007-0181-3

Thornton, J.M., Mariethoz, G., Brunner, P., 2018. A 3D geological model of a structurally complex alpine region as a basis for interdisciplinary research. Scientific Data 5, 180238. https://doi.org/10.1038/sdata.2018.238

Vollgger, S.A., Cruden, A.R., Ailleres, L., Cowan, E.J., 2015. Regional dome evolution and its control on ore-grade distribution: Insights from 3D implicit modelling of the Navachab gold deposit, Namibia. Ore Geology Reviews 69, 268–284. https://doi.org/https://doi.org/10.1016/j.oregeorev.2015.02.020

Wellmann, J.F., Horowitz, F.G., Schill, E., Regenauer-Lieb, K., 2010. Towards incorporating uncertainty of structural data in 3D geological inversion. Tectonophysics 490, 141–151. https://doi.org/10.1016/j.tecto.2010.04.022

Wellmann, J.F., Regenauer-Lieb, K., 2012. Uncertainties have a meaning: Information entropy as a quality measure for 3-D geological models. Tectonophysics 526–529, 207–216. https://doi.org/10.1016/j.tecto.2011.05.001

Wood, A.T.., 1994. Simulation of the von mises fisher distribution. Communications in Statistics - Simulation and Computation 23, 157–164. https://doi.org/10.1080/03610919408813161

Woodcock, N.H., 1977. Specification of fabric shapes using an eigenvalue method. Geological Society of America Bulletin 88, 1231. https://doi.org/10.1130/0016-7606(1977)88<1231:SOFSUA>2.0.CO;2

Wust, G.H., Silverberg, D.S., 1989. Northern Combin zone complex-Dent Blanche nappe contact: extension within the convergent Alpine belt. Schweizerische Mineralogische Und Petrographische Mitteilungen 69, 251–259.

Yuan, T., 2021. The 8-parameter Fisher–Bingham distribution on the sphere. Computational Statistics 36, 409–420. https://doi.org/10.1007/s00180-020-01023-w

3D implicit structural modelling leveraging inequality and structural constraints: a case study from the Pennine Alps

Gloria Arienti[1], Andrea Bistacchi[1], Guillaume Caumon[2,3], Jérémie Giraud[4],
Bruno Monopoli[5], Giovanni Dal Piaz[5]

[1]Dipartimento di Scienze dell'Ambiente e della Terra, Università degli Studi di Milano-Bicocca, 20126 Italy
[2]RING, GeoRessources – ENSG, Université de Lorraine - CNRS, 54000 France
[3]Institut Universitaire de France (IUF), 75000 France
[4]Centre for Exploration Targeting (School of Earth Sciences), University of Western Australia, 6009 Australia
[5]LTS s.r.l., Treviso, 31020 Italy

Abstract

We combine advanced 3D structural modelling techniques with high-resolution structural mapping to create a geomodelling workflow tailored for Alpine metamorphic settings. The workflow employs the implicit Discrete Smooth Interpolator, which represents geological structures as isovalue surfaces of a volumetric scalar field. We employ inequality position and gradient constraints to integrate off-contact information and structural measurements in the interpolation. To propagate the structural constraint from the topographic surface throughout the model volume, we perform 3D interpolation of an extensive structural dataset of schistosity measurements. We also introduce stochastic simulations of dip-dip direction measurements, generating suites of simulated vectors away from direct observations by replicating orientation distributions derived from the structural database. This accounts for structural uncertainties and produces a range of plausible subsurface scenarios for in-depth analysis. Our workflow is applied to the 3D structural modelling of the Roisetta-Tournalin ridge, located in the Italian Pennine Alps. Results reveal that the introduction of inequality constraints reduces uncertainty related to interpretations in the map and enables the creation of alternative, smoother solutions, while the uncertainty analysis highlights higher uncertainties away from direct measurements and oscillations of up to 100 meters orthogonal to the layers.

4.1. Introduction

Three-dimensional structural models are essential tools for the representation of the Earth's subsurface as they provide comprehensive visualisation of geological structures, thus serving as an advanced form

of geological knowledge expression and storage. Their creation is addressed by a broad range of geomodelling techniques (e.g., Wellmann and Caumon, 2018), among which implicit techniques represent a powerful approach (Jessell et al., 2014). The implicit approach achieves the numerical representation of the geological architecture by building a three-dimensional scalar field as a function of the relative distance (or relative geological time) among geological boundaries (Lajaunie et al., 1997; Mallet, 2002; Chilès et al., 2004; Calcagno et al., 2008), within which they are represented as isovalue surfaces. The first mathematical formulations of the implicit problem applied to geological contexts have been proposed by Houlding (1994) and Lajaunie et al. (1997) and they envisage the propagation of the scalar field in three dimensions through the imposition of different classes of geological and structural constraints, which ensure that the resulting models adhere to observed geological relationships and structures.

To account for observed geological information, implicit methods use mapped geological contacts, borehole markers, and interpretations on structural cross-sections or seismic lines as constraints that impose the value of the implicit function at specific locations (e.g., Kaufmann and Martin, 2009; Philippon et al., 2015; Thornton et al., 2018; Arienti et al., 2024 - Chapter 2). Noteworthy, this kind of constraints pertain to observations made exactly at the location of the boundary. A second class of constraints, known as inequality constraints, control the value of the scalar field introducing inequalities in the interpolation (Frank et al., 2007; Hillier et al., 2014). These constraints define regions based on "greater than" and "less than" relationships, effectively forcing the location of the boundary between units to lie within a specific spatial range. By enabling the use of off-contact observations, derived e.g. from outcrops internal to geological units, or boreholes that terminate within a unit, these constraints significantly enrich the input database for geomodelling.

Despite the abundance and relevance of off-contact observations in the majority of geological settings, inequality position constraints are not usually implemented in geomodelling software, primarily due to the mathematical complexities inherent to solving a system of equations under these constraints and to the computational expense they introduce (Caumon et al., 2013; Hillier et al., 2014). Exceptions are the approaches introduced by Chilès et al. (2004), which incorporates inequality constraints using a Gibbs sampler, Frank et al. (2007), which integrates inequalities into the Discrete Smooth Interpolator (Mallet, 2002), and Hillier et al. (2014), which achieves this through the resolution of a quadratic optimisation problem.

Implicit geomodelling workflows also allow the integration of direct observations of structural measurements into the interpolation process, thanks to the imposition of constraints on the orientation of the gradient of the scalar field (Frank et al., 2007; Calcagno et al., 2008; Hillier et al., 2013, 2014; Laurent et al., 2016; Grose et al., 2017), which is mathematically defined as normal to the isovalue

surfaces. This approach allows using a wide range of structural measurements as constraints, including bedding/schistosity, fold axes and axial planes, and mineral lineation.

To enhance the modelling of complexly folded terrains and to strengthen the structural control exerted by geological rules in areas with sparse input, the weight of structural constraints on the gradient can be further extended interpolating these vectorial data in three dimensions (Hillier et al., 2013; Laurent et al., 2016; Grose et al., 2017; Arienti et al., in prep. - Chapter 3).

The implicit geomodelling approach additionally features remarkable adaptability to accommodate changes in the input constraining dataset. This adaptability is reflected in efficient revision times when new input data becomes available, and in the possibility to introduce stochastic simulations to account for structural uncertainties (Chilès et al., 2004; Caumon et al., 2007; Wellmann et al., 2010; Lindsay et al., 2012; Wellmann and Regenauer-Lieb, 2012; Cherpeau and Caumon, 2015; Pakyuz-Charrier et al., 2018). The simulation of suites of scenarios allows managing uncertainty through exploration of the space of acceptable models, improving geological understanding and enhancing the model's robustness.

In this work, we apply the implicit geomodelling approach to the metamorphic Italian Pennine Alps. Although the method was initially developed for sedimentary settings, its suitability for addressing complex metamorphic settings has been well-established (Maxelon and Mancktelow, 2005; Bistacchi et al., 2008; Maxelon et al., 2009; Hillier et al., 2013; Perrouty et al., 2014; Vollgger et al., 2015; Philippon et al., 2015; de Kemp et al., 2016; Schneeberger et al., 2017; Thornton et al., 2018; Arienti et al., 2024 - Chapter 2). Specifically, we employ the Discrete Smooth Interpolator algorithm (DSI; Frank et al., 2007; Caumon et al., 2013) and incorporate the range of constraints mentioned earlier to guide the implicit algorithm in generating interpretations.

We represent the tectonic architecture exposed along the Roisetta-Tournalin ridge, a north-south trending sequence of mountain peaks above 3,000 meters (Mount Roisetta 3,334 m a.s.l., Mount Grand Tournalin 3,379 m a.s.l., Mount Petit Tournalin 3,207 m a.s.l.) comprised between the Valtournenche and Ayas Valleys (Fig. 4.1). The area displays a stack of ophiolitic tectono-metamorphic units which experienced both ductile and brittle deformation events during the Alpine orogeny, resulting in frequent thickness variations, multi-scale and disharmonic folding patterns. It is worth noting that this area falls within the extent of a prior regional geological modelling effort (Arienti et al., 2024 – Chapter 2), which represented the tectonic architecture exposed between the Mont Blanc and the Monte Rosa leveraging structural interpretations performed on vertical cross-sections. In the following sections, we increase the resolution of the representation and, by combining advanced modelling strategies with high-resolution geological mapping, we enhance the understanding of this Alpine region.

4.2.   Geological and tectonic setting

The Alps are the European collisional orogen originated from the Cretaceous-onward convergence between the Adriatic and European tectonic plates. The orogeny process involved the subduction of the Ligurian-Piedmont Ocean, which once separated the two continents, and later collision and subduction of the passive continental margins (Dal Piaz et al., 2003). The orogenic suture zone is exposed in the northwestern Alps, where it can be traced following the ophiolitic rock units of the Piedmont nappe system (Dal Piaz and Ernst, 1978). These ophiolites, along with minor continental slices, are now interleaved between the continental Adriatic and European nappes in the regional tectonic architecture, which as a whole constitutes the Austroalpine-Penninic collisional wedge (Dal Piaz and Ernst, 1978). Within the tectonic architecture of this collisional wedge, different tectono-metamorphic units, i.e. distinct crustal elements with distinct associations of lithology, metamorphic conditions and tectonic evolution, are recognised. These elements are stacked along tectonic boundaries that underwent a history of multiple contractional and extensional events (e.g., Reddy et al., 2003) which affected and transposed internal schistosity and structures as well.

Our study transect is situated in the Piedmont ophiolitic system (see Fig. 4.1 for the structural map), within which two first-order nappes, the Combin zone and the Zermatt-Saas unit, are recognised on the basis of lithological and metamorphic distinctions. The Combin zone is a structurally composite nappe that incorporates both ophiolites and minor metasedimentary cover units that underwent metamorphism under greenschist facies conditions during post-collisional times (Ernst and Dal Piaz, 1978). The ophiolitic succession within the Combin zone is characterised by a complex amalgamation of terrigenous metasediments, metabasalts, metagabbros and serpentinites. Remnants of oceanic and manganese-rich metasediments are also exposed (Dal Piaz et al., 1979).

In contrast, the non-ophiolite-related units are identified as decollement cover units, and they are represented by the Pancherot-Cime Bianche-Bettaforca unit (PCB; Passeri et al., 2018 and refs. therein) within our study area. These rocks correspond to the Frilihorn unit in the Swiss literature (Marthaler, 1984). Initially considered as the basal complex of the Combin zone (Dal Piaz and Ernst, 1978), the PCB unit was later reinterpreted as an independently evolved cover unit with an uncertain basement (Dal Piaz, 1999). The PCB unit exhibits affinities with the sedimentary succession of the Austroalpine nappe system and has been interpreted by Passeri et al. (2018) as the remnant of extensional allochtons originally positioned along the Adria-facing ocean-continent transition. In our study area, the PCB unit separates the Upper and Lower Combin ophiolitic units, (Ballèvre et al., 1986), which share similar characteristics, albeit with some variations in mineralogical content (Dal Piaz and Ernst, 1978).

The tectonic boundary separating the Combin and Zermatt-Saas units is represented by the Combin Fault, a major Alpine shear zone considered responsible for the exhumation of eclogitic units to

shallower crustal levels (Ballèvre and Merle, 1993). The Zermatt-Saas unit, underlying the Combin zone, is primarily composed of ophiolites covered by a thin metasedimentary layer. The ophiolitic succession within this unit includes thick serpentinised peridotites, discontinuous metagabbros and massive to pillowed metabasalts (Dal Piaz and Ernst, 1978). The rocks of the Zermatt-Saas unit have undergone a complex history of metamorphism. They initially experienced high-pressure, low-temperature metamorphism during the early stages of the Alpine orogeny related to subduction. Later, they underwent an overprinting phase under greenschist facies conditions as a result of decompression (Ernst and Dal Piaz, 1978; Bucher, 2005).

Additionally, bodies of eclogitic Austroalpine outliers are distributed along the Combin Fault and exhibit metamorphism coeval to the high-pressure events recorded in the Zermatt-Saas unit (Dal Piaz et al., 2001). In our study area, these eclogitic outliers are represented by the single lens of the Crebuchette unit (Fig. 4.1).

In this area, the Austroalpine-Penninic collisional wedge has additionally experienced two distinct phases of brittle tectonics, subsequent to the ductile deformation. The first phase involved NW-SE extension during the Oligocene, followed by a second phase characterised by SW-directed lateral extrusion from the Miocene onward (Bistacchi and Massironi, 2000; Bistacchi et al., 2000, 2001; Sue et al., 2007).

4.3. Methodology

Our implicit modelling workflow (Fig. 4.2) builds multiple 3D structural models of the tectonic sequence exposed along the Roisetta-Tournalin ridge by sequential integration of value and gradient constraints, and by introducing stochastic simulations of schistosity data. In the following sections, we describe each step in the workflow, before presenting the results in Sect. 4.4.

4.3.1. Input data

Our input working information includes the structural map in Fig. 4.1 and an extensive database of structural measurements of schistosity and fold axes, complemented by a 2-meter resolution LIDAR Digital Elevation Model (DEM) and aerial orthophotos with resolution of 20 cm per pixel (provided by the geological survey of Autonomous Aosta Valley Region). The structural map results from the combination of 1:10,000 mapped outcrops, available on the Aosta Valley Region geology portal (https://geoportale.regione.vda.it/; Dal Piaz et al., 2010, 2016; Perello et al., 2011; Polino et al., 2015), with the new 1:75,000 tectonic map of the northern Aosta Valley (presented in Arienti et al., 2024 – Chapter 2) that results from a recent upscaling of the same geological database. The study area is characterised by a remarkable 1,500 meters vertical relief, stretching from Mount Grand Tournalin (elevation 3,379 m a.s.l.) to the Valtournenche and Ayas Valleys, allowing for the truly three-

dimensionality of the geological dataset (Fig. 4.3).
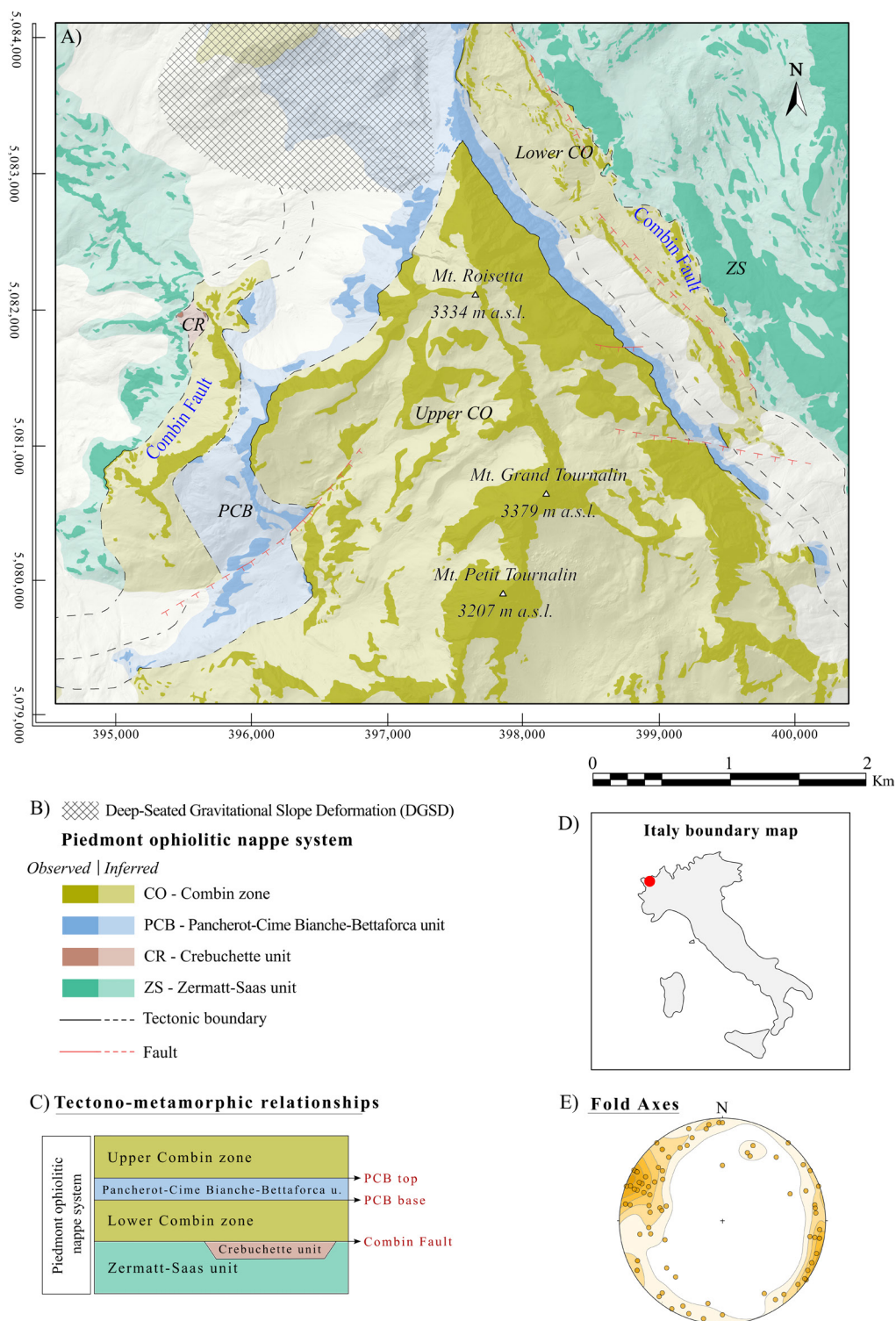
Figure 4.1. Surface input data of the Roisetta-Tournalin ridge region. A) Structural map, coordinates as WGS 1984 UTM Zone 32N. B) Tectonic legend. C) Scheme of the tectono-metamorphic relationships. D) Location of the study area in northwestern Italy in red. E) Fold axes measurements collected during fieldwork, with Kamb contouring with interval 1 σ and significance level 2 σ (Cardozo and Allmendinger, 2013; Allmendinger et al., 2015).

A. Input data
Tectonic map and database of geological and structural direct observations.

Tectonic contacts:
— *Observed*
- - - *Inferred*

B. Spherical statistics study
· Definition of homogeneous structural domains.
· Analysis of statistical distributions of schistosity data. Case for von Mises-Fisher distribution (concentration parameter *k*, mean direction).

C. Interpolation of schistosity data
3D interpolation of the normals to the schistosity planes using DSI.

D. Interpolation of geometries
3D implicit interpolation of the tectonic scalar field. Interpolated schistosity imposed as gradient constraint.

0 tectonic scalar field 1

Model 1

E. Inequality constraints
Defined at local extrema points on mapped outcrops.

0 tectonic scalar field 1

F. Interpolation of geometries leveraging off-contact information
The interpolation conforms to observed tectonic contacts and inequality constraints.

Tectonic contacts:
— *Observed*
- - - *Inferred*
········· *from interpolation with inequality constraints*

Model 2

G. Stochastic simulation of normal to schistosity data
Reproducing vMF distributions.

x 100
Parameters:
· concentration coeff. *k*
· mean direction

H. Interpolation of alternative geometries
For every simulated dataset. Both original and simulated data imposed as constraints.

0 tectonic scalar field 1

Model 3 - 102

x 100

Figure 4.2. Geomodelling workflow, detailed in Sect. 4.3 of the text.

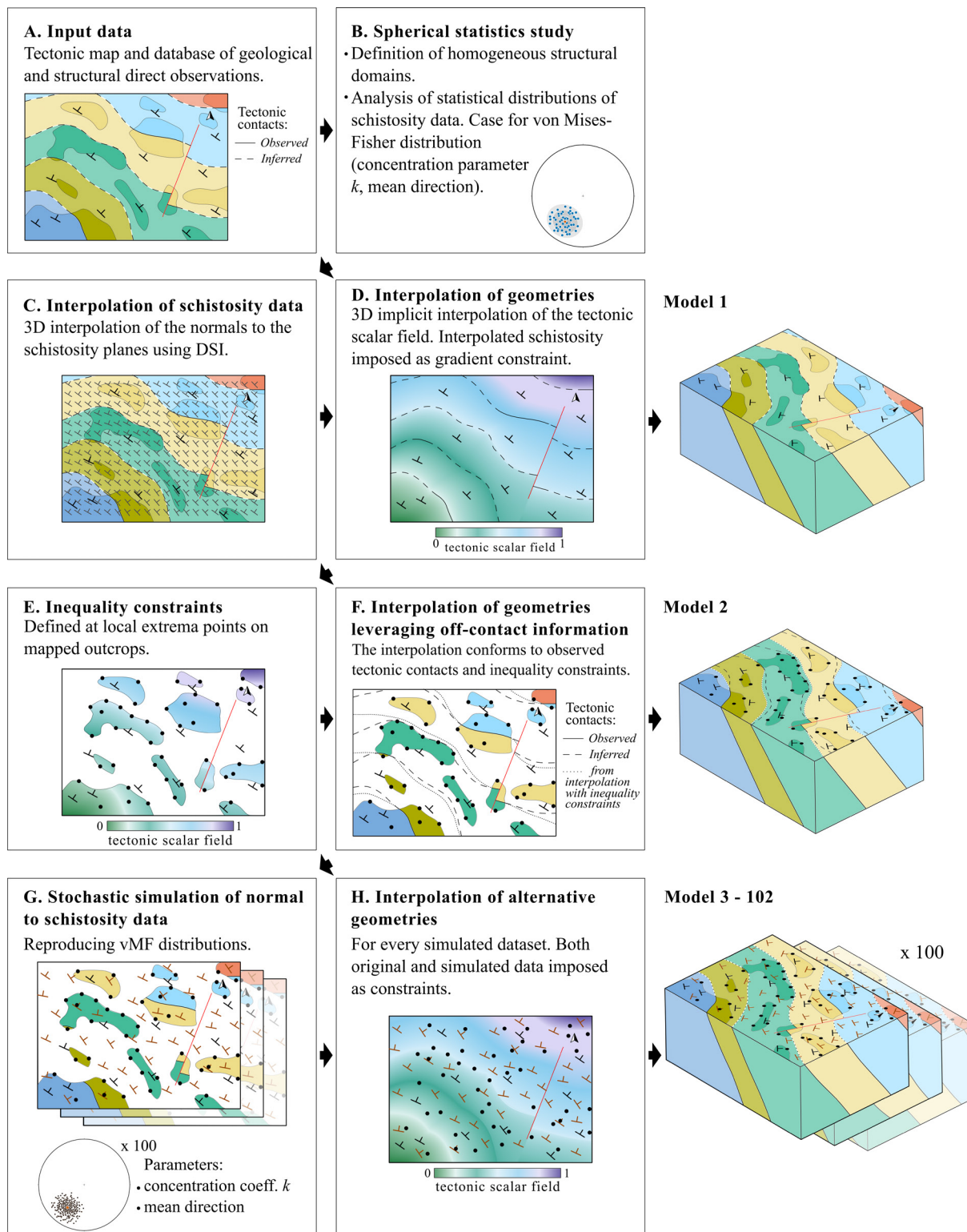Like in most traditional geological mapping studies, the geological data presented in our structural map are distinguished into "observed" and "inferred" on the basis on the level of certainty associated with the information they convey (Fig. 4.1). Most of the times, observed information corresponds to outcrops where a single unit is observed, classified as off-contact observations. In fact, outcrops where tectonic contacts are directly observed (on-contact observations) are not so common, also because tectonic contacts are quite often associated to strongly deformed rocks that tend to undergo selective erosion. In contrast, inferred information is composed of interpretations made by expert geologists, serving as a best guess of the bedrock geology undercover beneath Quaternary deposits. Even in our high mountain environment, on-contact observations account for only ca. 21% of the total length of tectonic contacts in map view (Fig. 4.1). This highlights the impact of expert interpretations on the final modelling results and underscores the importance of integrating off-contact observations into the modelling process through the imposition of inequality constraints.

4.3.2. Spherical orientation analysis

Orientation analysis is performed with the aim of (i) upscaling the structural database from the outcrop resolution to the model scale by defining one or more representative vectors for each investigated outcrop, (ii) providing insights into the structural behaviour and recognising structurally homogeneous domains, and (iii) characterising the statistical distributions of schistosity data in preparation for uncertainty analysis. The results of this analysis are in Sect. 4.4.1.

The structural database of metamorphic schistosity consists of direct measurements collected in the field, grouped by sampling location and with sample sizes sufficiently large to derive representative summary statistics (Fisher et al., 1987). We perform the spherical analysis on the normal directions to the schistosity data, described as three-component unit vectors ($easting, northing, elevation$) computed using direction cosines dip and $dip\ azimuth$:

$$easting = cos\left(\frac{\pi}{2} - dip\right) sin(dip\ azimuth - \pi), \tag{1}$$

$$northing = cos\left(\frac{\pi}{2} - dip\right) cos(dip\ azimuth - \pi), \tag{2}$$

$$elevation = -sin\left(\frac{\pi}{2} - dip\right). \tag{3}$$

To upscale the structural information from the outcrop scale and avoid local noise, we compute one or more mean directions (Borradaile, 2003) for each outcrop, focusing on manually recognised outcrop-scale fold's limbs. The mean direction represents the orientation ($\bar{x}, \bar{y}, \bar{z}$) of the resultant R of the sample of n measurements:

$$R^2 = \left(\sum_{i=1}^{n} easting_i\right)^2 + \left(\sum_{i=1}^{n} northing_i\right)^2 + \left(\sum_{i=1}^{n} elevation_i\right)^2, \tag{4}$$

$$\bar{x} = \frac{1}{R}\sum_{i=1}^{n} easting_i, \qquad \bar{y} = \frac{1}{R}\sum_{i=1}^{n} northing_i, \qquad \bar{z} = \frac{1}{R}\sum_{i=1}^{n} elevation_i. \quad (5)$$

Based on outcrop data, we identify structurally homogeneous domains, i.e. the portions of the study area that share similar deformation styles, and which can thus be described by a common average schistosity, or that display the same folding style. Each homogeneous domain can be characterised by the parameters of a statistical distribution that successfully describes its schistosity data. Firstly, we investigate the data sample through eigenanalysis (Woodcock, 1977) and obtain information about the three eigenvectors (v_1, v_2, v_3), corresponding to the three orthogonal principal axes of the sample, with v_1 being the major axis (and often an estimate of the mean direction), v_2 the intermediate and v_3 the minor axis. The corresponding eigenvalues (S_1, S_2, S_3) are directly related to the shape of the data sample and, in case of unimodal distributions, they give a first estimate of the isotropy or anisotropy around the mean axis and of the level of clustering thanks to the parameters K and C (Woodcock, 1977):

$$K = \frac{\ln(S_1/S_2)}{\ln(S_2/S_3)} \qquad and \qquad C = \ln(S_1/S_3). \qquad (6)$$

Low values of K ($0 \leq k < 1$) indicate data samples with girdle tendencies, clusters are indicated by high values of K ($1 < K \leq \infty$), while C quantifies the strength of the preferred orientation (Woodcock, 1977).

Successively, the hypothesis of the observations being successfully described by a particular spherical distribution can be supported by goodness-of-fit tests. In this work we present the case for a von Mises-Fisher distribution (vMF; Fisher, 1953; Fisher and Best, 1984) since, as we will see in Sect. 4.4.3, this distribution is accepted within a subarea of the model where we perform the uncertainty analysis. The von Mises-Fisher distribution (Fisher, 1953) is parameterised with the mean direction of the sample (5) and the concentration parameter k, which describes the clustering of data points assigning higher values to more tightly clustered distributions:

$$k = \frac{n-1}{n-R}. \qquad (7)$$

4.3.3. Overview of the Discrete Smooth Interpolator

Following the data analysis step, 3D interpolation is performed employing the implicit approach implemented in RING Toolkit (Frank et al., 2007; Caumon et al., 2013), which operates within the SKUA/GOCAD environment (https://www.aspentech.com/en/products/sse/aspen-skua). The RING Toolkit solves the interpolation on the nodes of a tetrahedral mesh by applying the Discrete Smooth Interpolator (DSI; Mallet, 2002; Frank et al., 2007; Caumon et al., 2013) using a least-squares weighted approach. In this section we briefly summarise the classes of geological and structural constraints leveraged by the DSI approach. In this section we briefly summarise the geological and structural constraints used in this approach.

The implicit DSI approach is a three-dimensional interpolation method that reproduces the tectonic architecture as a continuous and differentiable scalar field, with the exception of faults and unconformities that are modelled as mathematical as well as geological discontinuities. Geological features of interest are identified as isovalue surfaces within the scalar field, whose continuity, smoothness and well-posedness is ensured by a constant gradient constraint imposed at the interfaces between adjacent tetrahedra (Frank et al., 2007; Caumon et al., 2013).

The scalar field is interpolated using constraints, whose weights in the interpolation can be manually tuned, on both its value and its gradient. The value of the scalar field is controlled by equality constraints from on-contact geological observations and, when applicable, structural interpretations on cross-sections. Inequality constraints also guide the value of the scalar field but are instead, as the name implies, represented by inequalities in the mathematical implicit problem. These constraints result in the interpolation of scalar fields whose values are to be either "greater than" or "lower than" at the location of the inequality constraints and are therefore valuable for integrating off-contact observations, or more in general where specific thresholds need to be maintained within the model. Inequality constraints are potentially very numerous and in Sect. 4.3.5 we discuss a possible approach to reduce the number of these constraints while maximising geological information.
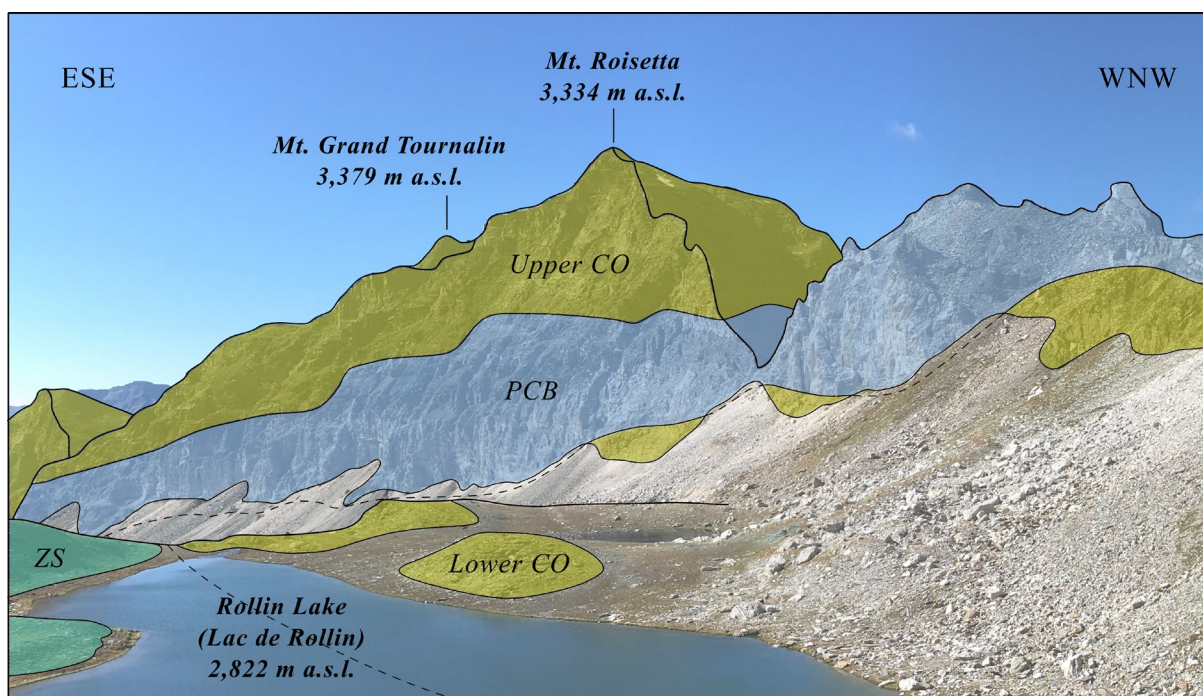

Figure 4.3. Interpreted landscape view of the Roisetta-Tournalin ridge. Colours and names of tectonic units as in the structural map in Fig. 4.1. Point of view is located north of the region represented in the structural map in Fig. 4.1.

Conversely, structural constraints enforce the orientation of the scalar field's gradient through the imposition of tangent and gradient constraints (Frank et al., 2007; Caumon et al., 2013). These constraints bind the gradient of the generated scalar field to be perpendicular to respectively a specified tangent direction (e.g., fold axis) or plane (e.g., schistosity).

Finally, structural features of interest, which have been obtained from the scalar field as isovalue surfaces, can be extracted as triangulates surfaces to create a boundary representation of the 3D structural model.

4.3.4. Interpolation of the normal to the schistosity using DSI

The imposition of gradient constraints on the interpolation process is a powerful methodology that extends its applicability to the three-dimensional interpolation of vectorial data. In our workflow, we perform 3D interpolation of schistosity data to address the challenge posed by sparse data sampling, in order to densify orientation constraints in the interpolation process. In fact, the distribution of field structural measurements is often uneven, confined to the topographic surface, and their sampling may not provide sufficient constraints to accurately represent the complexity of the scalar field in the three dimensions.

Data density is typically influenced by various factors, including outcrops availability and accessibility. Steep slopes or undercover areas (e.g., covered by Quaternary deposits), for instance, may lack direct observations due to the difficulties of data collection. Conversely, certain outcrops may be oversampled, and the data may become superfluous if geometries that are subscale compared to the model's resolution are described, offering more detail than the modelling solution can accurately incorporate. While upscaling methodologies (e.g., Carmichael and Ailleres, 2016) can help solving oversampled areas, the issue of sparse input data can be addressed performing the interpolation of schistosity measurements. The applicability of this approach to our case study is further enhanced by the three-dimensional nature of our input structural database, spread over the rugged topography.

Once the orientation of the normal vectors to the schistosity data is expressed as three-component vectors and upscaled (Sect. 4.3.2), we employ the DSI algorithm and perform the implicit interpolation of a three-dimensional scalar field in which the direction of the gradient is aligned with the orientation of the normal vectors, with the verse indicating the "stacking" of the succession. Affected by the "constant gradient" necessary for the interpolation, the process performs smoothing of the input data and interpolates across areas devoid of structural information. To minimise the smoothing effect, the weight of this constraint can be reduced.

Successively, we transfer the orientation of the gradient as a three-component property to a set of points randomly distributed throughout the model volume. These interpolated vectors will be imposed as

gradient constraints on the interpolation of the 3D structural models within our workflow (Fig. 4.2 for the workflow, steps 2C and 2D).

4.3.5. Efficient placement of inequality constraints

Our model area is situated in a mountainous region characterised by vast outcrops and limited vegetation which, combined with the rugged topography, provides ample opportunities for direct geological observations over large volumes. However, the precise location of tectonic contacts at surface often remains poorly constrained in comparison to the quantity of outcrop data available, since on-contact observations are usually scarce. Many geomodelling workflows tend to overlook this uncertainty, relying instead on expert interpretations to define constraining data for the modelling process. To reduce the need for these interpretations, we introduce inequality constraints at the locations of mapped outcrops to directly incorporate off-contact observations into the interpolation process. This also helps removing a class of uncertain information from the input database, and it encourages the interpolation process to suggest geologically plausible smoother solutions.

Nevertheless, it is important to note that the computational complexity of the RING Toolkit interpolator scales linearly with the number of mesh nodes times the number of inequality constraints (Frank et al., 2007; Caumon et al., 2013), making the efficient placement of inequality constraining crucial. To address this, we present a simple methodology for the selection of locations on the map that correspond to local extrema points, identified as follows.

After an initial interpolation of the tectonic geometries performed incorporating all available information from the structural map, including both observed and inferred portions of the tectonic contacts, we project the values of this scalar field at the mapped outcrop locations onto a two-dimensional grid. By iterating through neighbouring cells, the process identifies locations where the scalar field exhibit local minima or maxima values. These points are found both along the contacts of outcrops and within the outcrop regions themselves. For instance, if we consider a sub-horizontal geological feature, which will be described by the scalar field as a sub-horizontal isosurface, the workflow will register small depressions in the topography as local maxima (assuming a downward scalar field gradient). Conversely, in this specific scenario isolated peaks in the topography would correspond to local minima.

Following this approach, we identify both local maxima and minima to generate, for each tectonic surface we aim to represent, a pair of constraining datasets that define both "greater than" and "lower than" constraints. The locations of the local extrema are recorded as discrete punctual information. After associating each point with the respective tectonic unit to which it belongs, these data points can be introduced as constraining data in the interpolation process (Frank et al., 2007).

4.3.6. Stochastic simulation of schistosity data

Our workflow incorporates stochastic simulations of schistosity data, perturbed according to a suitable orientation distribution, to account for uncertainties in the structural database and to allow for the exploration of a range of plausible scenarios (e.g., Lindsay et al., 2012). In this section we discuss the case for a von Mises-Fisher distribution since, as we will see in Sect. 4.4.1, the schistosity data falling within the area of our uncertainty analysis can be assumed to be derived from this model.

The vMF distribution (Fisher, 1953) on the sphere is the analogue of the isotropic bivariate normal distribution, and it is described by the mean direction vector and by the concentration parameter k, computed in the structural analysis step of our workflow (Sect. 4.3.2). Employing a methodology introduced by Fisher et al. (1981), also applied by Wood (1994), and as formulated in Appendix A in Pakyuz-Charrier et al. (2018), we generate 100 sets of pseudo-random vectors that follow the vMF statistical model. The spatial position of these simulated vectors is assigned randomly within the investigated volume.

These simulated datasets are successively imposed, together with the direct measurements collected in the field, as gradient constraints for the creation of 100 alternative realisations of the tectonic architecture. The outcome is a suite of models that conform to both the direct observations collected in the field and to the simulated vectors (Fig. 4.2G and 4.2H).

The final step of the analysis involves the visualisation and interpretation of the uncertainty results. For this, we compute information entropy H (Shannon, 1948; Wellmann and Regenauer-Lieb, 2012) at each node of the 3D mesh, a measure that helps determine which tectonic unit is most likely to be represented at that location, defined as:

$$H = -\sum_{i=1}^{N} p_i \log p_i, \tag{8}$$

where N is the number of realisations and p_i is the probability of the node to belong to a specific unit. Higher values indicate higher entropy in the system and consequent higher uncertainty on the value of the scalar field at the node. Application of this uncertainty workflow is detailed in Sect. 4.4.3.

4.4. Results

In this section, we apply the geomodelling methodologies described in Sect. 4.3 to the interpolation of the tectonic architecture exposed along the Roisetta-Tournalin ridge in the Italian Pennine Alps. We represent the tectonic contacts that separates different tectono-metamorphic units, without considering internal lithological variations. Through the progressive introduction of supplementary constraining data in the interpolation process, we generate multiple geologically plausible models. We then engage in the description of the outcomes and their structural meaning.

4.4.1. Spherical statistics analysis

The input structural dataset for our geomodelling work includes approximately 2,200 schistosity measurements and about 100 observations of fold axes. Structural data falling within the boundaries of a Deep-Seated Gravitational Slope Deformation (i.e., slow slope instabilities characteristic of mountain environments) of ca. 2.2 km^2 have been excluded from the structural analysis and the subsequent geomodelling interpolation process (Fig. 4.4A), as these data may be affected by rotation and tilting, making them unreliable for our purpose.

Out of the entirety of schistosity measurements, approximately 2,050 are original and have been collected with sample sizes sufficiently large to derive statistics for each outcrop investigated. For every structural station, a spherical statistics analysis has been performed to determine the representative orientation of the schistosity exposed at the outcrop, as described in Sect. 4.3.2. Ultimately, the output structural database used in the three-dimensional interpolation steps is composed of 199 schistosity measurements.

The database of structural measurements collected in the field shows a distinct scale-dependent behaviour. At the outcrop scale, we observe the presence of smooth, ductile structures deformed with close to isoclinal folded geometries, where the fold axes exhibit predominant sub-horizontal orientations that span across all quadrants of the stereogram (Fig. 4.1E). We associate these trends with Alpine deformation phases of shearing (Reddy et al., 2003).

We successively increase our scale of observation and at the model scale we recognise two structurally homogeneous sectors (Fig. 4.4). The western portion of the model (Sector 1 in Fig. 4.4) is characterised by schistosity data scattered across all the quadrants of the stereogram, folded at the outcrop scale along the fold systems introduced before, and creating NE-SW and NW-SE trending girdles.

Conversely, schistosity data falling within the eastern portion of the study area describe a model-scale synform open fold (Sector 2 in Fig. 4.4). Here, schistosity measurements dip with low to medium angle towards the west-southwest and are organised in a cluster with axial symmetry. To preliminary analyse this dataset, we perform an eigenanalysis (methodology in Sect. 4.3.2) that highlights rotational symmetry around the mean axis and good level of clustering in a largely uniaxial way (shape parameter K of 30.80 and C of 3.91; Fig. 4.4C), which indicate that the vMF distribution might be a good candidate to describe the data.
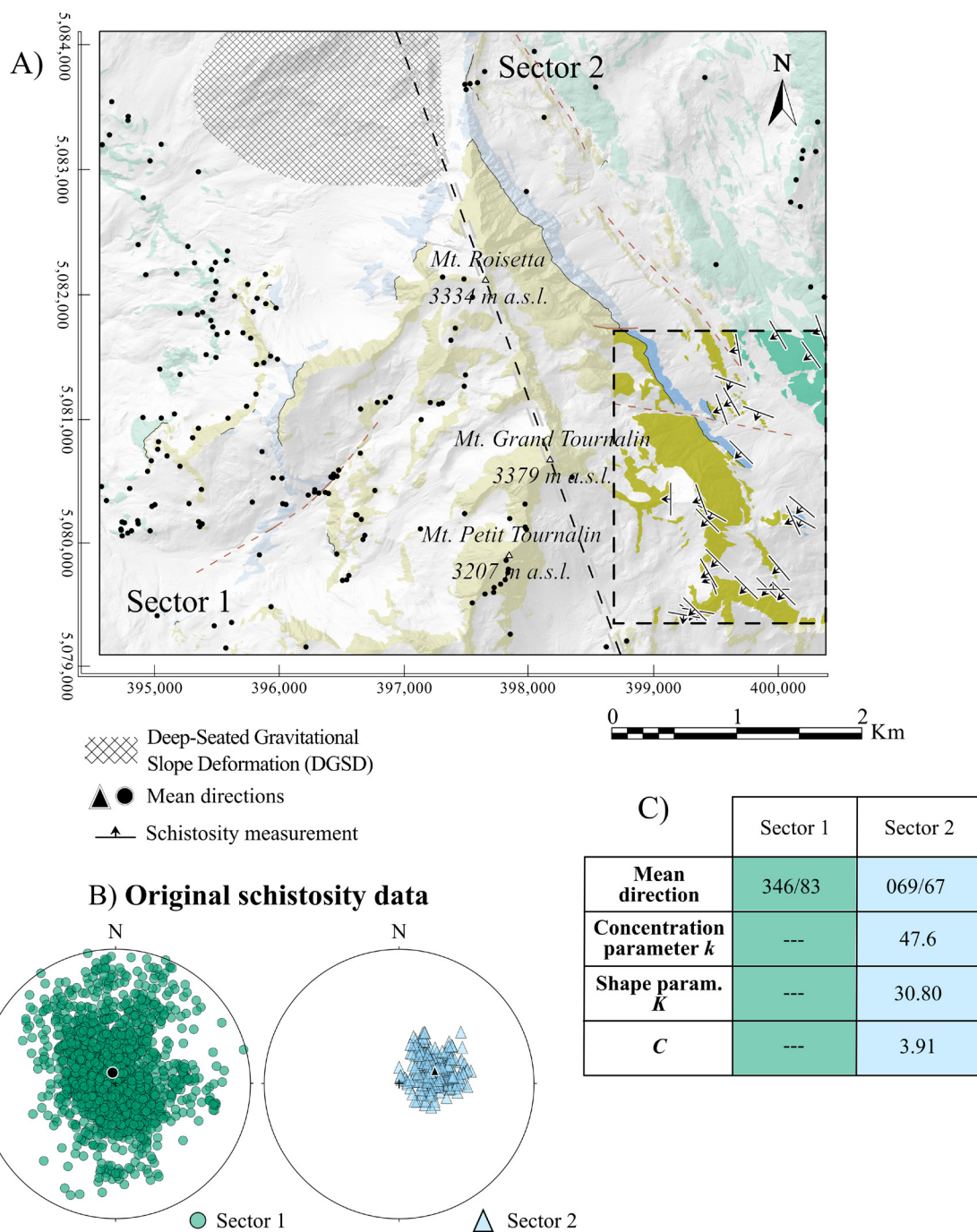
Figure 4.4. Spherical statistics analysis, as detailed in Sect. 4.3.2 (methodology) and 4.4.1 (application) of the text. A) Structural map. Structural measurements collected at the black dot's locations. Colours and names as in Fig. 4.1. Black and grey dashed line separates two structurally homogeneous domains, namely Sector 1 and 2. Black dashed rectangle in the eastern portion bounds the area for the uncertainty analysis described in Sect. 4.4.3 of the text. Within this area, direct measurements of schistosity data are represented. B) Stereogram of input schistosity data for each sector. 1872 primary observations for sector 1, and 324 for sector 2. Black symbols represent the mean vectors for the samples. C) Spherical parameters computed for sector 2, where the uncertainty analysis is focused.

To test this hypothesis, we employ a modified version of the goodness-of-fit tests for vMF models proposed by Fisher and Best (1984), which provides means to calculate a formal estimate of the adequacy of fit to the vMF. Fisher and Best (1984) rotate the original vectors (θ, Φ), with original mean direction $(\bar{\theta}, \bar{\Phi})$ and sample size n, to new coordinates (θ', Φ') with mean direction $(0, 0)$ and to (θ'', Φ'') with mean direction $(3\pi/2 - \bar{\theta}, \bar{\Phi} - \pi)$. On these rotated vectors, they compute the relations

$$S_{Exponential} \equiv \{c_i' = 1 - \cos\theta_i',\ 1 \le i \le n\}, \tag{9}$$

$$S_{Uniform} \equiv \{\Phi_i',\ 1 \le i \le n\}, \tag{10}$$

$$S_{Normal} \equiv \left\{z_i = \Phi_i'' \sqrt{\sin\theta_i''},\ 1 \le i \le n\right\}, \tag{11}$$

and propose to check:

(i)   the colatitude distribution ($S_{Exponential}$) of the sample for exponentiality,

(ii)   the assumption of rotational symmetry about the mean direction ($S_{Uniform}$) for uniformity

(iii)   and the correlation between colatitude and longitude (S_{Normal}) for normality.

We test (i-iii) by computing the corresponding Cumulative Density Functions (CDF) for the field measurements and comparing them with the Empirical CDFs fitted on the sample, allowing us a quantitative analysis. To compare theoretical and empirical CDFs, we perform the Lilliefors test (Lilliefors, 1967, 1969) for (i) and (iii), and the Kuiper test (Fisher and Best, 1984) for (ii), and complement them with the visual analysis of said CDFs (Fig. 4.5). Results provide both a graphical inspection of the differences and a quantitative interpretation thanks to the p-value and statistic outputs. We validated the assumptions using tabulated values, indicating sufficient fit to consider the sample as drawn from a vMF distribution.
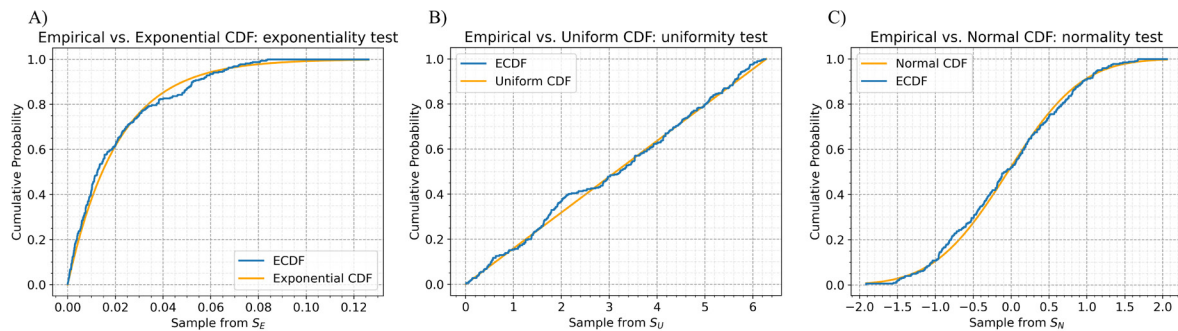

Figure 4.5. Goodness-of-fit test for vMF distribution, modified from Fisher and Best (1984). Tests validated using tabulated values. Sample of 324 measurements (Sector 2 in Fig. 4.4). A) Test for exponentiality. B) Test for uniformity. C) Test for normality.

The mean direction (trend/plunge 069/67) and concentration parameter for this cluster ($k = 47.6$, Fig. 4.4C) are computed using equations (5) and (7). In Sect. 4.4.3, we will focus on a subarea located within this sector (dashed rectangular area in Fig. 4.4) to perform the uncertainty analysis steps of our workflow. In this phase, the spherical statistics parameters will play a key role in guiding the stochastic simulation of schistosity data according to the derived vMF distribution.

4.4.2. 3D structural model of the Roisetta-Tournalin ridge

To model the Roisetta-Tournalin ridge, the implicit interpolations are performed on a three-dimensional tetrahedral mesh that covers 2,000 meters of vertical elevation, with a resolution of 70 meters (corresponding to the average distance between the nodes of the mesh). The mesh consists of a total of ca. 2.8×10^5 nodes and 1.6×10^6 tetrahedra. The combination of mesh resolution and extent allows for practical interpolation times that range, depending as we will see on the type of constraining data employed, between a couple of seconds and ca. 70 seconds on a desktop computer (AMD Ryzen 9 5950X Processor, NVIDIA GeForce RTX 3080 GPU, 64.0 GB RAM on a Windows system).

The 3D structural models introduced in this section represent the tectonic architecture by building the tectonic contacts (i.e., zones of tectonic displacement that separate different tectono-metamorphic units) that outcrop in the region. As described in the tectonic setting in Sect. 4.2, the tectonic sequence primarily consists of ophiolitic units associated with the oceanic Piedmont nappe system. These are the metamorphic units of the Combin zone, the Pancherot-Cime Bianche-Bettaforca and the Zermatt-Saas (Fig. 4.1). Within the extent of the model area, these units compose a conformable sequence. In our modelling steps, due to its limited dimensions we do not consider the Crebuchette unit and instead, given its metamorphic history, we integrate it into the Zermatt-Saas unit.

The tectonic architecture has been affected by brittle normal faulting, leading to offsets of the tectonic contacts. The faulting events are distinguished in two distinct sets with NE-SW and NW-SE trending directions (Fig. 4.1). These fault surfaces (for a total of five independent surfaces) are incorporated into the modelling workflow during the early stages of the interpolation process as mathematical discontinuities (Frank et al., 2007). The map extensions of these fault surfaces are contained within the spatial boundaries of the 3D model, making them "finite" faults (Fig. 4.1), while we have modelled them extending the vertical dimension to the model boundary by linear extrusion of their mapped geometries. These high-angle faults, with dip angles greater than 60 degrees, exhibit normal kinematics with displacements ranging from several meters to as much as 350 meters in our 3D realisations.

The distribution of input structural measurements within the model volume is heterogeneous, as they are only concentrated at the topographic surface. However, the rugged nature of the topography in our study area allows for strategic positioning of observations in three dimensions and is particularly suitable for representing the sub-horizontal or slightly inclined tectonic contacts exposed in our study region. To

homogenise the structural control on the interpolation, we opt for 3D interpolation of schistosity data as detailed in Sect. 4.3.4. We perform the interpolation of the 199 schistosity measurements (whose location is shown in Fig. 4.4A), which are the outcome of the vectorial means computed in the orientation analysis step (Sect. 4.4.1).

This interpolation yields a 3D scalar field, here referred to as "schistosity scalar field" for clarity, whose gradient follows the oscillations of the normal vectors associated with the input schistosity data while also performing a smoothing process due to the solving of the least-squares problem. The interpolation steps are represented in Fig. 4.6, as applied to a subarea of the model region. The gradient information from this scalar field is then transferred to 3,000 points randomly distributed throughout the 3D volume. This new set of interpolated schistosity data serves as an additional set of constraining data for the interpolation of the 3D structural models of the Roisetta-Tournalin ridge.

We proceed with the interpolation of the first of multiple interpretative scenarios, obtained through the incorporation of all the tectonic contacts delineated in the structural map shown in Fig. 4.1. We constrain the orientation of the interpolation using both the field-collected schistosity data and the values interpolated from the same schistosity data, assigning higher interpolation weights to the first constraining dataset (10 times higher) as allowed by the DSI interpolator. The outcome, obtained through a 20 seconds-long interpolation, is a 3D structural model that conforms to the input structural map and to the structural data observed in the field. This model serves as a baseline representation of the tectonic architecture, and it is improved in the following steps of the workflow, described in this section.
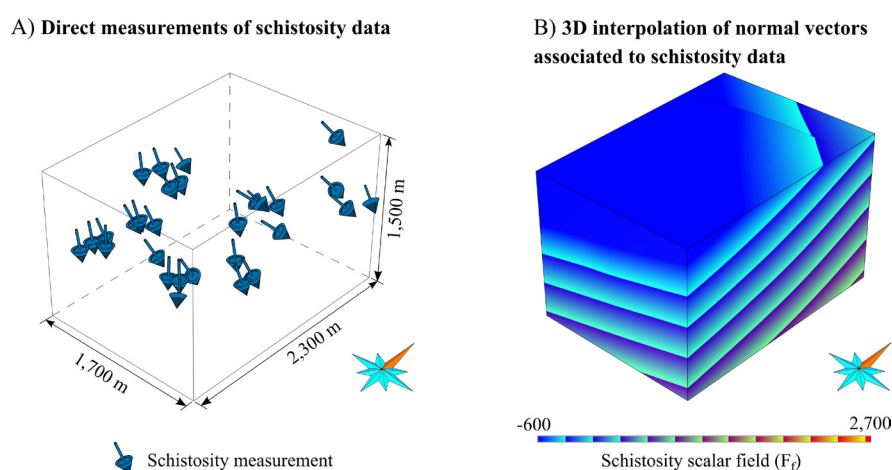

Figure 4.6. Interpolation of schistosity data, as detailed in Sect. 4.3.4 (methodology) and 4.4.2 (application) of the text. Location of the investigated volume is indicated in Fig. 4.4A by the dashed rectangle. A) Direct measurements of schistosity data. The vectors represent the normal directions associated with the schistosity data. B) Three-dimensional interpolation of schistosity data.
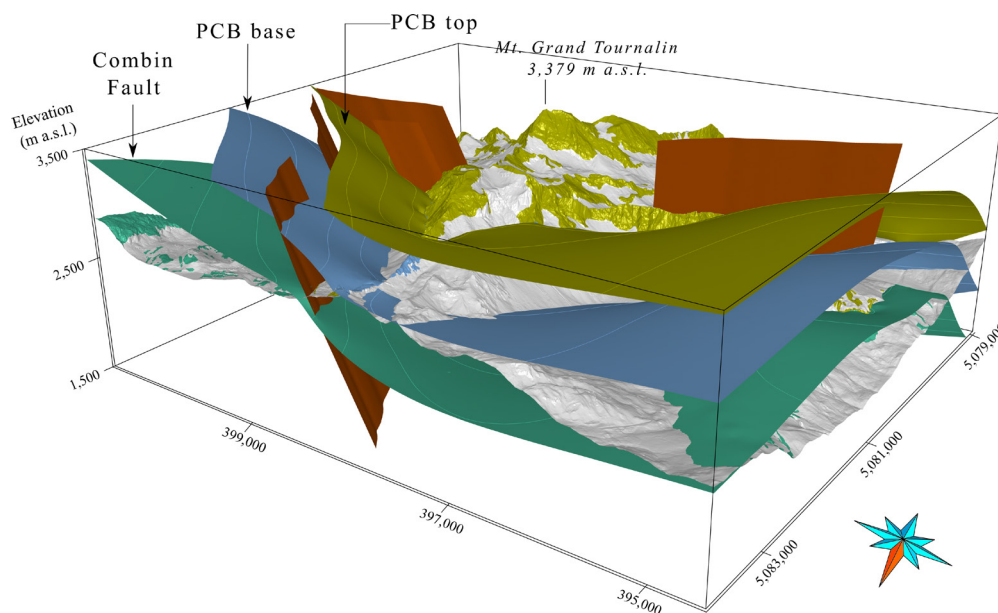
Figure 4.7. 3D view of the boundary representation of the structural model of the Roisetta-Tournalin ridge, obtained leveraging inequality constraints and interpolated schistosity data. Names as in the scheme of the tectono-metamorphic relationships in Fig. 4.1. Topographic surface draped with the structural map showing the outcrop locations.

The second model, shown in Fig. 4.7, is obtained through the introduction of inequality constraints in the interpolation process. Following the procedure outlined in Sect. 4.3.5, the scalar field produced by the interpolation of the first 3D structural model guides the placement of inequality constraints at the location of local extrema within the outcrop areas (Fig. 4.8), along the nodes of a two-dimensional regular grid (cells measuring 2.3 by 2.3 meters). A total of 7,124 inequality points is introduced in the interpolation, resulting in a longer running time, approximately 70 seconds on a desktop computer. The second 3D structural model is therefore governed by the observed portions of the tectonic contacts from the input structural map (Fig. 4.1), by the inequality constraints, and its orientation is conformable to both the original and interpolated schistosity data. The outcome consists of geometries that intersect the topographic surface at locations that might differ from the interpretation proposed in the input structural map (Fig. 4.8C). These intersection lines provide a fresh perspective on the tectonic interpretation of the region, and they could serve as valuable input for creating an enhanced structural map of the area.

4.4.3. Stochastic simulation of schistosity data for uncertainty analysis

We introduce stochastic simulation of the schistosity data with the purpose of accounting for uncertainties in the structural database. We perform the analysis in the rectangular area highlighted in Fig. 4.4A, located on the limb of a model-scale synform fold. Following the extent of this subarea, we

build a tetrahedral mesh with resolution of 30 meters and vertical extension of 1,500 meters (ranging from 1,500 m a.s.l. and 3,000 m a.s.l.). The mesh, on which we perform the interpolation of the simulations, totals 3.5×10^5 nodes and 2.0×10^6 tetrahedral cells.

Following the methodology detailed in Sect. 4.3.6 and employing the parameters derived from the spherical statistics analysis of vMF distribution (mean direction and concentration parameter k) in Sect. 4.4.1, we proceed to populate the 3D volume with a total of 1,000 randomly placed simulated vectors (Fig. 4.9A). This simulation process is carried out iteratively 100 times, and these vectors collectively represent the normal directions associated with the schistosity data.

Subsequently, each of these samples is incorporated in the interpolation process for the generation of 100 realisations of the tectonic architecture (Fig. 4.9B). Each iteration, comprising simulations of schistosity data and interpolations of the new scenarios, requires ca. 60 seconds on a desktop computer. In the interpolation step, we impose as constraining data the observed portions of the tectonic contacts, the set of inequality constraints and both the original schistosity obtained from the spherical analysis and the simulated schistosity vectors generated through the stochastic simulation process. These constraints are essential for producing geologically plausible realisations of the tectonic architecture, that account for both observed and simulated structural data.

The outcomes of the interpolation of 100 simulations of 3D structural models are represented using Information Entropy (Fig. 4.9C and Fig. 4.10) and by showing the intersections of the newly generated surfaces with cross-section planes and with the topography (Fig. 4.10). As it is intuitive, the outcomes highlight the presence of greater oscillations in the geometries of the tectonic contacts as one moves away from the constraints imposed by the structural map. In vertical cross-sections, this behaviour translates in higher uncertainty values away from the topography, while in map view higher uncertainties are concentrated away from on-contact observations (corresponding to the locations of equality constraints in the interpolation; Fig. 4.10).

The oscillations within the interpolated tectonic contacts do not result in overlapping among the three different tectonic units. Instead, they primarily indicate uncertainties in the precise location and orientation of these contacts. The modelled surfaces exhibit oscillations of up to 100 meters in the direction orthogonal to their evolution, which, in turn, influence the intersection points with faults and, consequently, the modelled offsets. Additionally, the interpolation process demonstrates a tendency to maintain relatively constant layer thicknesses. This behaviour is a consequence of the "constant gradient" constraint smoothing effect, which is a necessary component of the DSI algorithm as it is responsible for the well-posedness of the mathematical problem (Frank et al., 2007; Caumon et al., 2013).

A)

B) **Positioning of inequality constraints**

Local minima locations

Local maxima locations

C) **Interpolation leveraging inequality constraints**

- - - — Inferred/observed tectonic
contacts (Fig. 1)
——— Interpolation using
inequality constraints

CO - Combin Zone

PCB - Pancherot-Cime
Bianche-Bettaforca unit

ZS - Zermatt-Saas unit

Inequality constraint points

○ : F_t > PC top   □ : F_t < PC top

◇ : F_t > PC base   △ : F_t < PC base

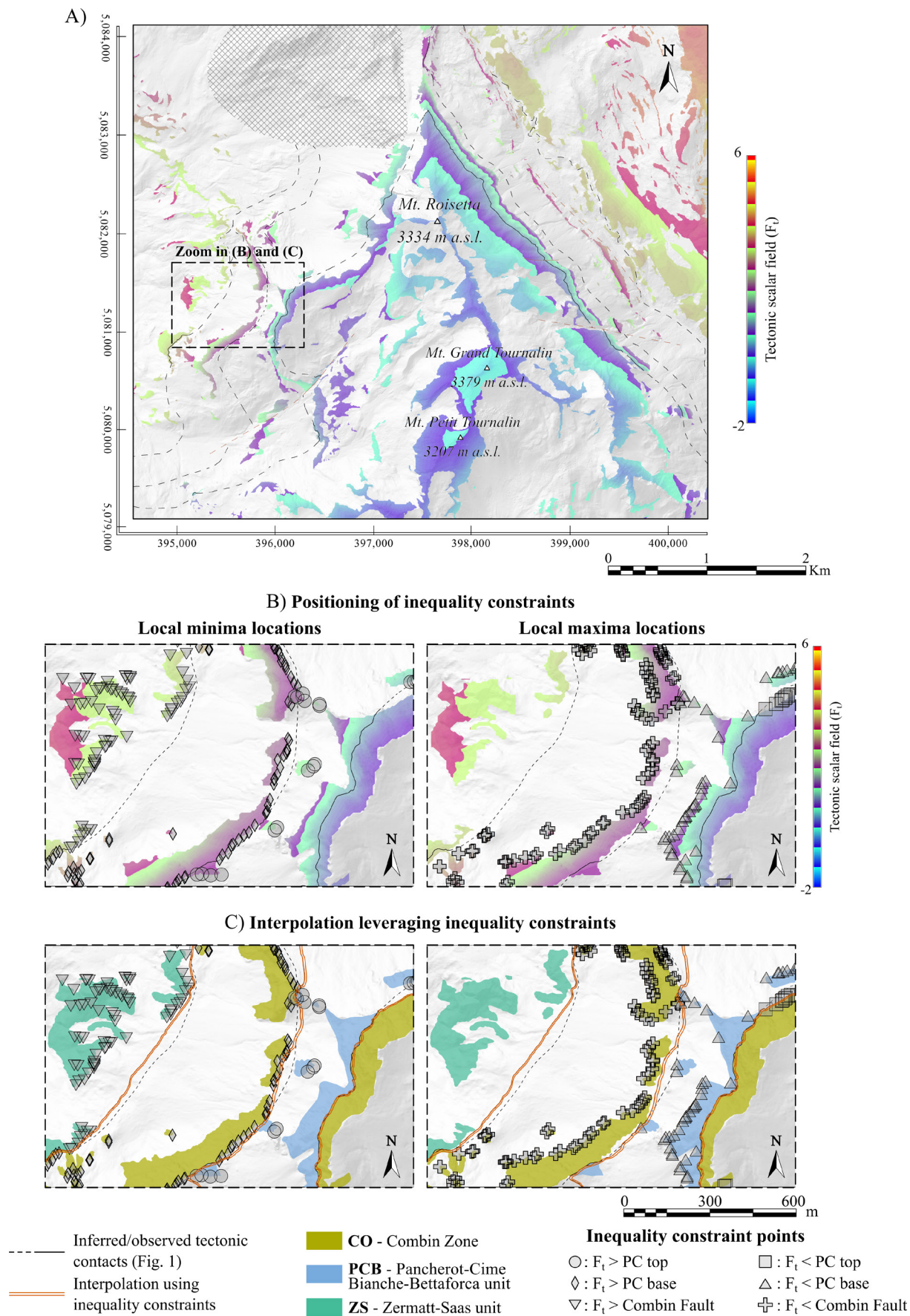▽ : F_t > Combin Fault   ⊕ : F_t < Combin Fault

Figure 4.8 (previous page). Introduction of inequality constraints in the geomodelling workflow, as detailed in Sect. 4.3.5 (methodology) and 4.4.2 (application) of the text. A) Map of the outcrop locations, painted with the value of the scalar field generated using both observed and interpreted tectonic contacts. B) Extract from the map in (A) with location of inequality constraints. The locations correspond to points of local maxima and minima in the scalar field painted on the topographic surface. C) Outcome of the interpolation that leverages inequality constraints.

Furthermore, in the northeastern part of the currently investigated area, some of the realisations of the Combin Fault boundary intersect the topography in correspondence of outcrops of the Zermatt-Saas unit (Fig. 4.10, map views and Section AA'). This occurs because of the similar inclination between the topographic slope and the average schistosity vector observed in the area. Herein lies a conflict between the inequality constraints, designed to prevent the tectonic contact from intersecting the topography in the region where Zermatt-Saas outcrops are mapped, and the orientation imposed by the simulated schistosity data. Despite both categories of constraints are assigned equal weights in the interpolation, in a subsample of the generated geometries the simulated schistosity data assert stronger influence and direct the interpolation of the tectonic contact to intersect the topography. This outcome therefore suggests the possibility of scattered outcrops of Combin rocks within the Zermatt-Saas domain, coinciding with the areas indicated by the results of the uncertainty study.
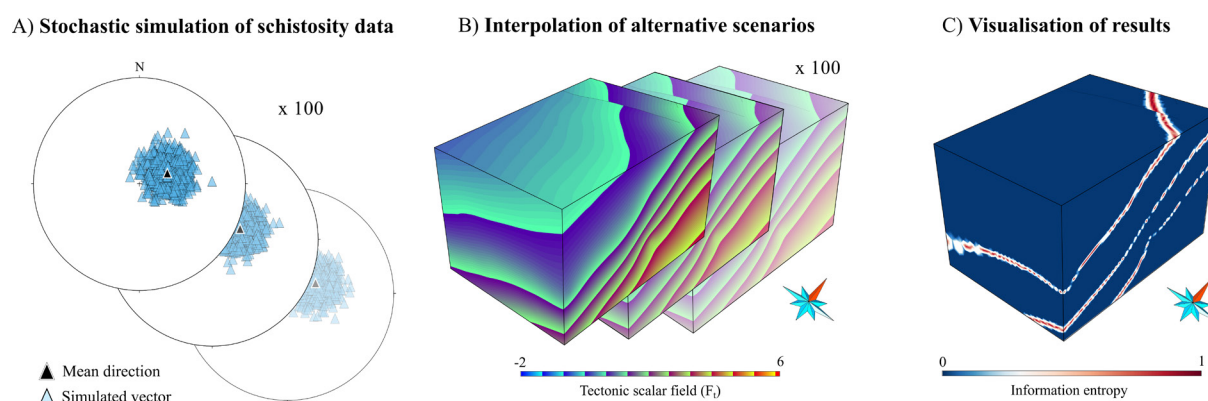

Figure 4.9. Uncertainty analysis workflow, as detailed in Sect. 4.3.6 (methodology) and 4.4.3 (application) of the text. Location of the investigated volume is indicated in Fig. 4.4A by the dashed rectangle. A) Stereogram of 1,000 simulated schistosity vectors. B) Interpolation of 100 new geometries. C) Visualisation of results with Information Entropy (Wellmann and Regenauer-Lieb, 2012).

A) __Map view__

Intersections with surfaces

Information Entropy

B) __Cross-section views__

Intersections with surfaces
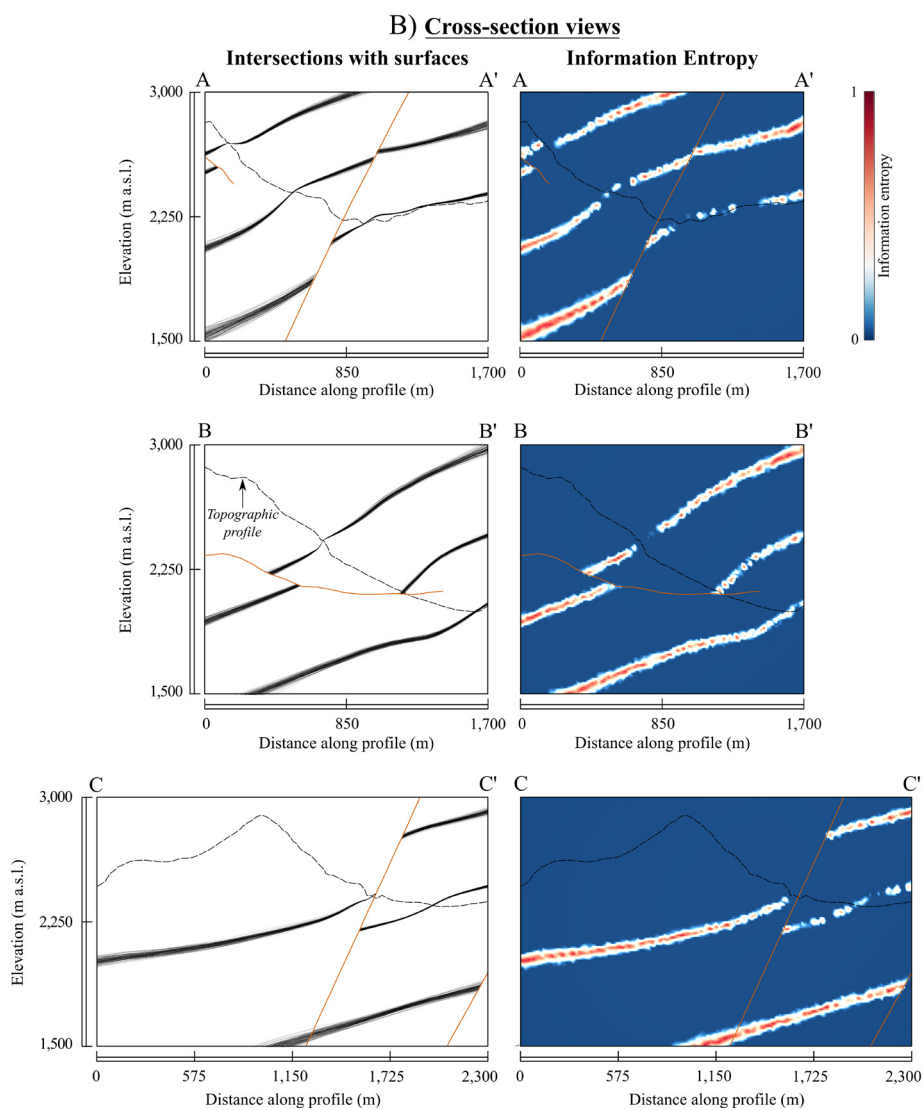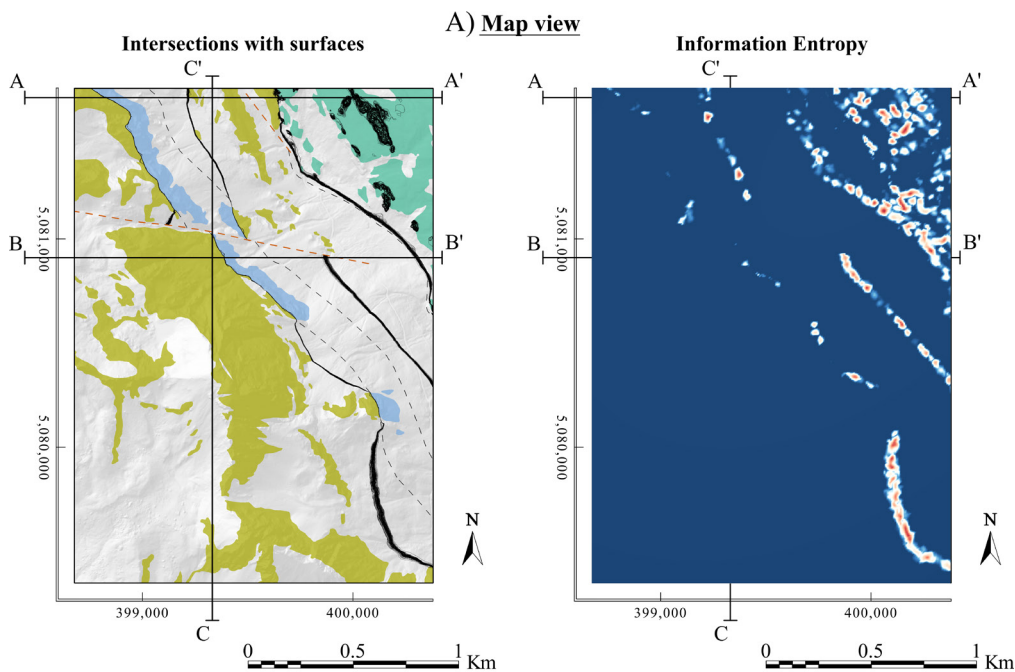
Information Entropy

Figure 4.10 (previous page). Results of the 100 realisations generated by the uncertainty analysis, as detailed in Sect. 4.3.6. Description of the results in Sect. 4.4.3 of the text. Location of the investigated volume is indicated in Fig. 4.4A by the dashed rectangle. On the left, intersection lines of the generated geometries with the map and the cross-sections planes. On the right, information entropy at the map and cross-section's locations. A) Map view. B) Representative cross-sections.

4.5.   Discussion

The presented workflow results from the combination of advanced implicit geomodelling techniques, which enable the integration of geological observations in the interpolation process, with high-resolution structural mapping. The methodology has been applied to a 29 km^2 challenging Alpine environment characterised by an ophiolitic tectonic sequence affected by multi-scale folding and brittle faulting. However, the potential of this approach extends beyond the specific Alpine setting and holds promise for a broader range of structural contexts where abundant structural data and a detailed structural map pinpointing the location of geological outcrops are available.

The integration of position inequality constraints in the interpolation process offers a means to reduce the impact of expert interpretation on the geomodelling outcome. This is achieved by excluding the portions of tectonic contacts that were interpreted between off-contact observations, and by instead directly integrating off-contact information itself into the modelling, greatly enriching the conventional approach to building structural models. By introducing this increased level of mathematical flexibility, the outcome solutions present smoother geometries that still fit the available data. In our workflow we employed independent "greater than" and "lower than" inequalities as implemented in the DSI algorithm of RING Toolkit (Frank et al., 2007; Caumon et al., 2013), however alternative strategies, such as defining bounding constraints to simultaneously restrict the value of the scalar field within defined limits, could also be effectively employed.

One limitation associated with the introduction of inequality constraints in the DSI algorithm relates to the increment in computational complexity, which scales with the number of nodes in the 3D mesh multiplied by the number of inequality constraints (Frank et al., 2007; Caumon et al., 2013). To ensure that interpolation times remain efficient, in our work we carefully considered the placement of inequality constraints, and we leveraged a prior implicit interpolation to define local extrema at outcrop locations at the surface (Sect. 4.3.5). Specifically, the replacement of interpreted tectonic contacts with inequality constraints led to a 3.5-fold increase in the interpolation time (from approximately 20 seconds to about 70 seconds). While this increase is significant in proportion, it is important to note that the overall interpolation time remains nearly instantaneous when compared to the time required for data collection and analysis. It is also worth mentioning that this approach could accommodate less accurate interpretations of the undercover tectonic contacts, since their primary purpose is to provide a basic

representation of geological boundary geometries and do not need high accuracy.

Nevertheless, there are alternative strategies for the sampling of inequality constraints that could be explored, to be used in combination or as substitution of the method implemented in this study. One potential strategy could involve leveraging the natural borders of geological outcrops, an approach particularly well-suited for settings where the topographic evolution of outcrops runs predominantly orthogonal to the geometries of the tectonic contacts to be represented. However, it may not be able to resolve settings where the average topography and the tectonic surfaces exhibit similar orientations, as observed in the eastern portion of our model where the orientation of the Combin Fault closely follows the topographic slope (Fig. 4.10). Other approaches would entail defining one inequality point at the centroid of each outcrop polygon or, albeit computationally more intense, covering the outcrop regions with a regular grid of points and using this set of points as inequality constraints in the interpolation process. Furthermore, an additional and straightforward approach, which we did not implement in this study to maintain a transparent representation of the limits of our method based on local extrema research, would involve the manual introduction of inequality points guided by expert knowledge. This approach could offer a more fine-tuned control over the constraints but would necessitate a higher degree of expert input.

The stack of metamorphic units exposed in our study area is characterised by abrupt lateral thickness variations and a limitation to their faithful representation arises from the uniformity of the gradient in the distance scalar field imposed by the DSI's regularisation term (Frank et al., 2007; Caumon et al., 2013). This term is essential as it ensures the well-posedness of the mathematical problem, also performing smoothing of the solution by minimising gradient variations between adjacent tetrahedra, but it is most suitable for sedimentary sequences with almost constant thicknesses of layers (Laurent, 2016). In our metamorphic setting, it leads to a "rebounding" effect away from equality constraints (on-contact observations) to maintain constant thicknesses at depth, even when minimising the effect of this constant gradient constraint by assigning lower weights compared to the other position and structural constraints (as low as 10^{-5}). However, to further enhance the geological realism of the modelled outcomes, future efforts should consider alternative approaches that involve introducing anisotropies into the gradient of the distance scalar field (e.g., Laurent, 2016; Laurent et al., 2016; Pizzella et al., 2022).

The orientation statistical analysis incorporated in our workflow has multiple effects on the modelled outcome, as it performs upscaling by defining, through vectorial means, one or more representative measurements for each investigated outcrop, and recognises the orientation distribution for the uncertainty study. The upscaling of vectorial data is a necessity aimed at smoothing outcrop-scale deformations (related to the complex nature of geological surfaces) that do not interest the geometry of

the tectonic contacts at the model scale.

The uncertainty analysis, on the other hand, aims at addressing the problem of sparse data sampling and at providing valuable insights into the effect that uncertainties in the structural database of plane measurements have on the geometry of tectonic contacts. This is done through simulation of schistosity data (randomly located in the 3D volume) that mirrors the statistical distribution recognised in the input dataset. In our work we have presented the case of a vMF distribution, however different statistical models could be stochastically simulated as pseudo-vectors, such as Kent distributions (e.g., Fisher et al., 1987; Arienti et al., in prep. – Chapter 3). Anticipating uncertainties concerning the locations of geological boundaries and the potential variations in the offset of faults holds far-reaching practical significance across various fields, including tunnelling projects, groundwater resource management, and resource explorations.

4.6. Conclusions

We presented a geomodelling workflow that combines advanced implicit algorithms with high-resolution structural mapping for the modelling of an ophiolitic tectonic sequence exposed in the Italian Pennine Alps. We modelled the tectonic contacts that outcrop along the Roisetta-Tournalin ridge employing the Discrete Smooth Interpolator implicit approach (Frank et al., 2007; Caumon et al., 2013), which leverages geological observations collected during fieldwork as direct constraints, including orientation and inequality constraints. We integrated off-contact observations into the interpolation process while filtering out interpretations performed on Quaternary deposits from the structural map, by imposing inequality constraints strategically placed at local extrema locations of a prior interpolation at surface. We also conducted 3D interpolation of schistosity data collected on the field. Finally, we generated stochastic simulations of schistosity data to reproduce the spherical distributions observed in the primary schistosity database. This last step addresses uncertainties within the structural database and generates a set of 100 plausible subsurface scenarios, demonstrating the absence of overlap between non-adjacent tectonic units, oscillations with magnitudes of up to 100 meters along the tectonic contacts, and varying fault offsets.

4.7. Author contributions

GA conceptualised the workflow, performed the data analysis, modelling and interpretation. GA, BM, GDP and AB carried out fieldwork in the study area. BM and GDP managed the GIS and created the structural map of the study area. JG and AB contributed to the statistical data analysis. GC provided geomodelling guidance. GA redacted the manuscript, with input from AB and JG. AB acquired funding.

4.8. Acknowledgements

the Interreg European Reservaqua project (ID 551749). G. Arienti acknowledges support from the European Union's Erasmus Traineeship + program. We thank Anna Losa and Matteo Pozzi for contributing to data collection.

4.9.   References

Arienti, G., Bistacchi, A., Caumon, G., Dal Piaz, G., Monopoli, B., Bertolo, D., 2024. Regional-scale 3D modelling in metamorphic belts: An implicit model-driven workflow applied in the Pennine Alps. Journal of Structural Geology 180, 105045. https://doi.org/10.1016/j.jsg.2023.105045

Arienti, G., Bistacchi, A., Caumon, G., Monopoli, B., Dal Piaz, G., in preparation. 3D structural implicit modelling of folded metamorphic units at Lago di Cignana with uncertainty assessment - Chapter 3 of this thesis.

Ballèvre, M., Kienast, J.-R., Vuichard, J.-P., 1986. La "nappe de la Dent-Blanche" (Alpes occidentales): deux unités austroalpines indépendantes. Eclogae Geologicae Helvetiae 79, 57–74. https://doi.org/https://doi.org/10.5169/seals-165826

Ballèvre, M., Merle, O., 1993. The Combin Fault : compressional reactivation of a Late Cretaceous-Early Tertiary detachment fault in the Western Alps. Schweizerische Mineralogische Und Petrographische Mitteilungen 73, 205–227. https://doi.org/https://doi.org/10/gfsjrz

Bistacchi, A., Dal Piaz, G., Massironi, M., Zattin, M., Balestrieri, M., 2001. The Aosta–Ranzola extensional fault system and Oligocene–Present evolution of the Austroalpine–Penninic wedge in the northwestern Alps. International Journal of Earth Sciences 90, 654–667. https://doi.org/10.1007/s005310000178

Bistacchi, A., Eva, E., Massironi, M., Solarino, S., 2000. Miocene to Present kinematics of the NW-Alps: evidences from remote sensing, structural analysis, seismotectonics and thermochronology. Journal of Geodynamics 30, 205–228. https://doi.org/https://doi.org/10.1016/S0264-3707(99)00034-4

Bistacchi, A., Massironi, M., 2000. Post-nappe brittle tectonics and kinematic evolution of the north-western Alps: an integrated approach. Tectonophysics 327, 267–292. https://doi.org/10.1016/S0040-1951(00)00206-7

Bistacchi, A., Massironi, M., Dal Piaz, Giorgio V, Dal Piaz, Giovanni, Monopoli, B., Schiavo, A., Toffolon, G., 2008. 3D fold and fault reconstruction with an uncertainty model: An example from an Alpine tunnel case study. Computers and Geosciences 34, 351–372. https://doi.org/10.1016/j.cageo.2007.04.002

Borradaile, G., 2003. Statistics of Earth Science Data. Springer Berlin Heidelberg, Berlin, Heidelberg. https://doi.org/10.1007/978-3-662-05223-5

Bucher, K., 2005. Blueschists, eclogites, and decompression assemblages of the Zermatt-Saas ophiolite: High-pressure metamorphism of subducted Tethys lithosphere. American Mineralogist 90, 821–835. https://doi.org/10.2138/am.2005.1718

Calcagno, P., Chilès, J.P., Courrioux, G., Guillen, A., 2008. Geological modelling from field data and geological knowledge. Part I. Modelling method coupling 3D potential-field interpolation and geological rules. Physics of the Earth and Planetary Interiors 171, 147–157. https://doi.org/10.1016/j.pepi.2008.06.013

Carmichael, T., Ailleres, L., 2016. Method and analysis for the upscaling of structural data. Journal of Structural Geology 83, 121–133. https://doi.org/10.1016/j.jsg.2015.09.002

Caumon, G., Gray, G., Antoine, C., Titeux, M.O., 2013. Three-dimensional implicit stratigraphic model building from remote sensing data on tetrahedral meshes: Theory and application to a regional model of la Popa

Basin, NE Mexico. IEEE Transactions on Geoscience and Remote Sensing 51, 1613–1621. https://doi.org/10.1109/TGRS.2012.2207727

Caumon, G., L. Tertois, A., Zhang, L., 2007. Elements for Stochastic Structural Perturbation of Stratigraphic Models. EAGE Conference on Petroleum Geostatistics. European Association of Geoscientists & Engineers. https://doi.org/10.3997/2214-4609.201403041

Cherpeau, N., Caumon, G., 2015. Stochastic structural modelling in sparse data situations. Petroleum Geoscience 21, 233–247. https://doi.org/10.1144/petgeo2013-030

Chilès, J.P., Aug, C., Guillen, A., Lees, T., 2004. Modelling the geometry of geological units and its uncertainty in 3D from structural data: the potential-field method. Proceedings of International Symposium on Orebody Modelling and Strategic Mine Planning. Perth, 313–320.

Dal Piaz, G., Cortiana, G., Del Moro, A., Martin, S., Pennacchioni, G., Tartarotti, P., 2001. Tertiary age and paleostructural inferences of the eclogitic imprint in the Austroalpine outliers and Zermatt–Saas ophiolite, western Alps. International Journal of Earth Sciences 90, 668–684. https://doi.org/10.1007/s005310000177

Dal Piaz, G.V., Bistacchi, A., Gianotti, F., Monopoli, B., Passeri, L., Schiavo, A., Bertolo, D., Bonetto, F., Ciarapica, G., Dal Piaz, G., Gouffon, Y., Massironi, M., Ratto, S., Toffolon, G., 2016. Foglio 070 Cervino e Note Illustrative. Carta Geologica d'Italia Alla Scala 1:50.000, ISPRA, Regione Autonoma Valle d'Aosta 432 pp.

Dal Piaz, G.V., Di Battistini, G., Venturelli, G., Kienast, J.-R., 1979. Manganiferous quartzitic schists of the Piemonte ophiolite nappe in the Valsesia-Valtournenche area (Italian Western Alps). Memorie Scienze Geologiche 32, 24 pp.

Dal Piaz, G.V., Gianotti, F., Monopoli, B., Pennacchioni, G., Tartarotti, P., Schiavo, A., Carraro, F., Bistacchi, A., Massironi, M., Martin, S., Ratto, S., 2010. Foglio 091 Chatillon e Note Illustrative. Carta Geologica d'Italia Alla Scala 1:50.000, ISPRA, Regione Autonoma Valle d'Aosta 152 pp.

Dal Piaz, G. V, 1999. The Austroalpine-Piedmont nappe stack and the puzzle of Alpine Tethys. Memorie Scienze Geologiche 53, 153–162.

Dal Piaz, G. V, Bistacchi, A., Massironi, M., 2003. Geological outline of the Alps. Episodes Journal of International Geoscience 26, 175–180. https://doi.org/10.18814/EPIIUGS/2003/V26I3/004

Dal Piaz, G. V, Ernst, W.G., 1978. Areal geology and petrology of eclogites and associated metabasites of the Piemonte ophiolite nappe, breuil—st. Jacques area, Italian Western Alps. Tectonophysics 51, 99–126. https://doi.org/10.1016/0040-1951(78)90053-7

de Kemp, E.A., Schetselaar, E.M., Hillier, M.J., Lydon, J.W., Ransom, P.W., 2016. Assessing the workflow for regional-scale 3D geologic modeling: An example from the Sullivan time horizon, Purcell Anticlinorium East Kootenay region, southeastern British Columbia. Interpretation 4, SM33–SM50. https://doi.org/10.1190/INT-2015-0191.1

Ernst, W.G., Dal Piaz, G. V, 1978. Mineral parageneses of eclogitic rocks and related mafic schists of the Piemonte ophiolite nappe, Breuil-St. Jacques area, Italian Western Alps. American Mineralogist 63, 621–640.

Fisher, N.I., Best, D.J., 1984. Goodness-of-fit tests for Fisher's distribution on the sphere. Australian Journal of Statistics 26, 142–150. https://doi.org/10.1111/j.1467-842X.1984.tb01228.x

Fisher, N.I., Lewis, T., Embleton, B.J.J., 1987. Statistical analysis of spherical data. Cambridge University Press.

Fisher, N.I., Lewis, T., Willcox, M.E., 1981. Tests of Discordancy for Samples from Fisher's Distribution on the Sphere. Applied Statistics 30, 230. https://doi.org/10.2307/2346346

Fisher, R.A., 1953. Dispersion on a sphere. Proceedings of the Royal Society of London 217, 295–305.

Frank, T., Tertois, A.L., Mallet, J.L., 2007. 3D-reconstruction of complex geological interfaces from irregularly distributed and noisy point data. Computers and Geosciences 33, 932–943. https://doi.org/10.1016/j.cageo.2006.11.014

Grose, L., Laurent, G., Aillères, L., Armit, R., Jessell, M., Caumon, G., 2017. Structural data constraints for implicit modeling of folds. Journal of Structural Geology 104, 80–92. https://doi.org/10.1016/j.jsg.2017.09.013

Hillier, M., de Kemp, E., Schetselaar, E., 2013. 3D form line construction by structural field interpolation (SFI) of geologic strike and dip observations. Journal of Structural Geology 51, 167–179. https://doi.org/https://doi.org/10.1016/j.jsg.2013.01.012

Hillier, M.J., Schetselaar, E.M., de Kemp, E.A., Perron, G., 2014. Three-Dimensional Modelling of Geological Surfaces Using Generalized Interpolation with Radial Basis Functions. Mathematical Geosciences 46, 931–953. https://doi.org/10.1007/s11004-014-9540-3

Houlding, S.W., 1994. The Geological Characterization Process. 3D Geoscience Modeling. Springer Berlin Heidelberg, Berlin, Heidelberg, 7–26. https://doi.org/10.1007/978-3-642-79012-6_2

Jessell, M., Aillères, L., de Kemp, E., Lindsay, M., Wellmann, F., Hillier, M., Laurent, G., Carmichael, T., Martin, R., 2014. Next Generation Three-Dimensional Geologic Modeling and Inversion. Building Exploration Capability for the 21st Century. Society of Economic Geologists. https://doi.org/10.5382/SP.18.13

Kaufmann, O., Martin, T., 2009. Reprint of "3D geological modelling from boreholes, cross-sections and geological maps, application over former natural gas storages in coal mines" [Comput. Geosci. 34 (2008) 278-290]. Computers and Geosciences 35, 70–82. https://doi.org/10.1016/S0098-3004(08)00227-6

Lajaunie, C., Courrioux, G., Manuel, L., 1997. Foliation fields and 3D cartography in geology: Principles of a method based on potential interpolation. Mathematical Geology 29, 571–584. https://doi.org/10.1007/BF02775087

Laurent, G., 2016. Iterative Thickness Regularization of Stratigraphic Layers in Discrete Implicit Modeling. Mathematical Geosciences 48, 811–833. https://doi.org/10.1007/s11004-016-9637-y

Laurent, G., Ailleres, L., Grose, L., Caumon, G., Jessell, M., Armit, R., 2016. Implicit modeling of folds and overprinting deformation. Earth and Planetary Science Letters 456, 26–38. https://doi.org/10.1016/j.epsl.2016.09.040

Lilliefors, H.W., 1969. On the Kolmogorov-Smirnov Test for the Exponential Distribution with Mean Unknown. Journal of the American Statistical Association 64, 387–389.

Lilliefors, H.W., 1967. On the Kolmogorov-Smirnov Test for Normality with Mean and Variance Unknown. Journal of the American Statistical Association 62, 399–402.

Lindsay, M.D., Aillères, L., Jessell, M.W., de Kemp, E.A., Betts, P.G., 2012. Locating and quantifying geological uncertainty in three-dimensional models: Analysis of the Gippsland Basin, southeastern Australia. Tectonophysics 546–547, 10–27. https://doi.org/10.1016/j.tecto.2012.04.007

Mallet, J.L., 2002. Geomodeling. Oxford University Press.

Marthaler, M., 1984. Géologie des unités penniques entre le val d'Anniviers et le val de Tourtemagne. Eclogae Geologicae Helvetiae 77, 395–448.

Maxelon, M., Mancktelow, N.S., 2005. Three-dimensional geometry and tectonostratigraphy of the Pennine zone, Central Alps, Switzerland and Northern Italy. Earth-Science Reviews 71, 171–227. https://doi.org/10.1016/j.earscirev.2005.01.003

Maxelon, M., Renard, P., Courrioux, G., Brändli, M., Mancktelow, N., 2009. A workflow to facilitate three-dimensional geometrical modelling of complex poly-deformed geological units. Computers & Geosciences 35, 644–658. https://doi.org/10.1016/j.cageo.2008.06.005

Pakyuz-Charrier, E., Lindsay, M., Ogarko, V., Giraud, J., Jessell, M., 2018. Monte Carlo simulation for uncertainty estimation on structural data in implicit 3-D geological modeling, a guide for disturbance distribution selection and parameterization. Solid Earth 9, 385–402. https://doi.org/10.5194/se-9-385-2018

Passeri, L., Ciarapica, G., Dal Piaz, G.V., 2018. The problematic origin of the Pancherot-Cime Bianche-Bettaforca unit (PCB) in the Piemonte zone (Western Alps). Italian Journal of Geosciences 137, 478–489. https://doi.org/doi.org/10.3301/IJG.2018.21

Perello, P., Gianotti, F., Monopoli, B., Carraro, F., Venturini, G., Fontan, D., Schiavo, A., Bonetto, F., 2011. Foglio 089 Courmayeur e Note Illustrative. Carta Geologica d'Italia Alla Scala 1:50.000, ISPRA, Regione Autonoma Valle d'Aosta 152 pp.

Perrouty, S., Lindsay, M.D., Jessell, M.W., Aillères, L., Martin, R., Bourassa, Y., 2014. 3D modeling of the Ashanti Belt, southwest Ghana: Evidence for a litho-stratigraphic control on gold occurrences within the Birimian Sefwi Group. Ore Geology Reviews 63, 252–264. https://doi.org/10.1016/j.oregeorev.2014.05.011

Philippon, M., de Veslud, C.L.C., Gueydan, F., Brun, J.P., Caumon, G., 2015. 3D geometrical modelling of post-foliation deformations in metamorphic terrains (Syros, Cyclades, Greece). Journal of Structural Geology 78, 134–148. https://doi.org/10.1016/j.jsg.2015.07.002

Pizzella, L., Alais, R., Lopez, S., Freulon, X., Rivoirard, J., 2022. Taking Better Advantage of Fold Axis Data to Characterize Anisotropy of Complex Folded Structures in the Implicit Modeling Framework. Mathematical Geosciences 54, 95–130. https://doi.org/10.1007/s11004-021-09950-0

Polino, R., Malusà, M.G., S, M., Carraro, F., Gianotti, F., Bonetto, F., Perello, P., Schiavo, A., Gouffon, Y., 2015. Foglio 090 Aosta e Note Illustrative. Carta Geologica d'Italia Alla Scala 1:50.000, ISPRA, Regione Autonoma Valle d'Aosta 144 pp.

Reddy, S.M., Wheeler, J., Butler, R.W.H., Cliff, R.A., Freeman, S., Inger, S., Pickles, C., Kelley, S.P., 2003. Kinematic reworking and exhumation within the convergent Alpine Orogen. Tectonophysics 365, 77–102. https://doi.org/10.1016/S0040-1951(03)00017-9

Schneeberger, R., de La Varga, M., Egli, D., Berger, A., Kober, F., Wellmann, F., Herwegh, M., 2017. Methods and uncertainty estimations of 3-D structural modelling in crystalline rocks: a case study. Solid Earth 8, 987–1002. https://doi.org/10.5194/se-8-987-2017

Shannon, E.C., 1948. A mathematical theory of communication. Bell System Technical Journal 27, 379–423.

Sue, C., Delacou, B., Champagnac, J.D., Allanic, C., Tricart, P., Burkhard, M., 2007. Extensional neotectonics

around the bend of the Western/Central Alps: An overview. International Journal of Earth Sciences 96, 1101–1129. https://doi.org/10.1007/S00531-007-0181-3

Thornton, J.M., Mariethoz, G., Brunner, P., 2018. A 3D geological model of a structurally complex alpine region as a basis for interdisciplinary research. Scientific Data 5, 180238. https://doi.org/10.1038/sdata.2018.238

Vollgger, S.A., Cruden, A.R., Ailleres, L., Cowan, E.J., 2015. Regional dome evolution and its control on ore-grade distribution: Insights from 3D implicit modelling of the Navachab gold deposit, Namibia. Ore Geology Reviews 69, 268–284. https://doi.org/https://doi.org/10.1016/j.oregeorev.2015.02.020

Wellmann, F., Caumon, G., 2018. 3-D Structural geological models: Concepts, methods, and uncertainties. Advances in Geophysics 59, 1–121. https://doi.org/10.1016/bs.agph.2018.09.001

Wellmann, J.F., Horowitz, F.G., Schill, E., Regenauer-Lieb, K., 2010. Towards incorporating uncertainty of structural data in 3D geological inversion. Tectonophysics 490, 141–151. https://doi.org/10.1016/j.tecto.2010.04.022

Wellmann, J.F., Regenauer-Lieb, K., 2012. Uncertainties have a meaning: Information entropy as a quality measure for 3-D geological models. Tectonophysics 526–529, 207–216. https://doi.org/10.1016/j.tecto.2011.05.001

Wood, A.T.., 1994. Simulation of the von mises fisher distribution. Communications in Statistics - Simulation and Computation 23, 157–164. https://doi.org/10.1080/03610919408813161

Woodcock, N.H., 1977. Specification of fabric shapes using an eigenvalue method. Geological Society of America Bulletin 88, 1231. https://doi.org/10.1130/0016-7606(1977)88<1231:SOFSUA>2.0.CO;2

<div align="right">Chapter 5</div>

Concluding remarks and perspectives

5.1.   Conclusion of the presented research

This PhD thesis presented workflows aimed at incorporating detailed geological and structural data derived from fieldwork, traditionally presented as structural maps, into modelling endeavours using the implicit Discrete Smooth Interpolator (DSI) as implemented in SKUA/GOCAD and in the RING Toolkit plugin (Frank et al., 2007; Caumon et al., 2013). The resulting models adhere to directly observed information and represent the tectonic setting of the Pennine Alps.

The structural map used as starting point throughout the thesis and presented in Chapter 2 (Fig. 2.1) is the culmination of over 30 years of fieldwork in the region (https://geoportale.regione.vda.it/; Dal Piaz et al., 2010, 2016; Perello et al., 2011; Polino et al., 2015) and offers continuous coverage across the entire study areas, spanning from the Mont Blanc to the Monte Rosa. Equipped with this detailed structural map (derived from fieldwork performed at the 1:10,000 resolution), the emphasis of this thesis has been on employing workflows that can incorporate the greatest amount of data out of the available database (i.e., outcrop observations, dataset of structural measurements, faults). Simultaneously, I have directed my efforts towards implementing modelling solutions designed to reduce the subjective input of the interpreter through the gradual introduction of additional constraints and modelling strategies, a progression that develops across the Chapters of this thesis.

In the initial segment of this thesis, covered in Chapter 2, I employed a more traditional modelling workflow for the representation of a regional area spanning 1,500 km^2 between the Mont Blanc and the Monte Rosa. This workflow relied on structural interpretations conducted on vertical cross-sections to propagate geological information from the outcrop scale to the broader model scale. Interpretations,

constructed by projection of geological data onto cross-section planes and application of conventional structural interpretation patterns, were later interpolated to obtain the resulting 3D structural model. However, since this approach was reliant on the interpretations provided to the interpolator, the modelled outcome was affected by high subjectivity and represents a "best guess" interpretation.

Topics such as upscaling of outcrop-scale observations aimed at smoothing small-scale deformations, which may not be relevant at the model scale, and the impact that building the 3D model had on the final tectonic interpretation of the area were introduced and discussed, emphasising the importance of three-dimensional reasoning over purely two-dimensional approaches. As discussed in Chapter 2 (Arienti et al., 2024) and throughout the entire thesis, the process of building 3D models motivated the creation of tectono-metamorphic schemes (legends) summarising hierarchical relationships among units, thus enhancing discussions about relative timing of geological events and also facilitating efficient data transfer between two-dimensional (e.g., tectonic map and cross-sections) and three-dimensional models (e.g., the structural model). Moreover, the creation of 3D models that adhere to field data and observations provided insights into a subset of the ensemble of plausible geological models, considering the validity of the proposed interpretation. It is also crucial to acknowledge the importance of 3D visualisation in facilitating effective geological communication and providing holistic representations that can be used for further validation (through classic geological reasoning) of interpretations of the tectonic architecture. However, for a more detailed discussion on the topic of "modelling informing geology", I direct the interested reader to Chapter 2's discussion section.

The introduction of synthetic interpretations, a common practice in modelling of large geographical areas (e.g., Maxelon et al., 2009; Thornton et al., 2018), is acknowledged in the first section of the work (Arienti et al., 2024 - Chapter 2) as a "necessary evil" essential for generating a model that adheres to the principles of geological realism, evaluated through geological reasoning. Therefore, significant expert contribution was indispensable to build cross-sections, analyse and interpret field data, and experiment with modelling parameters until an acceptable 3D geometry was achieved, requiring extensive working time. Overall, this initial segment of the thesis highlighted that building a regional-scale structural model from field data in a region characterised by significant structural complexity (e.g., a collisional orogenic wedge paired with a thrust sequence of semi-parallel structures as in our tectonic setting) is a task that is far from fully automated and requires substantial modelling expertise.

In the subsequent Chapters (3 and 4), I applied the implicit modelling approach to smaller areas (extensions less than 30 km^2) located within the boundaries of the regional-scale model, as indicated in the map in Fig. 1.1. Capitalising on the more confined dimensions of these regions, corresponding to more stationary deformation patterns, and on the wealth of the database of structural measurements, the workflows aimed to reduce the subjective contribution of the interpreter by replacing expert

interpretations on vertical cross-sections with robust structural control permitted by the implicit constraints of the Discrete Smooth Interpolator (Frank et al., 2007; Caumon et al., 2013).

The representation of non-cylindrical, isoclinal recumbent folds, presented in Chapter 3, was performed by employing a strategy based on the work of Laurent et al. (2016) which entailed 3D interpolation of fold axes collected on the field, and additional densification of position constraints through projection of the mapped tectonic contacts. The same dataset of fold axes was moreover analysed with spherical statistics methods and replicated using stochastic simulations, to produce suites of vectors mirroring the same orientation distribution derived from the observed measurements (both von Mises-Fisher and Kent models). This approach introduced simulated vectorial data away from field observations, emulating the introduction of new input data samples (e.g., additional fieldwork), and resulted in the generation of suites of geologically plausible alternative scenarios, which yielded particularly interesting insights on the location of fold hinges and possible fold plane rotations.

Overall, this section of the thesis showed that, by changing the scale of the modelling problem and increasing the resolution of the representation (compared to the regional-scale study presented in Chapter 2), it was possible to model complex isoclinal, non-cylindrical folds such as the ones outcropping in the Austroalpine tectono-metamorphic unit. It also showed that, by employing modelling strategies such as vectorial interpolation of field fold axes in a region with relatively stationary patterns, it was possible to overcome the need for structural interpretations on vertical cross-sections that was instead necessary for the previous regional-scale model.

In Chapter 4, for the modelling of a conformable ophiolitic succession, the workflow integrated inequality position constraints as permitted by the Discrete Smooth Interpolator implemented in RING Toolkit (Frank et al., 2007; Caumon et al., 2013) and performed 3D interpolation of dip-dip direction measurements to homogenise structural control and mitigate the effects of sparse data sampling. Moreover, the incorporation of position inequality constraints into the interpolation process provided an additional means to diminish the influence of expert interpretation on the modelling outcome and enhanced the conventional modelling approach by utilising direct observations of outcrop locations to influence the value of the scalar field with "greater than" and "lower than" constraints. This was achieved by excluding portions of tectonic contacts that were interpreted between off-contact observations and, instead, integrating off-contact outcrop information directly into the 3D structural modelling process while strategically positioning inequality constraints at outcrop locations. In addition to this, Chapter 4 also employed a similar approach to the one employed in Chapter 3 for the stochastic simulation of vectorial data to the dataset of foliation planes, yielding insights into the position of the tectonic contacts.

These two works (Chapters 3 and 4) can be viewed as a progression toward a more comprehensive,

mature modelling workflow. In fact, the modelling strategies employed could potentially be combined in a new workflow or used independently, depending on the requirements of the setting to model, showcasing the great flexibility of the implicit modelling method. The use of implicit constraints that allow the seamless integration of geological data traditionally accessible in structural maps into the interpolation process not only enhances the accuracy and robustness of the model, but also diminishes interpretation bias, while allowing the integration of classes of information characterised by relatively low uncertainties at the location of the observation.

5.2.   Discussion and future work

From the modelling endeavours outlined in this thesis, it emerged that despite the power inherent in the implicit modelling approach for representing the geological subsurface, there is still much to be done to enhance the geological realism in complex metamorphic settings.

As extensively discussed in the preceding Chapters, the modelling conducted in this thesis has revealed limitations in the ability of the DSI algorithm to accommodate abrupt lateral thickness variations in geological layers. This behaviour, previously reported also by Laurent (2016), arises from the regularisation term that minimises gradient variations between adjacent tetrahedra, ensuring the well-posedness of the interpolation problem (Frank et al., 2007; Caumon et al., 2013). While the commercial tools of SKUA/GOCAD allow enabling anisotropies in the gradient of the scalar field (e.g., Chapter 2), we are instead limited to reducing the weight of this regularisation terms when employing RING toolkit algorithms (Frank et al., 2007; Caumon et al., 2013). However, one potential approach to address this challenge, which could benefit this work, involves introducing oriented anisotropies in the gradient of the scalar field (Laurent, 2016; Laurent et al., 2016; Pizzella et al., 2022) in order to tailor the implicit solution to settings characterised by heterogeneous layer thicknesses and similar folding geometries. Moreover, since other implicit algorithms also rely on various regularisation terms targeting the minimisation of local variation in the second derivatives of the scalar field, it is conceivable that handling large thickness variations might be a common challenge, as preliminary studies might suggest (Caumon et al., 2020).

The representation of the tectonic framework of the Pennine Italian Alps at different scales (from the regional-scale in Chapter 2 to the small scales in Chapters 3 and 4) starting from a common tectonic map (the new tectonic map of the Northern Aosta Valley presented in Chapter 2), enabled different levels of detail on the interpretations. While higher resolution models clearly allow for a better fit to field observations, this also highlighted the need for robust upscaling methodologies for both the vectorial database (e.g., Jessell et al., 2014; Carmichael and Ailleres, 2016) and the geological geometries (e.g., mapped polylines). In this thesis, to upscale the structural dataset to match the scale of the models, we relied on techniques of averaging using vectorial means (Chapter 2 to 4). In particular,

in Chapter 2 we upscaled foliation measurements along the nodes of a regular grid, to have the structural database match the scale of the regional model. On the other hand, in Chapters 3 and 4 we used averaging methodologies supported by validation with eigenanalysis with the aim to compute one or more representative structural measurements for each indagated outcrop. In these latter cases (Chapters 3 and 4), being the 3D models at a smaller scale, the structural database did not require further upscaling as instead performed for the regional-scale 3D model. Similarly, for the upscaling of mapped geometries, for the regional model (Chapter 2) we relied on expert interpretations to perform smoothing of the small-scale deformations, while at the smaller scale (Chapters 3 and 4) the tectonic boundaries did not need upscaling since already similar to the resolution of the models.

Inherent to the utilisation of upscaling techniques, there is important loss of information and simplification of the structures. A significant enhancement in the direction of a unique, seamless representation that may be considered in future works is the integration of multi-scale modelling workflows, which would be particularly beneficial for the modelling of geological terrains characterised by geometries that propagate across different scales, such as in our study areas, while minimising loss of information. In this direction, in this thesis I proposed a strategy of manual breakdown of the modelling problem into multiple sub-models (the local 3D models of Chapters 3 and 4), whose resolution can be adjusted to accommodate the complexity of the geological structures. This approach represents a tentative to overcome computational problems related to mesh resolution and it breaks down the interpolation complexity by portraying settings with relatively stationary deformation patterns. However, this approach does not represent a seamless solution and produces completely independent models, highlighting the need for seamless multi-scale modelling workflows.

Regarding the assessment of uncertainties, this thesis presented the case of stochastic simulations of vectorial data mimicking statistical distributions recognised in the input field database, and we presented the case for von Mises-Fisher (Fisher, 1953) and Kent distributions (or Fisher-Bingham; Kent, 1982). However, the same rationale could be easily transferred to the generation of pseudo-random vectors belonging to other statistical distributions (e.g., Fisher et al., 1987). The presented approach consists in the generation of samples of vectorial data (uniformly distributed in the 3D volume) based on spherical statistical distributions derived from the field samples, and their introduction in the implicit interpolation together with field input data for the generation of suites of plausible scenarios. The outcomes of this uncertainty analysis, quantified using information entropy (Shannon, 1948; Wellmann and Regenauer-Lieb, 2012), are influenced by various sources of uncertainty that, nonetheless, often cannot be readily distinguished or easily identified. First, there exists uncertainty regarding the accuracy of the field measurements themselves, as they are subject to instrumental and sampling errors. Secondly, the inherently chaotic nature of geological processes and features contributes to a dispersion of

measurements that merges with the previous source of uncertainty. Lastly, there is uncertainty that stems from incomplete sampling of data, which is inevitably sparse and limited to the observations located at the topographic surface in our case, a source of uncertainty that the approach outlined in the Chapters of this thesis (Chapters 3 and 4) aims to tackle using statistical methods. To address this, simulated vectorial samples are treated as plausible representations of measurements that could be collected through additional data sampling across the model volume (e.g., through borehole drilling at depth or exploration of undercover outcrops). Overall, the results of this uncertainty analysis could be used to evaluate the expected range of variations in geological surfaces and behaviours along for instance fold segments (Chapter 3) or geological boundaries.

Moreover, a consideration not included in this thesis due to the absence of clear spatial correlation between structural measurements at the model scale is the incorporation of perturbation algorithms that consider spatial relationships among data (e.g., Caers, 2011; Cherpeau and Caumon, 2015). Integrating these algorithms would necessitate an alignment between the scale of data sampling and the scale of the deformation to be perturbed, overall contributing to enhancing the robustness of the uncertainty analysis.

Finally, a number of new approaches, building on or using implicit modelling techniques, have been recently presented, such as the use of spatial agents for geological modelling (de Kemp, 2021), or Implicit Neural Representation methods (Hillier et al., 2021, 2023), representing a growing set of valid alternatives for the representation of tectonic settings, including metamorphic ones.

I would also like to mention the transformative impact of open-source technologies on the future of 3D structural modelling. Throughout my PhD journey, I collaborated on an open-source modelling platform called PZero (https://github.com/andrea-bistacchi/PZero), as discussed in the thesis introduction (Sect. 1.4). Despite the change in focus and the utilisation of commercial algorithms in the modelling presented in this thesis, this initial exposure to open-source technologies influenced my perspective and presented the potential of open source algorithms in the future landscape of implicit modelling. Projects such as Loop (https://loop3d.org/; Grose et al., 2021b) and GemPy (https://www.gempy.org/; De La Varga et al., 2019) mark significant strides in advancing open-source implicit modelling. As the field evolves, the adoption of open-source methodologies emerges as a powerful choice, not only for encouraging collaboration and transparency but also for its capacity to democratise three-dimensional structural modelling, fostering accessibility and contributing to the continued expansion and improvement of implicit modelling methodologies.

5.3. References

Arienti, G., Bistacchi, A., Caumon, G., Dal Piaz, G., Monopoli, B., Bertolo, D., 2024. Regional-scale 3D modelling in metamorphic belts: An implicit model-driven workflow applied in the Pennine Alps. Journal of Structural Geology 180, 105045. https://doi.org/10.1016/j.jsg.2023.105045

Caers, J., 2011. Modeling uncertainty in the earth sciences. John Wiley & Sons.

Carmichael, T., Ailleres, L., 2016. Method and analysis for the upscaling of structural data. Journal of Structural Geology 83, 121–133. https://doi.org/10.1016/j.jsg.2015.09.002

Caumon, G., Gray, G., Antoine, C., Titeux, M.O., 2013. Three-dimensional implicit stratigraphic model building from remote sensing data on tetrahedral meshes: Theory and application to a regional model of la Popa Basin, NE Mexico. IEEE Transactions on Geoscience and Remote Sensing 51, 1613–1621. https://doi.org/10.1109/TGRS.2012.2207727

Caumon, G., Renaudeau, J., Irakarama, M., Grose, L., De La Varga, M., Hillier, M., de Kemp, E., Wellmann, F., Collon, P., Laurent, G., Ailleres, L., 2020. Progresses in the implicit structural modeling benchmark. 2020 RING Meeting. ASGA.

Cherpeau, N., Caumon, G., 2015. Stochastic structural modelling in sparse data situations. Petroleum Geoscience 21, 233–247. https://doi.org/10.1144/petgeo2013-030

Dal Piaz, G.V., Bistacchi, A., Gianotti, F., Monopoli, B., Passeri, L., Schiavo, A., Bertolo, D., Bonetto, F., Ciarapica, G., Dal Piaz, G., Gouffon, Y., Massironi, M., Ratto, S., Toffolon, G., 2016. Foglio 070 Cervino e Note Illustrative. Carta Geologica d'Italia Alla Scala 1:50.000, ISPRA, Regione Autonoma Valle d'Aosta 432 pp.

Dal Piaz, G.V., Gianotti, F., Monopoli, B., Pennacchioni, G., Tartarotti, P., Schiavo, A., Carraro, F., Bistacchi, A., Massironi, M., Martin, S., Ratto, S., 2010. Foglio 091 Chatillon e Note Illustrative. Carta Geologica d'Italia Alla Scala 1:50.000, ISPRA, Regione Autonoma Valle d'Aosta 152 pp.

de Kemp, E.A., 2021. Spatial agents for geological surface modelling. Geoscientific Model Development 14, 6661–6680. https://doi.org/10.5194/gmd-14-6661-2021

De La Varga, M., Schaaf, A., Wellmann, F., 2019. GemPy 1.0: Open-source stochastic geological modeling and inversion. Geoscientific Model Development 12, 1–32. https://doi.org/10.5194/gmd-12-1-2019

Fisher, N.I., Lewis, T., Embleton, B.J.J., 1987. Statistical analysis of spherical data. Cambridge University Press.

Fisher, R.A., 1953. Dispersion on a sphere. Proceedings of the Royal Society of London 217, 295–305.

Frank, T., Tertois, A.L., Mallet, J.L., 2007. 3D-reconstruction of complex geological interfaces from irregularly distributed and noisy point data. Computers and Geosciences 33, 932–943. https://doi.org/10.1016/j.cageo.2006.11.014

Grose, L., Ailleres, L., Laurent, G., Jessell, M., 2021. LoopStructural 1.0: Time-aware geological modelling. Geoscientific Model Development 14, 3915–3937. https://doi.org/10.5194/gmd-14-3915-2021

Hillier, M., Wellmann, F., Brodaric, B., de Kemp, E., Schetselaar, E., 2021. Three-Dimensional Structural Geological Modeling Using Graph Neural Networks. Mathematical Geosciences 53, 1725–1749. https://doi.org/10.1007/s11004-021-09945-x

Hillier, M., Wellmann, F., de Kemp, E.A., Brodaric, B., Schetselaar, E., Bédard, K., 2023. GeoINR 1.0: an implicit neural network approach to three-dimensional geological modelling. Geoscientific Model Development 16, 6987–7012. https://doi.org/10.5194/gmd-16-6987-2023

Jessell, M., Aillères, L., de Kemp, E., Lindsay, M., Wellmann, F., Hillier, M., Laurent, G., Carmichael, T., Martin, R., 2014. Next Generation Three-Dimensional Geologic Modeling and Inversion. Building Exploration Capability for the 21st Century. Society of Economic Geologists. https://doi.org/10.5382/SP.18.13

Kent, J.T., 1982. The Fisher-Bingham Distribution on the Sphere. Journal of the Royal Statistical Society 44, 71–80.

Laurent, G., 2016. Iterative Thickness Regularization of Stratigraphic Layers in Discrete Implicit Modeling. Mathematical Geosciences 48, 811–833. https://doi.org/10.1007/s11004-016-9637-y

Laurent, G., Ailleres, L., Grose, L., Caumon, G., Jessell, M., Armit, R., 2016. Implicit modeling of folds and overprinting deformation. Earth and Planetary Science Letters 456, 26–38. https://doi.org/10.1016/j.epsl.2016.09.040

Maxelon, M., Renard, P., Courrioux, G., Brändli, M., Mancktelow, N., 2009. A workflow to facilitate three-dimensional geometrical modelling of complex poly-deformed geological units. Computers & Geosciences 35, 644–658. https://doi.org/10.1016/j.cageo.2008.06.005

Perello, P., Gianotti, F., Monopoli, B., Carraro, F., Venturini, G., Fontan, D., Schiavo, A., Bonetto, F., 2011. Foglio 089 Courmayeur e Note Illustrative. Carta Geologica d'Italia Alla Scala 1:50.000, ISPRA, Regione Autonoma Valle d'Aosta 152 pp.

Pizzella, L., Alais, R., Lopez, S., Freulon, X., Rivoirard, J., 2022. Taking Better Advantage of Fold Axis Data to Characterize Anisotropy of Complex Folded Structures in the Implicit Modeling Framework. Mathematical Geosciences 54, 95–130. https://doi.org/10.1007/s11004-021-09950-0

Polino, R., Malusà, M.G., S, M., Carraro, F., Gianotti, F., Bonetto, F., Perello, P., Schiavo, A., Gouffon, Y., 2015. Foglio 090 Aosta e Note Illustrative. Carta Geologica d'Italia Alla Scala 1:50.000, ISPRA, Regione Autonoma Valle d'Aosta 144 pp.

Shannon, E.C., 1948. A mathematical theory of communication. Bell System Technical Journal 27, 379–423.

Thornton, J.M., Mariethoz, G., Brunner, P., 2018. A 3D geological model of a structurally complex alpine region as a basis for interdisciplinary research. Scientific Data 5, 180238. https://doi.org/10.1038/sdata.2018.238

Wellmann, J.F., Regenauer-Lieb, K., 2012. Uncertainties have a meaning: Information entropy as a quality measure for 3-D geological models. Tectonophysics 526–529, 207–216. https://doi.org/10.1016/j.tecto.2011.05.001